

14230
2002
C.2

**GAS PERMEAMETERS:
OPERATION, MODIFICATION, AND DESIGN**

by

Benjamin James Lechler

NMIMT
LIBRARY
SOCORRO, NM

Submitted in Partial Fulfillment
of the Requirements for the Degree of
Master of Science in Hydrology

New Mexico Institute of Mining and Technology
Department of Earth and Environmental Science
Socorro, New Mexico

August, 2002

SEP 17 2002

51939735

ABSTRACT

Gas permeameters are widely used in the fields of hydrology, soil science, and petroleum engineering to characterize the spatial heterogeneity of hydraulic properties, in particular permeability. The spatial distribution of permeability governs fluid flow and transport, affecting such processes as contaminant migration, groundwater recharge, and petroleum recovery. Laboratory scale and field-portable permeameters, based on steady or transient gas flow, are used to map the distribution of permeability. Most permeameters are optimized for use on a particular type of material (lithified rock or unconsolidated sediments) with a certain permeability range. A good field-permeameter must be highly portable and allow for rapid measurement of permeability across a wide range of materials. Many outcrop studies have been performed on high permeability poorly consolidated sand bodies dissected by nearly vertical zones of lower permeability material (small-displacement faults or clastic dikes). The lightweight syringe-based air-minipermeameter (LSAMP) designed by Davis et al. [1994] and modified LSAMP II [Suboor and Wilson, personal communication] were the primary permeameters used in many of these studies. Difficulty was encountered when attempting measurements on low permeability materials with these devices; the measurement duration was too long.

Three studies were performed to better understand and improve permeability estimation with gas permeameters, with particular focus on increasing the amount of data that can be collected in the field (making measurements faster) with a single permeameter. The first study compares the operational characteristics of the LSAMP with those of the improved LSAMP II. The second deals with modification of the

LSAMP II to increase the range (decrease measurement duration) of permeability that it can effectively measure in the field. The third study involves the development, design, and testing of a new field-portable transient pressure decay permeameter to allow for rapid estimation of permeability across a wide range of materials.

Over 1,000 permeability measurements were collected to compare the operational characteristics of the LSAMP and LSAMP II as they apply to measurement repeatability (measurement variance at a point). The major operational differences are: (1) the LSAMP uses a hand held tip seal, while the LSAMP II has a pistol grip-mounted tip seal with a gauge to monitor application force and (2) the LSAMP's tip seal must be removed between measurements to refill the syringe with air, while the LSAMP II has a 3-way solenoid valve and air pump which automatically refill the syringe, eliminating the need to remove the tip seal between measurements. Results suggest removing the tip seal when making multiple measurements at a point produces a significantly higher variance than not removing it, while the amount variability attributed to applying the tip seal by hand or with the pistol grip-mounted tip seal (monitoring application force) is relatively the same. Instrument error was also quantified and found to account for less than 2 % of the total measurement variability for all materials tested, but results indicate it could be an issue at the high end of the instruments measurement range.

Two modifications were tested to decrease the required measurement duration of the LSAMP II: (1) changing tip seal inner radius and geometric factor and (2) increasing the gas injection pressure by adding weight. 30 measurements were made at relatively the same location on an aluminum oxide sharpening block using three different tip seal geometries (inner radii and/or geometric factor). Measurements were made on different

lengths of POREX® porous plastic standards with no weight, 1 lb, and 2.5 lbs added weight. Increasing the tip seal ratio (geometric factor) for a given tip seal inner radius did not prove to have a significant effect on measurement duration. Increasing the tip seal inner radius, for a given geometric factor, significantly decreases the measurement duration, though application of this modification is limited due to practical considerations. The addition of weight proved to significantly decrease measurement duration: 5 times faster than the un-weighted duration for 1 lb, and 10 times faster than the un-weighted duration for 2.5 lb. Reduction of the measurement duration by a factor of 10 (for 2.5 lb added weight) effectively adds an order of magnitude permeability to the low end of the measurement range.

A mathematical model was developed and a prototype device was built to test the range and corresponding measurement duration of a transient pressure decay permeameter. Experiments were performed on multiple sample materials, at a range of initial tank pressures, using two different volume tanks (with and without a heat capacitor in the tank). Results suggest use of a heat capacitor in the tank is essential to dampen thermodynamic effects resulting from rapidly decaying pressure at the onset of a measurement. Derivative plots and steady-flow measurements indicate the presence of nonlinear effects, occurring at the transition to turbulent flow, in high permeability materials at higher pressure. For data in which thermodynamic and nonlinear effects were unnoticeable, pressure decay permeability estimates agree fairly well with steady flow measurements, but are consistently biased low. Though only tested in the laboratory, the pressure decay permeameter could significantly improve data collection in

the field, allowing for rapid ($\Delta t_{\text{measurement}} < 20$ s) permeability measurement across at least four orders of magnitude permeability ($1 \times 10^{-11} - 3 \times 10^{-15}$ m²) using a single permeameter.

ACKNOWLEDGMENTS

This research was supported by the New Mexico Tech Geophysical Research Center, the Hanford Clastic Dike Study under the Environmental Management Science Program of the U.S. Department of Energy.

I would like to thank my committee members: Mike Fort, Brian McPherson, and John Wilson. John deserves thanks for providing me with a Research Assistantship and acting as both my Academic and Research Advisor. It was a pleasure to have worked with John. Mike provided guidance throughout the design and testing of the pressure decay permeameter. Brian offered many helpful suggestions during the writing and organization of the final draft.

I thank my fellow students (especially Dan, Dave, and Eric) for the many intellectual exchanges along the way. I wouldn't have gotten through the research or the class-work without you people. Lastly, thanks to the many friends and family who gave their love and support throughout my stay at New Mexico Tech.

TABLE OF CONTENTS

	<u>pages</u>
<u>CHAPTER 1 - INTRODUCTION</u>	1
1.1 Background.....	3
1.2 Purpose and Scope.....	7
1.3 Organization.....	8
<u>CHAPTER 2 - OPERATOR ERRORS AND GAS PERMEABILITY MEASUREMENTS</u>	9
2.1 Background.....	9
2.2 LSAMP and LSAMP II Operation.....	10
2.2.1 LSAMP.....	11
2.2.2 LSAMP II.....	12
2.3 Questions and Hypotheses.....	13
2.4 Methods.....	14
2.4.1 Repeat Type.....	15
2.4.2 Application Type.....	16
2.4.3 Sample Type.....	17
2.4.4 Sampling Scheme.....	18
2.4.5 Data Analysis.....	18
2.4.6 Instrument Error.....	19
2.5 Results and Discussion.....	19
2.5.1 ANOVA Results.....	20
2.5.2 Instrument Effect on Measurement Variance.....	23
2.5.3 Measurement Averaging.....	26
2.5.4 LSAMP vs. LSAMP II.....	26
2.6 Conclusions.....	28
<u>CHAPTER 3 - MODIFICATION OF SYRINGE-BASED PERMEAMETERS FOR INCREASED MEASUREMENT RANGE</u>	31
3.1 Background.....	31
3.2 Controls on Measurement Duration.....	32
3.2.1 Increasing Gas Injection Pressure.....	35
3.2.2 Changing the Sample Volume.....	39
3.3 Results.....	40
3.3.1 Effect of Sample Volume.....	40

	<u>pages</u>
3.3.2 Effect of Injection Pressure	41
3.4 Conclusions.....	47
<u>CHAPTER 4 - DESIGN AND TESTING OF A PORTABLE PRESSURE DECAY</u>	
<u>GAS PERMEAMETER.....</u>	<u>50</u>
4.1 Background.....	50
4.2 Questions and Issues.....	52
4.3 Scope.....	54
4.4 Mathematical Model.....	55
4.5 Methods.....	59
4.5.1 Permeameter Fabrication.....	60
4.5.2 Testing Materials.....	62
4.5.3 Pressure Decay Measurement Procedure.....	63
4.5.4 Steady-Flow Methods.....	64
4.6 Results and Discussion.....	65
4.6.1 Pressure Anomalies.....	69
4.6.2 Derivative Plots.....	76
4.6.3 Nonlinear Flow.....	81
4.6.4 Comparison of Pressure Decay and Steady-Flow Methods.....	85
4.6.5 Instrument Range.....	90
4.7 Conclusions.....	93
4.7.1 Model Validation.....	93
4.7.2 Recommendations for Future Work.....	96
<u>CHAPTER 5 - CONCLUSIONS.....</u>	<u>98</u>
5.1 Gas Permeameter Operation.....	98
5.2 LSAMP II Modification.....	100
5.3 Pressure Decay Permeameter.....	101
REFERENCES.....	103
APPENDIX 1: POREX [®] Porous Plastic Standards.....	106
APPENDIX 2: LSAMP II Modification, Pressure vs. Time Plots.....	109
APPENDIX 3: Pressure Decay Permeameter Model Sensitivity to Atmospheric Pressure.....	112
APPENDIX 4: Pressure Decay Permeameter Plots (Small Reservoir).....	115

LIST OF FIGURES

	<u>pages</u>
Figure 1.1	Schematic diagram of gas permeameter flow field.5
Figure 1.2	Geometric factor for infinite half-space as a function of tip seal ratio. After Kerr and Wilson [personal communication].5
Figure 1.3	Schematic diagram of a syringe-based permeameter.7
Figure 2.1	Photos showing improvements incorporated into the LSAMP II design. (A) Addition of valve and air pump automatically refills the syringe with air between measurements. (B) A third photo sensor was added to stop the refill and reset the timer: (1) shuts off air pump and resets the timer, (2) starts timer and (3) stops timer. (C) Pistol grip-mounted tip seal with close up of force gauge.13
Figure 2.2	Application types used in repeatability study. (A) The pistol grip-mounted tip seal with a force gauge, (B) a hand held tip seal with a board, and (C) a hand held tip seal with no board.17
Figure 2.3	Instrument variability as a function of syringe fall time.23
Figure 3.1	Pressure ratio (3.3) as a function of injection pressure.34
Figure 3.2	A) Weight holder, arrow points to the blind hole fit for the piston. B) Holder and weights connected to the permeameter. C) Shows permeameter fit with bag for field use.38
Figure 3.3	Pressure vs. time plots for measurements on std. 1 with (A) no added weight, (B) 1 lb added weight, and (C) 2.5 lb added weight. The legend indicates the trial number. Similar plots for other standard lengths are located in Appendix 2.42
Figure 3.4	Permeability of 20-micron standard as a function of length (combination of lengths) of standard used for measurement.44
Figure 3.5	Ratio of standard length to permeability as a function of standard length.47
Figure 4.1	Schematic diagram of prototype pressure decay permeameter. (1) tip seal; (2) ¼ inch lab cock ball valve; (3) PVC end caps; (4) PVC threaded nipple; (5) quick disconnect couplings.61

Figure 4.2 Typical plot showing the rate of pressure decay in the source tank. Measurement made on the Berea Sandstone with the small tank with an initial (gauge) pressure of 30 kPa.65

Figure 4.3 Diagnostic dimensionless time vs. transformed pressure plot. (A) The model-predicted linear plot (Berea, small tank, $p_i = 30$ kPa gauge). (B) An actual plot from recorded pressure-time data showing a steeper slope in the early time data (Berea, small tank, $p_i = 30$ kPa gauge). (C) An actual plot from recorded pressure-time data showing an increasing slope after the early time data (Massillon, small tank, $p_i = 20$ kPa gauge).68

Figure 4.4 Diagnostic plot with corresponding tank temperature. The time at which the 0.5 °C drop in temperature occurs corresponds to the valve opening.70

Figure 4.5 Pressure drop due to pressurization of the valve/tip seal volume at the onset of a measurement for reservoir with and without a heat capacitor. The 0.25 second offset in the data is for visual purposes.72

Figure 4.6 Diagnostic plots for: (A) Berea Sandstone, (B) Massillon Sandstone, and (C) Standard 3. Experiments were performed at four initial pressures for each material: 10, 15, 20, 30 kPa gauge pressure.73

Figure 4.7 Transformed pressure derivative vs. time plots for (A) Berea Sandstone, (B) Massillon Sandstone, and (C) Standard 3. The derivative axis is stretched to accentuate differences between data collected at different initial pressures. Large in title refers to the tank used.78

Figure 4.8 Transformed pressure derivative vs. pressure plots for (A) Berea Sandstone, (B) Massillon Sandstone, and (C) Standard 3. The derivative axis is stretched to accentuate differences between data collected at different initial pressures. Large in title refers to the tank used.79

Figure 4.9 Transformed pressure derivative vs. pressure for all samples. The initial tank pressure was 30 kPa for all samples.81

Figure 4.10 Evaluation of possible non-Darcian behavior for: (A) Berea Sandstone, (B) Massillon Sandstone, and (C) Standard 3.83

Figure 4.11 Estimated permeability dependence on injection pressure at the tip seal of a steady flow permeameter, where permeability is estimated using Darcy's Law, ignoring non-linear effects.86

Figure A2.1 Pressure vs. time plots for all three weight classes on (A-C) Std. 2, (D-F) Std. 1 + 4, and (G-I) Std. 2 + 3 + 4.109

	<u>pages</u>
Figure A3.1	Pressure decay model sensitivity to atmospheric pressure. Sensitivity depends on whether pressure data is in (A) absolute or (B) differential pressure.114
Figure A4.1	Diagnostic plots for Berea Sandstone. Title refers to material, tank size, and initial tank gauge pressure.115
Figure A4.2	Diagnostic plots for Massillon Sandstone. Title refers to material, tank size, and initial tank gauge pressure.116
Figure A4.3	Diagnostic plots for Standard 3. Title refers to material, tank size, and initial tank gauge pressure.117
Figure A4.4	Transformed pressure derivative vs. time plots for (A) Berea Sandstone and (B) Massillon Sandstone. The derivative axis is stretched to accentuate differences between data collected at different initial pressures. Small in title refers to the tank used.118
Figure A4.5	Transformed pressure derivative vs. pressure plots for (A) Berea Sandstone and (B) Massillon Sandstone. The derivative axis is stretched to accentuate differences between data collected at different initial pressures. Small in title refers to the tank used.119

LIST OF TABLES

	<u>pages</u>
Table 2.1	ANOVA tables for repeatability study organized by Sample type. (A) Berea Sandstone, (B) Massillon Sandstone, and (C) Popatosa Formation.21
Table 2.2	Percent of total measurement variability attributable to the operator and sample heterogeneity for the tested material.25
Table 3.1	Measurement duration as a function of added weight.43
Table 3.2	Comparison of weighted permeability estimates (m^2) with those obtained using the un-weighted instrument.45
Table 4.1	Comparison of pressure decay permeability estimates (m^2) with two steady-state methods: syringe-based (LSAMP) and continuous flow (CFP) permeameters.88
Table A1.1	Average and standard deviation in permeability by Porex plastic pore size.107
Table A1.2	Measured length of permeability standards used to test weighted LSAMP. Statistics for each length are based on five LSAMP II measurements.108

CHAPTER 1

INTRODUCTION

One of the major problems facing scientists and engineers interested in fluid flow and transport phenomena in porous media is the spatial distribution of permeability. Gas permeameters are used in the field, as well as in the laboratory, to make dense samples of permeability on porous rocks and sediments. Estimates of permeability with gas permeameters are achieved by injecting gas, either at constant pressure (monitoring flow rate), or of a known initial pressure and volume (monitoring pressure decay), through a probe (or tip seal) into the material of interest. Historically, petroleum engineers and hydrogeologists have used steady-flow gas permeameters [Dykstra and Parsons, 1950; Eijpe and Weber, 1971; Goggin et al., 1988; Davis et al., 1994], and soil scientists have used transient pressure decay air permeameters [Kirkham, 1946; Smith et al., 1997]. Steady-flow field-portable gas permeameters, consisting of a compressed gas source and rotameters to measure flow rate, have long been used in the petroleum industry [Eijpe and Weber, 1971; Goggin et al., 1988] to estimate the permeability of petroleum bearing rock units. Use of a compressed gas source and multiple flow meters provides the necessary pressures/flow rates to measure permeability over a wide range. Well-lithified sedimentary rocks, of interest in the petroleum industry, are less susceptible to

deformation during air permeability measurements than are the friable sediments often encountered in hydrogeologic studies. Davis et al. [1994] developed a lightweight syringe-based air-minipermeameter (LSAMP) that operated under the same principles as steady-flow permeameters used in petroleum engineering, but allowed for non-destructive measurements on poorly-lithified sediments. Modifications were made to the LSAMP by Suboor and Wilson [personal communication] to enhance the permeameter's operational characteristics. Both the LSAMP and LSAMP II have been used in numerous outcrop studies [Davis et al., 1993; Davis, 1994; Ferris, 1995; Sigda, 1997; Taylor, 1997; Titzel, 1997; Hong, 1999; Sigda, 1999; Rawling et al., 2001]. The outcrops that are the focus of these studies often involve materials that span four to five orders of magnitude permeability. The practical range of syringe-based permeameters is limited to approximately two orders of magnitude because measurements take too long on lower permeability materials.

The limitations of the syringe-based devices prompted the search for a new field-portable method to rapidly measure permeability over a wider range. Jones [1992] addressed the problem of rapid permeability measurement over a wide range. He used a laboratory scale gas permeameter (PDPK-200) based on transient methods to measure materials spanning eight orders of magnitude permeability, with no measurement longer than 35 seconds. The PDPK-200 achieved this wide range (and corresponding short measurement duration) by incorporating multiple reservoir volumes into its design. The volume of the gas used controls the rate of pressure decay in the reservoir (for a given permeability), and therefore the measurement duration. The impressive performance of Jones' permeameter prompted investigation into transient methods for a field portable

device, and resulted in the design of a new pressure decay permeameter.

1.1 Background

Gas permeameters provide a relatively inexpensive method for estimating permeability both in the laboratory and in the field. Steady-flow gas permeameters have been employed in a wide range of studies; permeability measurement of drill-core plugs [Goggin et al., 1988], mapping the spatial distribution of permeability [Chandler et al., 1989; Davis et al., 1993], and recently to address the issue of permeability upscaling [Tidwell and Wilson, 1997]. Permeability estimates from steady-flow gas permeameters are achieved by injecting a gas at a constant pressure into one end of a sample material (with a known pressure, usually atmospheric, maintained at the other end) and measuring the flow rate. If the flow rate is not too high and steady-flow has been achieved, Darcy's Law applies. Provided that the sample dimensions are known, permeability can be estimated from the mathematical model

$$k = \frac{L}{A} \frac{2Qp_1\mu(T)}{[p_1^2 - p_0^2]}, \quad (1.1)$$

where k is permeability, L is the sample length, A is the cross-sectional area of the sample, Q is the measured gas flow rate, μ is the gas viscosity as a function of temperature, p_1 is the gas inlet pressure, and p_0 is the gas outlet pressure (usually atmospheric pressure). The volumetric moisture content of the material also must be taken into account. If the water content is too high ($> 5\%$), the calculated values of permeability will be underestimated (see Taylor, 1997, for complete discussion of moisture contents effect on air permeability). The above expression is limited in that it can only be used to describe flow through a sample with regular dimensions.

Gas permeameters have long been used to make measurements on consolidated and unconsolidated sediment outcrops. A new method (using a probe or tip seal) of injecting gas into the sample was developed to accommodate the non-uniform and laterally extensive geometry of outcrops. Tip seal designs have advanced through the years, but originally many consisted of tubing with a rubber ring or gasket at the end to make a seal on the material surface. Eijpe and Weber [1970] acknowledged that the measured permeabilities were an average value for the rock surrounding the tip seal. Since the dimension of the sample was unknown, permeability estimates were acquired through calibration of gas permeability against more conventional permeability measurement techniques. Searching for a more rigorous treatment of gas permeability estimation, Goggin et al. [1988] modeled the gas flow field in the vicinity of the tip seal. They found that the volume of material sampled could be described by a geometrical factor, G_o , which varies with the ratio of outer to inner tip seal radii and the sample dimensions. A schematic diagram of the gas permeameter flow field is shown in **Figure 1.1**. Analytical solutions for the geometric factor have since been developed [Tartakovsky et al., 2000; Kerr and Wilson, personal communication]. **Figure 1.2** shows the geometric factor as a function of tip seal ratio for a material represented by an infinite half-space. Inserting the geometric factor into Darcy's Law yields an expression for divergent gas flow from a tip seal

$$k = \frac{2Qp_1\mu(T)}{r_i G_o \left(\frac{r_o}{r_i}\right) [p_1^2 - p_0^2]}, \quad (1.2)$$

where r_i is the inner tip seal radius, r_o is the outer tip seal radius, and $G_o \left(\frac{r_o}{r_i}\right)$ is the geometric factor.

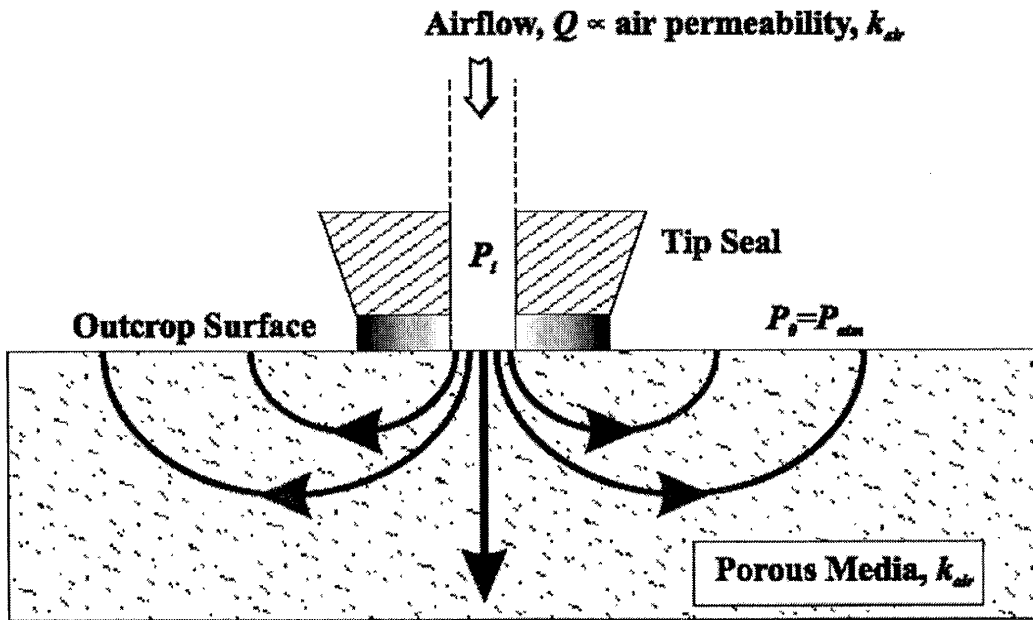


Figure 1.1. Schematic diagram of gas permeameter flow field.

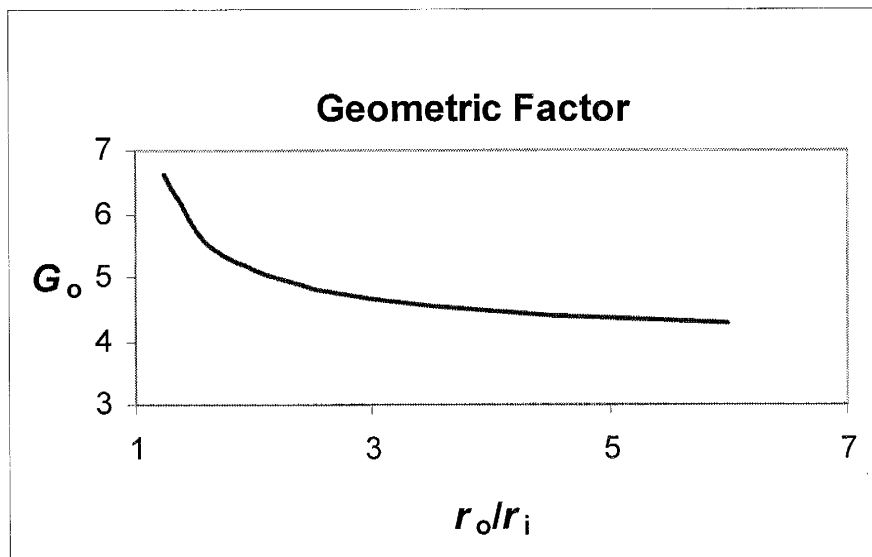


Figure 1.2. Geometric factor for infinite half-space as a function of tip seal ratio. After Kerr and Wilson [personal communication].

Historically steady-flow gas permeameters used in the field have consisted of a pressure source (typically a scuba-sized compressed gas tank) and a series of rotameters or mass flow meters to measure the gas flow rate. This permeameter design works well for consolidated sedimentary rocks, but is not optimized for use on unconsolidated sediments. Measuring permeability on friable sediments requires the use of low-pressure devices to ensure no grain rearrangement during the measurement. To address this situation, Davis et al. [1994] designed a gas permeameter that consisted of a low pressure source, but that was both lightweight and highly portable for use in the field. As part of his PhD thesis, Davis developed a lightweight syringe-based air minipermeameter (LSAMP) specifically for measuring permeability on unconsolidated sediments of the Rio Grande Rift Basin. A schematic diagram of the LSAMP is shown in **Figure 1.3**. The LSAMP uses a glass syringe as the pressure source to be applied to the material. The basic design is described in Davis et al. [1994]. The LSAMP proved to be an effective means for measuring permeability on friable sands, but there were a few key design limitations: (1) the tip seal had to be removed from the material surface between measurements for the syringe to be refilled with air, (2) there was no means for monitoring the force with which the tip seal was pressed on the outcrop, and (3) measurement of less-permeable materials required a long time for the piston to drop between the photo sensors (**Figure 1.3**). The force used in tip seal application determines the quality of the seal made at the material surface, and therefore the accuracy of the permeability estimate. Suboor and Wilson [personal communication] modified Davis's LSAMP (LSAMP II, explained in Chapter 2) to address limitations 1 and 2 outlined above, but the required time to make a measurement (3) remained essentially unchanged.

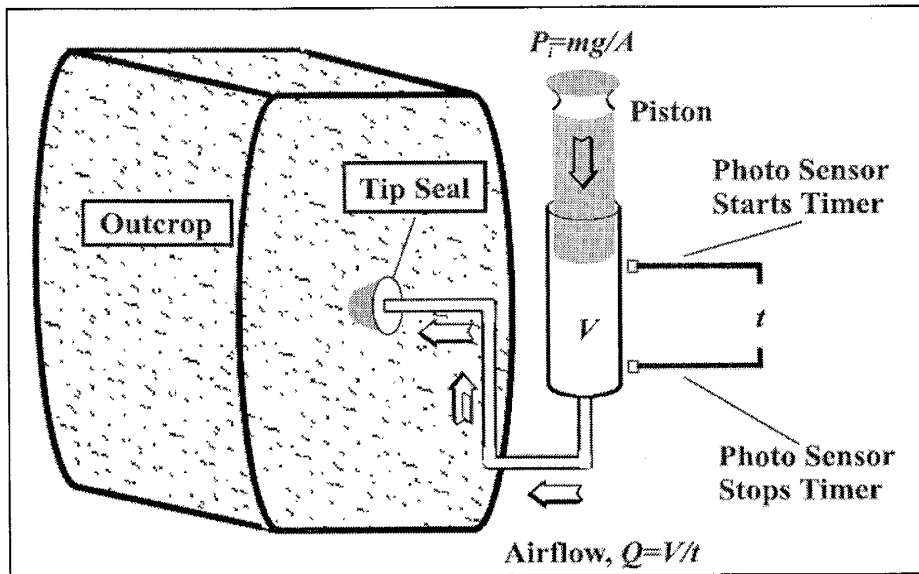


Figure 1.3. Schematic diagram of a syringe-based permeameter.

1.2 Purpose and Scope

The general goal of this research is to develop and improve instrument and operational characteristics of field portable gas permeameters for the spatial characterization of permeability across a wide range of geologic materials. Focuses include the operation and modification of an existing permeameter design and development of a new method to improve permeability estimation in the field, with emphasis on making fast measurements over a wide permeability range.

This research has three specific objectives:

- (1) Investigate the LSAMP II modifications, developed by Suboor and Wilson, as they apply to air permeameter operation. Specifically, do the modifications

- increase measurement repeatability, decrease operator introduced bias, and improve the overall quality of the data collected?
- (2) Modify the existing design of LSAMP II to allow for permeability estimation across a greater range of permeabilities.
 - (3) Develop and test a new field-portable pressure decay instrument capable of rapidly measuring a wider range of permeability than is permitted by syringe-based permeameters.

The scope of this research covers the design characteristics and operation of air permeameters for use in the field. The findings apply to the many branches of science and engineering in which the rapid collection of permeability data in the field is desirable. The results of Chapter 2 apply specifically to air permeameters which incorporate the use of a hand held tip seal. The results of Chapter 3 apply only to syringe-based permeameters.

1.3 Organization

Chapters 2-4 cover different research projects corresponding respectively to the above objectives, and all of which focus on a different aspect of air permeameters. Each chapter is written such that it can be presented in and of itself. Chapter 2 involves the analysis of design improvements made on the LSAMP (LSAMP II), and a discussion of the operational characteristics of gas permeameters. Chapter 3 discusses the operation performance of a modified LSAMP II device. In Chapter 4 we present the design, testing, and analysis of a new pressure decay permeameter.

CHAPTER 2

OPERATOR ERRORS AND GAS PERMEABILITY

MEASUREMENTS

2.1 Background

In order to make progress in any scientific or engineering related field, methods for collecting data must continually be reevaluated, modified, and improved. Methods and the accompanying instrumentation for the estimation of permeability have become better understood and more sophisticated over the past 50 years. When evaluating a data collection method it is important to define the potential sources of uncertainty. Considering permeability estimation in the field, there are three sources of variability in a measurement: (1) the instrument, (2) the operator, and (3) the material for which permeability is being estimated. The variability due to the porous material is the result of complicated depositional and diagenetic processes, and it is usually this variability that we wish to characterize. Measurement variability resulting from the instrument and operator can often be separated, and measures can be made to reduce these errors, but it is difficult to desegregate the variability induced by the operator and the natural variability of the porous media.

Instrument error associated with gas permeameters consists of fluctuations in precision of one or more of the components of the measurement system. For compressed gas permeameters, the pressure transducers (monitoring pressure at the tip seal) and rotameters (measuring flow rate) are common sources of instrument error. Imperfections in the syringe and fluctuations in the timing system (combination of photo sensors and stopwatch) contribute the most to instrument error for syringe-based permeameters. To average out the effect of instrument noise, it is common practice when using syringe-based permeameters to make multiple measurements at a point.

Operator errors for gas permeameters, used to estimate permeability on outcrops, are for the most part a function of the process of tip seal positioning on the material surface. Two factors must be considered when placing the tip seal on the material of interest: (1) the force with which the tip seal is held to the surface and (2) the degree to which the tip seal is oriented normal to the surface. These factors control the quality of the seal at the material/tip seal interface, which has a direct effect on the reliability of the estimated permeability. Tidwell and Wilson [1997] observed an exponential decrease in permeability with increasing tip seal compression stress (force per unit area) for a lithified sandstone. The use of insufficient force when applying the tip seal to the surface allows for gas that would otherwise be forced through the material to leak out at the material/seal interface, and permeability to be overestimated. Deviations from normality to the material surface result in similarly biased permeability estimates.

2.2 LSAMP and LSAMP II Operation

Modifications were made to the LSAMP (LSAMP II) to address the issues of instrument and operator errors. The LSAMP and LSAMP II operate under the same

conditions and the schematic diagram of a syringe-based permeameter (**Figure 1.3**) applies to both permeameters. Calculation of permeability for both devices is governed by Equation (1.2), where all terms are known except the gas pressure at the tip seal, p_1 , and the volumetric flow rate, Q . The flow rate is calculated by measuring the time to displace a known volume of air and the pressure at the tip seal is obtained through calibration (although it can be directly monitored using a pressure transducer). The following summarizes the differences in design and operation of the LSAMP and operation of the LSAMP II.

2.2.1 LSAMP

The LSAMP consists of a box housing the syringe and circuitry with a length of tubing and inline air filter connecting the syringe to the tip seal. The LSAMP's tip seal is composed of a rubber stopper with a foam-rubber pad fixed to the narrow end. A brass grommet is placed in the inner orifice to keep the inner tip seal radius relatively constant. See Davis et al. [1994] for a full description of the LSAMP design. To make a measurement with the LSAMP, the piston is manually pulled above the upper set of photo sensors. This draws ambient air in through the tip seal orifice, tubing, and filter, to fill the syringe casing. The tip seal is then pressed, by hand, on the rock or sediment surface and the piston is released. As the piston passes the upper set of photo sensors a stopwatch begins to record the time for the piston to displace a known volume of air (the volume between the two sets of photo sensors). The time of measurement is then recorded, the timer is manually reset to zero, and another measurement may be made. In order to make another measurement, the tip seal must be removed from the material surface to allow air to be brought in through the tip seal orifice, refilling the syringe.

Therefore, when attempting to average permeability measurements at a point, the volume of rock sampled changes with each measurement due to movement of the tip seal.

2.2.2 LSAMP II

The LSAMP II was designed by Suboor and Wilson [personal communication] to improve the basic design of Davis et al. [1994]. The modifications include (see **Figure 2.1**): (1) addition of a 3-way solenoid valve and a micro-air pump to automatically refill the syringe after each measurement, (2) a third set of photo sensors to automatically stop the refill and reset the timer between measurements, (3) a pistol grip-mounted tip seal with a force gauge, and (4) a silicone tip seal with inner and outer guide rings after that described in Tidwell and Wilson [1997]. To make a measurement with the LSAMP II, the pistol grip-mounted tip seal is compressed on the material surface (monitoring application force on the force gauge), and the trigger is pulled or button pushed activating the air pump to fill the syringe. After the piston has reached the upper most set of photo sensors the timer is reset, the air pump is shut off, the 3-way valve closes the line to the air pump and opens the line to the tip seal, and the piston begins to fall. When the piston reaches the middle set of photo sensors, the stopwatch begins to record the time to displace a known volume of air. The measurement is complete (timer is stopped) when the piston has reached the lower set of photo sensors. With the addition of the air pump and 3-way valve multiple measurements can now be made without removing the tip seal, and the same volume of rock is interrogated with each measurement.

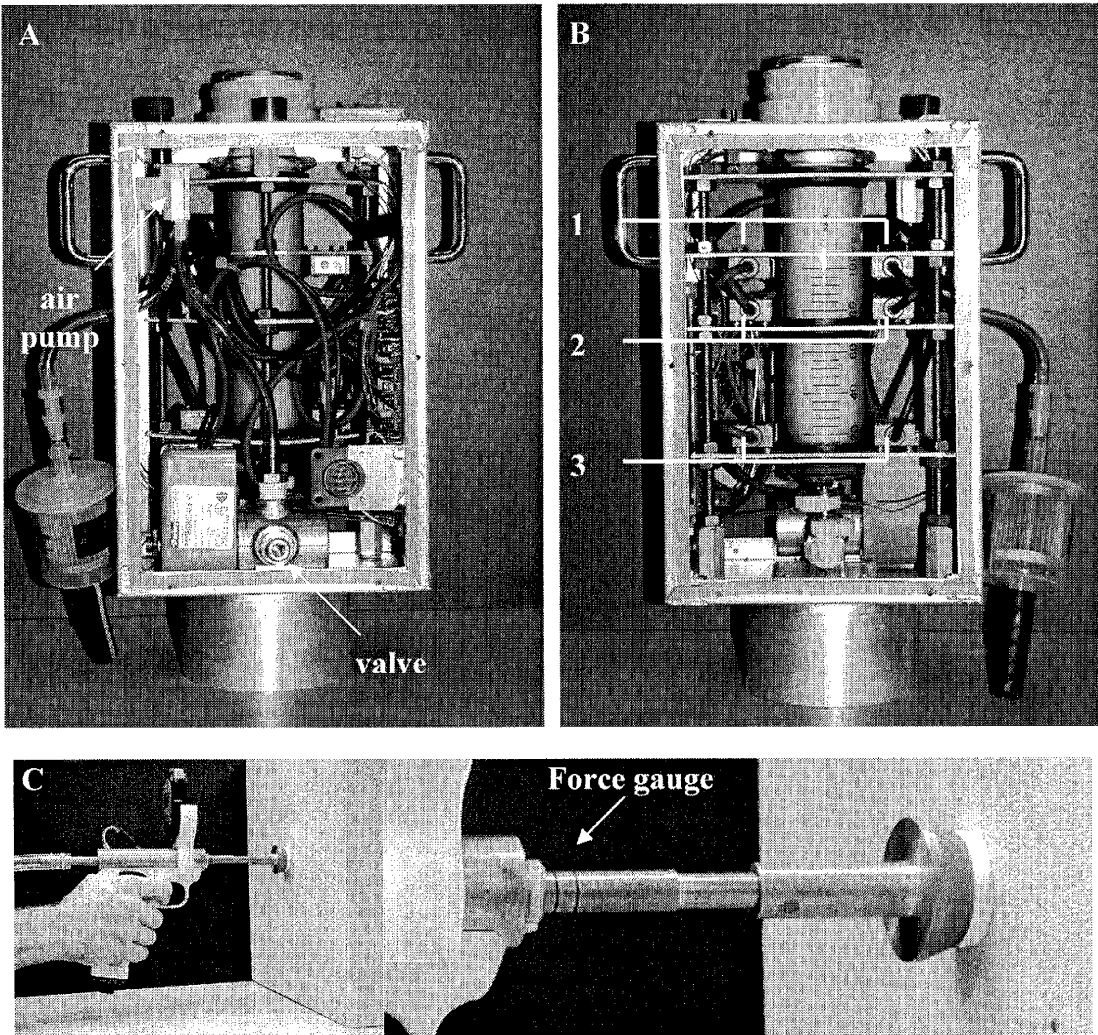


Figure 2.1. Photos showing improvements incorporated into the LSAMP II design. (A) Addition of valve and air pump automatically refills the syringe with air between measurements. (B) A third photo sensor was added to stop the refill and reset the timer: (1) shuts off air pump and resets timer, (2) starts timer and (3) stops timer. (C) Pistol grip-mounted tip seal with close up of force gauge.

2.3 Questions and Hypotheses

The LSAMP II was designed to improve the operational characteristics of syringe-based permeameters, specifically the LSAMP. The major modifications made in the construction of the LSAMP II are described in the previous section. To test whether

or not the above modifications significantly improved the performance of the LSAMP, we posed the following hypotheses:

- (1) Making repeated measurements at a point decreases measurement variability due to instrument noise.
- (2) Removing the tip seal while repeating measurements at a point causes an increase in measurement variance.
- (3) Using consistent application force decreases measurement variability.

2.4 Methods

To test the above hypotheses, each related modification (LSAMP II) had to be isolated and compared with the corresponding operational characteristic of the LSAMP. Differences in the LSAMP and LSAMP II that were not investigated in this study were the effects of: (1) manually filling the syringe between measurements, (2) the use of different tip seal designs, and (3) the inline air filter of the LSAMP. To negate the influence of these design differences, the LSAMP II was used to make all measurements. Using the LSAMP II with a hand held tip seal that was removed between measurements mimicked the relevant operational characteristics of the LSAMP. Suites of measurements were made in an attempt to quantify the differences in the operation of the LSAMP and the LSAMP II. Three variables were considered for any given measurement, including (1) the method of repeating measurements (Repeat type), (2) the method for holding the tip seal to the material surface (Application type), and (3) the sample material used (Sample type).

2.4.1 Repeat Type

It is common practice when collecting air permeability samples with syringe-based permeameters to make repeated measurements at a given point. Repeated measurements are made to average out the effects of operator and instrument error. When operating the LSAMP, the tip seal must be removed after each measurement to fill the syringe with air. Removing the tip seal, while using the other hand to pull up the piston (filling the syringe with air), makes it very difficult for the operator to replace the tip seal exactly where the prior measurement was made. Addition of the 3-way valve and air pump in the design of the LSAMP II made it possible to make repeated measurements at a point without lifting the tip seal from the material surface between measurements. The method of repeating measurements (Repeat type) was varied to test the significance of the 3-way valve and air pump additions with respect to measurement repeatability at a point. Three different Repeat types were used; (RT1) no tip seal removal between measurements, (RT2) removal of the tip seal after each measurement with immediate replacement, and (RT3) removal of the tip seal between each measurement with some distraction before replacing it. RT1 pertains directly to the operation of the LSAMP II and the addition of the 3-way valve and air pump. RT2 and RT3 involve removing the tip seal from the material surface between each measurement and were both designed to mimic the operation of the LSAMP. Making repeated measurements at a point with the LSAMP can be a complicated process due to the preparations that must be made between measurements. Skilled operators can become very good at performing the necessary tasks between measurements without losing sight of the location of the prior measurement. RT2 was designed to impersonate a skilled operator on the LSAMP, while

RT3 was designed to imitate an LSAMP operator unfamiliar with the instrument. To achieve consistency, and distinction between RT2 and RT3, the following routine was invoked. When using RT2, after a measurement the tip seal was lifted from the surface and replaced all in one motion, attempting to replace the tip seal in its prior location. The protocol for RT3 was to remove the tip seal, hand record the piston fall-time (the actual measured quantity), and then replace the tip seal to its previous location.

2.4.2 Application Type

When making gas permeability measurements, a major contribution to operator error is the way in which the tip seal is applied to the rock or sediment surface. A quality seal must be provided at the rock/seal interface so that a steady-state flow field can be achieved in the porous medium. Two factors control the quality of the seal: the force with which the seal is applied and degree to which the seal is held normal to the material surface. To examine the effect of tip seal application on measurement variability, three different Application types were used (**Figure 2.2**): (AT1) the pistol grip-mounted tip seal with a force gauge, (AT2) a hand held tip seal with a board, and (AT3) a hand held tip seal with no board. AT1 is the method of tip seal application designed for use with the LSAMP II, which allows the operator to monitor application force. The LSAMP was traditionally operated using a hand held tip seal with no board (AT3). Hand held tip seals are often equipped with a small board near the tip seal to provide balance and comfort for the operator when making many measurements, and thus AT2 was also included as an Application type.

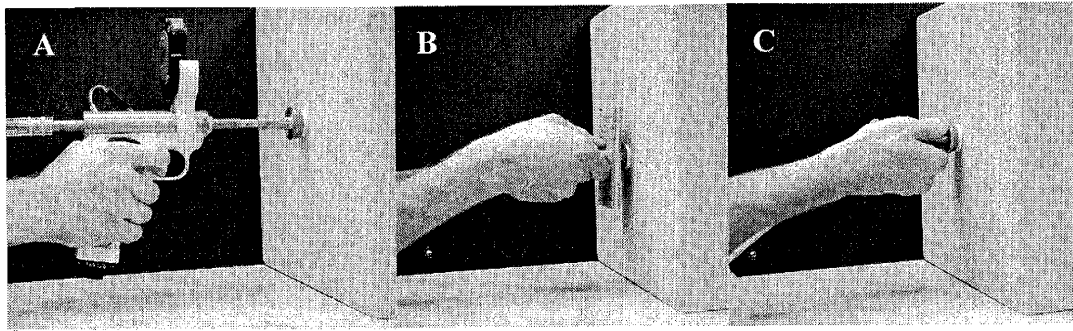


Figure 2.2. Application types used in repeatability study. (A) The pistol grip-mounted tip seal with a force gauge, (B) a hand held tip seal with a board, and (C) a hand held tip seal with no board.

2.4.3 Sample Type

The tests were performed on three different porous media types (Sample type). The materials were selected to represent varying degrees of heterogeneity and span the range of permeability capable of being measured with syringe-based permeameters. Sample type 1 (ST1) was a block of Berea Sandstone. The Mississippian age Berea Sandstone is a very clean (~ 90 % silica) medium grained sandstone. Berea Sandstone was chosen because of its wide use in laboratory applications and extremely low degree of heterogeneity. Sample type 2 (ST2) was a slab of Massillon Sandstone. The Pennsylvanian aged Massillon Sandstone, in contrast to Berea Sandstone, is cross-stratified sandstone exhibiting small-scale heterogeneity. All measurements on the Berea Sandstone and Massillon Sandstone were made under laboratory conditions. The third Sample type (ST3) was an outcrop of Rio Grande Rift sediments located at the Canyon Trail Site of the Bosque Del Apache, San Antonio, New Mexico. All measurements on ST3 were made in the field. Herrin [2001] identified this outcrop as the Popatosa Member (Miocene in age) of the Santa Fe Group and interpreted it to be of eolian origin

based on its depositional structure. The Canyon Trail Site was chosen because it has been the focus of numerous studies involving deformation bands [Hong 1999; Herrin, 2001; Sigda and Wilson, 2002] in which permeability measurements were made.

2.4.4 Sampling Scheme

Suites of data were collected using every combination of the three measurement variables (Repeat type, Application type, and Sample type) for a total of nine different types of measurements. For each of the nine permutations, data were collected in sets of three measurements at a point. In other words, for a given combination of the three variables, three measurements were made (or were attempted to be made) at one point on the rock, the tip seal was moved to a new location (on the same material), and three more measurements were made at that point. This process was repeated until there were at least ten sets of three point measurements for each of the nine possible combinations of variables.

2.4.5 Data Analysis

Ten sets of three measurements (at a point) were collected for all combinations of Repeat, Application, and Sample types. We were interested in the amount of variation within the set of three measurements as a function of Repeat type and Application type. The average, variance, and coefficient of variation were calculated for each set (3 data points) for initial comparison. To test the presence of significant differences in set variance, MINITAB (release 12.22) was used to perform a Two-way Analysis of Variance (Two-way ANOVA) on the set variances. Syringe piston fall-time was the response variable used for the ANOVA. The calculated permeability for LSAMP-type

devices depends inversely on piston fall-time (for a given instrument calibration), and because of this, variability in fall-time is inversely proportional to variability in permeability. The balanced Two-way ANOVA was used to discern differences in set variance due to Application type, Repeat type, and any interaction between the two variables.

2.4.6 Instrument Error

The sampling scheme described above was intended to isolate different types of operator error to test the significance of improvements incorporated in the design of the LSAMP II. The instrument used to collect the data (LSAMP II) contributed some amount of variability to the data (due to imperfections in the timing device and syringe) and therefore a technique was needed to quantify instrument error. Isolation of the variability attributable to the instrument required that measurements be simulated with no operator or sample. To accomplish this, a needle valve was attached to the LSAMP II outlet to provide a constant resistance. Series of pseudo-measurements were made at various valve settings ranging from completely open to nearly closed. Summary statistics, including variance and coefficient of variation, were then calculated for the each of the data series. The range of valve settings provided a wide range of resistance to flow and also helped examine the possibility of time dependent instrument error (due to frictional heating of the instrument).

2.5 Results and Discussion

Over 1,000 permeability measurements were made to help distinguish the effects of tip seal application (Application type) and tip seal removal (Repeat type) on

measurement variance at a point. Results of the Two-way ANOVA suggest that no one of the three different methods for applying the tip seal (pistol grip-mounted, or hand-held with and without a board) is better for reducing measurement variability than the others. On the other hand, of the three ways measurements were repeated at a point (no tip seal removal, removal with immediate replacement, and removal with distraction before replacement), not removing the tip seal significantly reduced measurement variability for all Sample and Application types. The contribution of instrument error to the total variability when making three measurements at a point was found to be minor (less than 2% of total variability) for all sample materials.

2.5.1 ANOVA Results

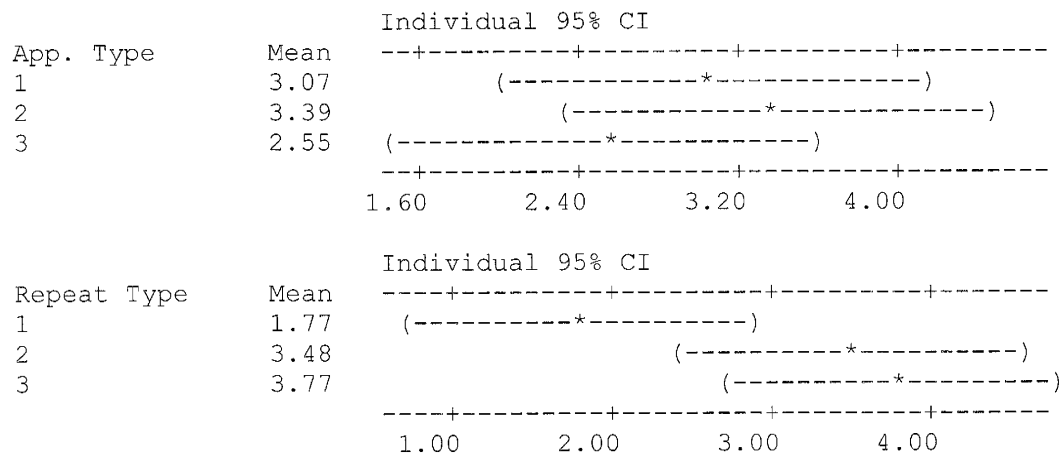
The null hypothesis for the Two-way ANOVA was that sample set variance is equal across all Application and Repeat types. **Table 2.1 A-C** summarizes the results of the ANOVA for each Sample type. The null hypothesis is evaluated using the F-statistic, which is given by the ratio of the mean squares (MS) for a given treatment (Application type, Repeat type, or Interaction) to the mean squares error (MSE). The null hypothesis is rejected if the F-value is greater than the critical F-value (F_{α}) at a prescribed confidence level ($1-\alpha$). The test can be significant at different confidence levels. The ANOVA tables (**Table 2.1**) give the alpha value (in the column labeled P) with which the null hypothesis can be rejected.

Results for the three treatments were consistent across all Sample types. Application type and Interaction (between Application and Repeat types) were found to cause insignificant variability in the data for all Sample types. The null hypothesis could not be rejected for Application type with confidence greater than 75 %, or for Interaction

with confidence greater than 54 % for any Sample type. Variability due to Repeat type was found to be much more significant. The null hypothesis could be rejected for Repeat type with the following confidence levels: 97.6 % for Berea Sandstone, 99.8 % for Massillon Sandstone, and 93.9 % for the Popatosa Formation.

Table 2.1A. Two-way ANOVA table for Berea Sandstone sample. See key for abbreviations and units.

Source	DF	SS	MS	F	P
Application Type	2	10.60	5.30	0.60	0.553
Repeat Type	2	69.72	34.86	3.92	0.024
Interaction	4	18.64	4.66	0.52	0.718
Error	81	719.68	8.88		
Total	89	818.64			



KEY

DF, Degrees of Freedom [-]

MS, Mean Squares [s^2]

P, P value for F-test [-]

SS, Sum of Squares [s^2]

F, F ratio [-]

CI, Confidence interval [-]

Table 2.1B. Two-way ANOVA table for Massillon Sandstone sample. See Table 2.1A for key of abbreviations and units.

Source	DF	SS	MS	F	P
Application Type	2	11.04	5.52	1.43	0.245
Repeat Type	2	52.23	26.12	6.77	0.002
Interaction	4	14.09	3.52	0.91	0.461
Error	81	312.48	3.86		
Total	89	389.84			

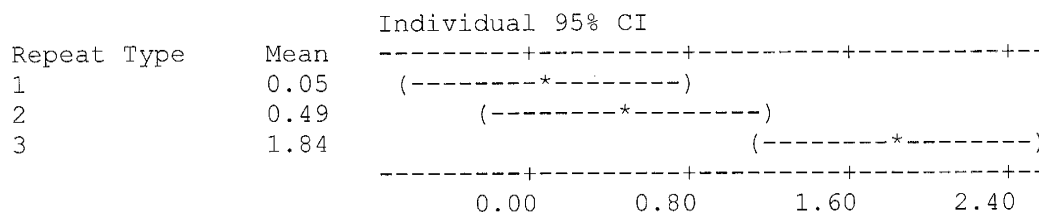
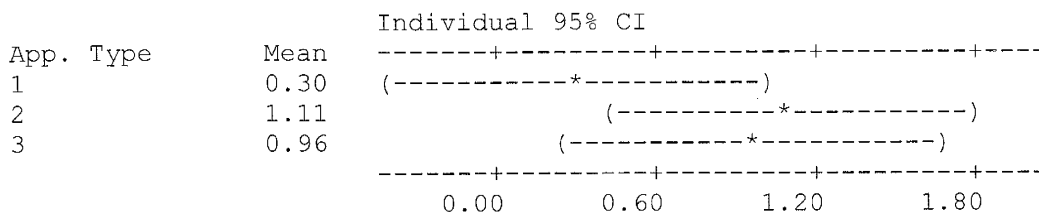
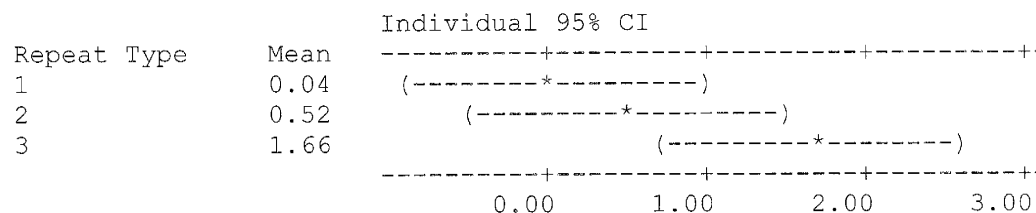
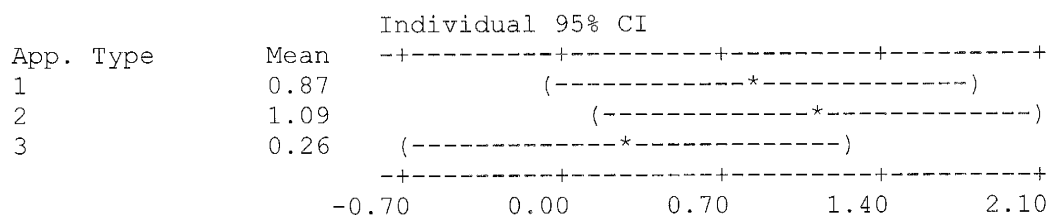


Table 2.1C. Two-way ANOVA table for Popatosa Formation sample. See Table 2.1A for key of abbreviations and units.

Source	DF	SS	MS	F	P
Application Type	2	11.21	5.61	0.78	0.463
Repeat Type	2	41.68	20.84	2.89	0.061
Interaction	4	13.07	3.27	0.45	0.770
Error	81	584.31	7.21		
Total	89	650.28			



As previously stated, the Massillon Sandstone was the most heterogeneous sample used. This fact is supported by the high confidence level with which the null hypothesis for Repeat type can be rejected. As small-scale heterogeneity increases, measurement set variance will be more significant if the tip seal is removed between repeated measurements at a point.

2.5.2 Instrument Effect on Measurement Variance

Measurements were simulated for a range of resistances by placing a valve on the downstream port of the permeameter. The valve provided a constant resistance and could be adjusted to produce syringe fall times comparable to those produced by the three Sample types. The amount of instrument error varies as a function of the syringe fall time. **Figure 2.3** shows the coefficient of variation in fall time exponentially decreasing from syringe freefall (no resistance, 0.4 s) to a fall time of 5 seconds. The coefficient of variation was used to compare the relative amount of instrument error for a range of fall times. For the materials investigated, instrument error appears to be constant for fall times greater than 5 seconds.

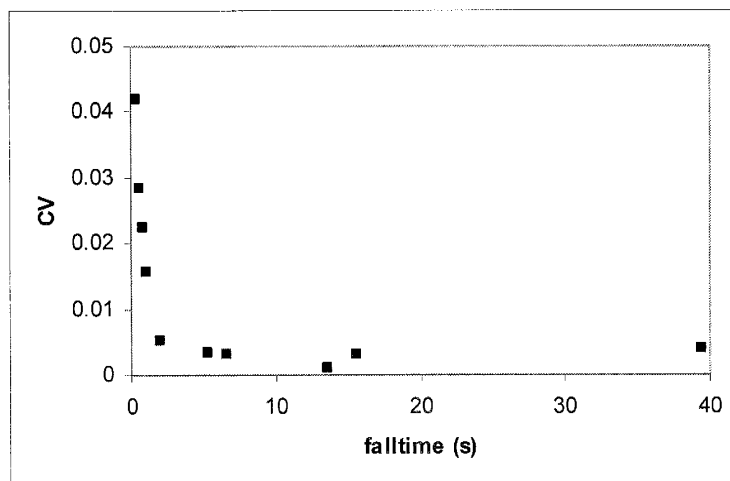


Figure 2.3. Instrument variability as a function of syringe fall time.

The average syringe fall time for each Sample type was: 40 s for Berea Sandstone, 7 s for Massillon Sandstone, and 6 s for the Popatosa Formation. All three Sample types fall within the region of constant coefficient of variation (**Figure 2.3**), and thus relative instrument error should be constant for all tests. For any given set of measurements at a point, the total measurement variability can be attributed to three components: (1) instrument variability, (2) sample heterogeneity, and (3) operator error. Assuming variances are additive and neglecting cross-correlation, the variation in syringe fall time attributable to each is given by:

$$\sigma^2_{total} = \sigma^2_{instrument} + \sigma^2_{sample} + \sigma^2_{operator} . \quad (2.1)$$

Instrument variability ($\sigma^2_{instrument}$) was quantified as outlined above. The sample heterogeneity and operator error were more difficult to quantify and for practical purposes were inseparable. For the following analysis sample variability and operator error were combined and referred to as measurement variability ($\sigma^2_{measurement}$). The average variance was calculated from each measurement set for each Sample type as a function of Repeat type. Variability due to Application type was not taken into consideration because the Two-way ANOVA indicated no significant difference in measurement set variance due to Application type. The total measurement variability and the instrument variability were used to calculate the percentage of variability attributable to the operator/sample:

$$\%_{measurement} = \left[\frac{\sigma^2_{measurement}}{\sigma^2_{total}} \right] * 100 = \left[\frac{\sigma^2_{total} - \sigma^2_{instrument}}{\sigma^2_{total}} \right] * 100 . \quad (2.2)$$

Table 2.2 shows percentage of total variability as a function of Sample type and Repeat type. The variability due to the operator/sample ranges from 98.3% - 100.0%. A higher percentage means instrument variability plays a minor role in total measurement variability. Lower values equate to more of the error due to the instrument. Because instrument variability is extremely small, this translates to a better method for repeating measurements at a point. For all Sample types, Repeat type 1 (no tip seal removal) shows the lowest and Repeat type 3 (removal of the tip seal with distraction before replacement) shows the highest percentage of error due to the operator/sample.

Table 2.2. Percent of total measurement variability attributable to the operator and sample heterogeneity for the tested material.

	Sample type	Repeat type		
		1	2	3
$\sigma_{\text{measurement}}$ (% of total)	Berea	98.7	99.3	99.4
	Massillon	98.3	99.9	100.0
	Popatosa	98.7	99.9	100.0

The contribution of instrument variability to the total variability of a measurement was very small (and relatively constant) for all Sample types tested. This result is consistent with the relationship shown in **Figure 2.3**, which shows the coefficient of variation to be nearly constant for materials producing fall times greater than 5 seconds. For fall times less than 5 seconds the coefficient of variation increases rapidly as fall time decreases. The values in **Table 2.2** would likely increase significantly as the high end of the instrument's measurement range was approached. This suggests making repeated measurements at a point (measurement averaging) to reduce instrument noise may not be necessary for lower permeability materials (high fall time), but as the instrument

approaches the high end of its measurement range (low fall time) repeating measurement could help reduce instrument noise.

2.5.3 Measurement Averaging

During this study the purpose of measurement averaging was questioned by many colleagues. Most frequently, people questioned whether or not the tip seal should be moved during measurement averaging. More specifically, it was argued that since the LSAMP II interrogates such a small volume of rock, moving the tip seal slightly between measurements would provide a better average of the local permeability. If the instrument used to acquire permeability estimates does not introduce much variability into the measurement, making repeated measurements to filter out instrument noise is unnecessary.

Moving the tip seal a small amount between measurements could aid in better characterization of small scale heterogeneity. Making many measurements at relatively (only small tip seal movement) the same location would better estimate the variogram nugget when mapping permeability heterogeneity. If the material's permeability is not at the high end of the LSAMP II's measurement range (see **Figure 2.3**) and the operator provides a good seal at the material surface, small movement of the tip seal could provide more useful permeability information than a precise point estimate.

2.5.4 LSAMP vs. LSAMP II

Other than the proven increase in measurement repeatability resulting from not lifting the tip seal between measurements, the LSAMP II also offers other design and operational improvements not formally tested here. The addition of the 3-way solenoid

valve and micro-air pump not only alleviate the need to remove the tip seal between measurements, but also remove the need for an inline air filter and eliminate the burden of manually filling the syringe. The use of a tip seal with inner and outer guide rings provides more constancy in the tip seal ratio (geometric factor).

The air filter on the LSAMP is located between the syringe outlet and the tip seal. Placing the filter inline presents a few problems relating to instrument range and precision. The filter introduces an additional head loss (increases resistance to flow) which decreases the high end of the measurement range. If the filter is not changed frequently the head loss will increase and the precision of the instrument will be jeopardized. The LSAMP II employs an air filter, but it is not placed inline with the measurement. The three way valve allows for air to be brought in through the filter to fill the syringe, and then forces the air out to the tip seal through a different port (bypassing the valve). Removal of the inline valve in the LSAMP II eliminates a possible source of instrument drift and increases precision in the high end of the measurement range.

The 3-way valve and air pump in the LSAMP II automatically fill the syringe with air between successive measurements. The effect of automatically filling the syringe as it applies to repeating measurements (removing the tip seal) was addressed, but the effect of manually filling the tip seal was not. The ANOVA results suggest removing the tip seal with a distraction (recording the syringe fall time) caused a significant increase in measurement variance at a point. When using the LSAMP, the distraction between successive measurements also includes resetting the clock and manually filling the syringe. If these other distractions were accounted for, the LSAMP II's relative performance would only increase when compared to the performance of the LSAMP.

The tip seal differences between the LSAMP and the LSAMP II also were not tested. The LSAMP's tip seal consists of soft foam-rubber pad fixed to the base of a rubber stopper with a brass grommet placed in the center of the foam pad to control the inner tip radius [Davis et al., 1994]. The LSAMP II's tip seal was modeled after that of Tidwell and Wilson [1997]. This tip seal has guide rings to control both the inner and outer tip seal radii. Though differences in these two tip seals should not affect measurement repeatability, there are implications regarding the precision and accuracy of permeability estimates. The outer to inner tip seal ratio determines the geometric factor that is used to calculate permeability. The use of guides for not only one (LSAMP), but both of the tip seal radii with the LSAMP II produces a more consistent tip seal ratio and therefore a more precise and accurate permeability estimate.

2.6 Conclusions

Suites of data were collected to assess improvements made to the original LSAMP device design of Davis et al. [1994]. The design of the LSAMP was altered to improve field productivity (make operation easier) and to increase the repeatability of measurements at a point. The major design improvements were: (1) the addition of a 3-way valve and air pump and (2) a pistol grip-mounted tip seal with a force gauge. The valve and air pump automatically fill the syringe with air between successive measurements. This allows multiple measurements to be made without moving the tip seal. The force gauge on the pistol grip-mounted tip seal helps the operator achieve consistency in the application force used during measurements. The objective was to compare the operational characteristics of the LSAMP and the LSAMP II as they apply to the repeatability of measurements at a point (measurement averaging).

Data were collected on three different materials (Sample type) using all combinations (nine total combinations) of three methods for holding the tip seal (Application type) and three ways for repeating measurements (Repeat type). The Application and Repeat types were designed to mimic operation of the LSAMP and LSAMP II. Sets of three measurements at a point were made at multiple locations on each sample for all nine types of measurements.

The variance within a set of three measurements was used as the response in a Two-way ANOVA. The ANOVA tests for any significant differences in variance due to Application type, Repeat type, or interaction between the Application and Repeat types. There are no significant differences in variance resulting from Application type or interaction between Application and Repeat types. However, the ANOVA reports measurement set variances to differ as a function of Repeat type with a confidence level of 94-99 % depending on Sample type.

Multiple pseudo-measurements (i.e. using a needle valve in lieu of porous medium) were made at a constant resistance to quantify instrument error. Measurements were made at various resistances to investigate the possibility of time dependent instrument error. The coefficient of variation in syringe fall time was chosen to represent the variability in a measurement because it is normalized by the mean. The coefficient of variation exponentially decreases from syringe freefall (no resistance, 0.4 s) to a fall time of 5 seconds. For fall times greater than 5 seconds instrument error is constant.

Instrument error plays only a minor role in the total variability within a set of measurements at a point. A majority of the variability within a measurement set is a

result of the small-scale heterogeneity of the material and the method used for repeating measurements. Successive measurements made without removing the tip seal produced the least variable measurements, while measurements for which the tip seal was removed (with some distraction) between measurements were the most variable. Since instrument error is minor for most permeability materials, there may be some benefit to moving the tip seal slightly between measurements. Small movement of the tip seal would result in a more local permeability average and could be useful in estimating the variogram nugget.

The results of the sampling study and Two-way ANOVA are indicative of the effect of design improvements on measurement repeatability (averaging values at a point), and other improvements that were not officially tested also improve the operational characteristics of the LSAMP II. The addition of the 3-way valve and air pump significantly decreases measurement variance at a point. With the addition of the valve and air pump many distracting tasks are removed for the operator. The operator no longer has to manually fill the syringe while pressing the tip seal to the surface. This allows the operator to focus attention on the tip seal, ensuring a good seal at the surface (no leakage). The use of the valve and air pump also allow for removal of the inline air filter. Removal of the air filter significantly reduces internal head loss and removes a potential source of instrument drift. The use of the pistol grip-mounted tip seal (with the force gauge), though more comfortable for the operator, does not significantly decrease measurement variability.

CHAPTER 3

MODIFICATION OF SYRINGE-BASED PERMEAMETERS FOR INCREASED MEASUREMENT RANGE

3.1 Background

The lightweight syringe-based air-minipermeameter (LSAMP), designed by Davis et al. [1994], and the LSAMP II designed by Suboor and Wilson [personal communication], were both manufactured to estimate permeability on high permeability poorly lithified sediments. The weight of the piston supplies moderately low and relatively constant pressures at the tip seal (see discussion of LSAMP, Ch. 2), which prevents grain deformation/rearrangement during the measurement. The use of a constant pressure source (the weight of the piston over the area of the syringe-casing) makes the volumetric flow rate, and therefore the measurement duration, a function of the volume of the material sampled and the material's permeability. Without modification, the practical measurement range of the LSAMP devices is limited to two orders of magnitude permeability. The upper limit of the practical range corresponds to flow rates just below those produced with no resistance at the tip seal. The lower limit can be extended by holding the tip seal on the material for a longer time. The practical lower

limit corresponds to the permeability for which measurements take an unreasonable amount of time (more than two minutes), resulting in operator fatigue and impatience. Poorly consolidated sand deposits fall within the measurement range of the LSAMP, but most outcrops of poorly consolidated sediments also contain fine-grained materials that are outside the range of the device. Some of the studies conducted by LSAMP users involve outcrops with a poorly consolidated sand matrix dissected by thin, nearly vertical low permeability bands (small displacement faults and clastic dikes). LSAMP measurements on the low permeability zones encountered in these studies fell far outside the practical lower limit of the measurement range. The time required to make a measurement on the low permeability material had to be decreased for the instrument to be effective in the field. A shorter measuring period could be achieved by using a compressed gas source, but the amount of equipment would triple, making the setup less portable in the field. To maintain a manageable amount of equipment in the field, modifying the existing LSAMP for increased measurement range became desirable.

3.2 Controls on Measurement Duration

The controls on measurement time for the LSAMP can be determined by examining Equation (1.2). For the LSAMP the flow rate, Q , is determined by measuring the length of time, t , required to displace a constant volume of gas, V , where $Q = V/t$. Using this relationship we can solve Equation (1.2) for time,

$$t = \frac{2Vp_1\mu(T)}{kr_iG_o\left(\frac{r_o}{r_i}\right)[p_1^2 - p_o^2]}, \quad (3.1)$$

where the gas viscosity, μ , atmospheric pressure, p_0 , and permeability, k , are constant for a given measurement, and the volume of gas displaced, V , is constant for a given permeameter. The gas injection pressure, p_1 , and the effective sample size defined by,

$$\frac{1}{r_i G_o}, \quad (3.2)$$

are the only two controls on measurement duration.

Increasing the pressure at the tip seal causes the ratio of the injection pressure to the difference of squared injection and atmospheric pressures,

$$\frac{p_1}{[p_1^2 - p_0^2]}, \quad (3.3)$$

to decrease, which in turn decreases the measurement duration for a given material (see **Figure 3.1**). The gas injection pressure is given by [Davis et al., 1994]:

$$p_1 = \frac{F}{A_p} - R_F = \frac{m_p g}{A_p} - R_F, \quad (3.4)$$

where F is the force exerted by the weight of the piston, m_p is the syringe piston mass, g is acceleration due to gravity, A_p is the cross-sectional area of the piston casing, and R_F is frictional resistance. The resistance term is a function of the surface roughness and surface area of the syringe piston/casing contact. Assuming the frictional resistance is constant for a given permeameter (syringe piston/casing combination), the injection pressure can only be increased by increasing the weight or decreasing the cross-sectional area of the syringe piston. Suboor [1994] noted the use of weights to decrease measurement duration when using Scanning Minipermeameter (SMP), a syringe-based permeameter similar to the LSAMP II. A significant difference between the LSAMP II

and the SMP it that the LSAMP II is designed for use in the field, while the SMP is a laboratory scale device.

The effective volume of material sampled for measurements made using a tip seal, inversely related to Equation (3.2), is a function of the tip seal dimensions. For a circular tip seal, the sample volume increases with the tip seal inner radius and, through the geometric factor, G_o (see **Figure 1.2**), the ratio of the tip seal's outer to inner radii [Aronson, 1999; Tartakovsky et al., 2000; Molz et al., 2002]. The ratio given by Equation (3.2) must decrease to shorten the measurement duration. A decrease in the ratio can be achieved by increasing the sample volume, by either increasing the geometric factor, G_o , or increasing the tip seal inner radius, r_i [Tartakovsky et al., 2000]. A decrease in the tip seal ratio corresponds to an increase in the geometric factor. The following two sections outline the different methods used to investigate the effect of gas injection pressure (Section 3.21) and tip seal geometry (Section 3.22) on measurement duration.

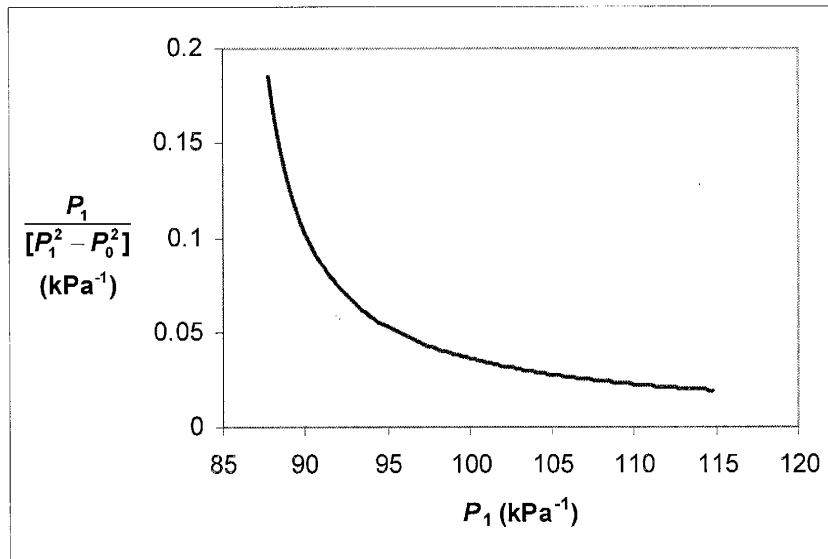


Figure 3.1. Pressure ratio (3.3) as a function of injection pressure.

3.2.1 Increasing Gas Injection Pressure

The gas injection pressure is a function of the weight and the cross-sectional area of the falling syringe piston. Increasing the pressure at the tip seal requires either increasing the force exerted by the syringe piston, or decreasing the cross-sectional area of the piston. Rewriting Equation (3.4) for the addition of weight, or

$$p_1 = \frac{F}{A_p} - R_F = \frac{W_p + W_A}{A_p} - R_F, \quad (3.5)$$

where W_p is the weight of the piston and W_A is the added weight. The piston weight, W_p , can be written as the product of the piston density, ρ_p , piston volume, V_p , and acceleration due to gravity, or

$$W_p = \rho_p V_p g = \rho_p A_p L_p g, \quad (3.6)$$

where L_p is the length of the syringe piston. Combining Equations (3.5) and (3.6), the gas injection pressure is given by

$$p_1 = \rho_p L_p g + \frac{W_A}{A_p} - R_F. \quad (3.7)$$

The injection pressure can be increased by: increasing the piston density, increasing piston length, increasing the weight added, or decreasing the piston cross-sectional area. For standard size syringes, as the cross-sectional area decreases, the piston length also decreases. Due to the impracticality of manufacturing custom syringes, it was decided that increasing the weight would be the main focus for this study. Two options present themselves for increasing the injection pressure by adding weight: (1)

increasing the syringe density by filling the syringe piston with a liquid or granular material, and (2) fixing weights externally to the piston.

Filling the piston has an advantage in that no external change is made to the permeameter. Disadvantages to filling the piston are: (1) the piston must be removed from its casing to take out the added mass allowing for dust and fine particles to collect in the casing (should this change be made in the field) and (2) the piston has a finite volume and therefore, barring access to materials with a wide range of density (i.e. mercury), there is a limit to the amount of mass that can be added. (As a hazardous material, mercury could not be used in field devices with the glass syringe pistons.) Adding mass to the top of the piston is advantageous because: (1) removal of the piston is not required to add or take off mass, and (2) weights can easily be added in various combinations to achieve a wide range of injection pressures. Due to these advantages and the limited amount of mass that could be added by filling the syringe, it was decided to externally add weight to the piston. The drawback to adding weight externally is that it raises the piston's center of mass and could mechanically perturb the surface contact made between the falling piston and the syringe casing. Previous attempts to add weight to the LSAMP II have been made [John Wilson, personal communication]. During these attempts, the addition of an excessive amount of weight during the measurement produced a shockwave that propagated through the plumbing of the instrument and caused it to shake. The shockwave was a result of gas compression in the tubing between the valve, located in the LSAMP II instrument box, and the tip seal. The shockwave could be eliminated by installing a valve at the tip seal, but this design change was not implemented on the LSAMP II.

A method for securing weight to the top of the piston had to be devised before the effectiveness of adding weight could be tested. A holder for weights was fashioned out of a No. 13 rubber stopper (see **Figure 3.2**). A blind hole (2 cm radius, 1 cm deep) was drilled into the base of the stopper to provide a snug fit between the stopper and the piston. The top of the stopper was fit with a ¼ inch threaded rod, washers, and a nut to secure weights to the stopper. A plastic bag, cinched at the end by a rubber band, was manufactured to keep dust out of the system under field conditions. A short length of tubing was used between the tip seal and the permeameter to decrease the volume of gas that had to be compressed at the onset of a measurement.

Before extensive work was done using a weighted instrument, exploratory measurements were made to test the performance of the weight holder and estimate the mechanical upper limit for the addition of weight. After fixing the holder to the top of the syringe piston, different amounts of weight were added and measurements were attempted on materials with a wide range of permeability. Across the range of permeability for which the addition of weight was productive, it was determined that 2.5 lbs. could be safely added. An interesting phenomenon was observed over multiple trials. Occasionally the weighted syringe piston would chatter (i.e. bounce up and down in the syringe casing) during a measurement while during other measurements it would fall smoothly. Through investigation it was determined that the chattering could be attributed to the holder and/or weights not being secured levelly on top of the piston.

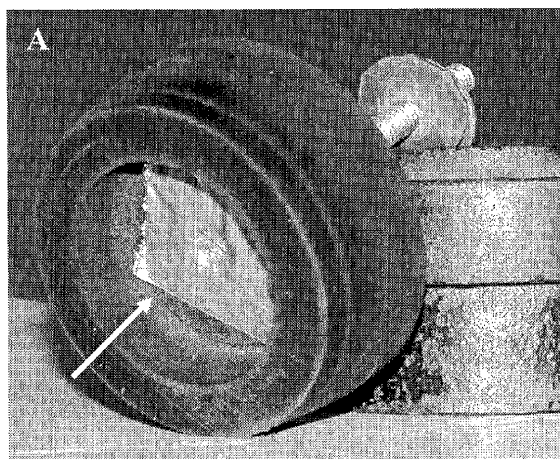
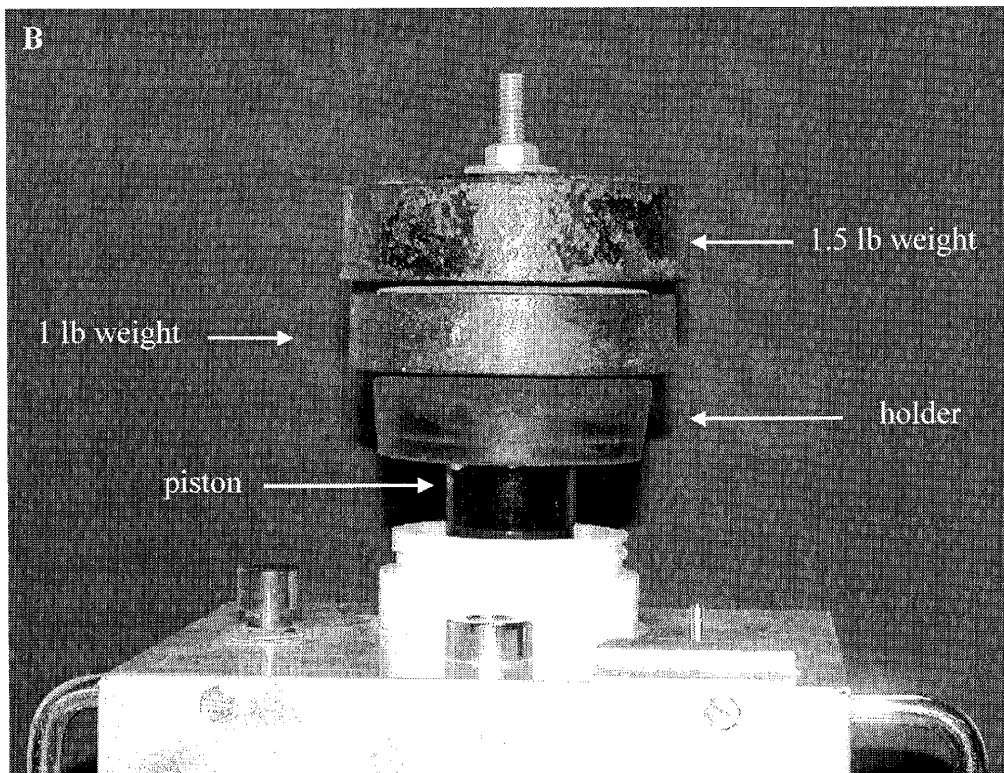


Figure 3.2. A) weight holder, arrow points to the blind hole fit for the piston.
B) Holder and weights connected to the permeameter. C) Shows permeameter fit with bag for field use.

Measurements were made using combinations of different lengths of 20-micron POREX® porous plastic standards (see Appendix 1) and combinations of 1 and 1½ lb weights. The more precise weights were: the 1 lb weight was 452.73 g and the 1.5 lb weight was 680.35 g. When adding weight to the syringe piston the rubber holder must also be included as an additional weight. It weighs 106.45 g. From here forward, 1 lb and 2.5 lb added weight refers to the addition of the 696.67 g (1 lb weight + holder) and 1377.02 g (1 + 1.5 lb weights + holder), where the weight of the holder is implied. Various combinations of four 20-micron standards of length 1, 2, 3, and, 4 cm were connected in series to vary resistance to flow while maintaining a constant permeability. Three different types of measurements were made with respect to weight: (1) no weight, (2) 1 lb, and (3) 2.5 lb added to the syringe piston. Measurements were made for each of the three weight classes using all combinations of the four standards to study the increase in the pressure ratio (3.3) as a function of increased injection pressure. The injection pressure was monitored for a subset of the measurements to verify if steady-flow conditions occurred as the piston fell between sensors.

3.2.2 Changing the Sample Volume

The volume of rock interrogated by gas permeability measurements made with a tip seal is dependent on the tip seal geometry. The sample volume is changed by using different tip seal ratios having different inner radii. Three tip seals were used to investigate their effect on measurement duration: (1) a 2:1 (ratio of outer to inner radii) tip seal with an inner radius of 3 mm, (2) a 4:1 tip seal with an inner radius of 3 mm, and (3) a 4:1 tip seal with an inner radius of 1.5 mm. The dimensions of the tip seal were measured before it was compressed on the material surface and thus it was assumed that

deformation due to compression of the tip seal was negligible. 30 measurements were made on a knife sharpening block (Ace Hardware aluminum oxide 6 x 2 x ¾ inch block) at the same location, with each of the three tip seals, to determine the relative differences in measurement time for each tip seal. The sharpening block used was chosen as the test material because of its relatively homogeneous properties. The use of a homogenous material is crucial for distinguishing between time differences produced by the tip seal and those that would result from material heterogeneities.

3.3 Results

Experiments were performed to test the effects of sample volume and gas injection pressure on the time required to make a permeability measurement. The volume sampled by the permeameter was varied using three different tip seal geometries. For the three tip seals used, preliminary tests showed the inner tip seal radius to be a more effective means for controlling the measurement duration than the outer to inner tip seal ratio (geometric factor, see **Figure 1.2**). The addition of weight to the syringe piston proved to allow for more control over the duration of a measurement.

3.3.1 Effect of Sample Volume

30 measurements were made at the same location on a sharpening block with each of the three tip seal geometries to investigate the control of the tip seal ratio and the tip seal inner radius on the length of a measurement. The mean measurement time for each tip seal geometry was as follows: (1) 2:1 tip seal, $r_i = 3$ mm, $\Delta t = 12.63$ s, (2) 4:1 tip seal, $r_i = 3$ mm, $\Delta t = 12.92$ s, (3) 4:1 tip seal, $r_i = 1.5$ mm, $\Delta t = 25.01$ s. Measurements made with the same inner tip seal radius and different tip seal ratio (1 & 2 above) showed little

difference in measurement time. Measurements made with tip seals having the same tip seal ratio and different inner tip seal radii (2 & 3 above) exhibited more of an effect on measurement duration. The duration of a measurement is inversely proportional to the inner tip seal radius (Equation 3.1). If the tip seal ratio is increased by a factor of two, but keeping the same geometric factor, the measurement duration should decrease by a factor of two. Our results showed that for a twofold increase in the inner tip seal radius (from 1.5 mm to 3 mm) the duration of the measurement decreased by a factor of 1.94, which agrees well with the model.

3.3.2 Effect of Injection Pressure

The estimation of permeability using an LSAMP device assumes steady-flow conditions. This translates to the falling syringe piston reaching terminal velocity (zero acceleration) before passing the middle set of photo sensors (start of the timer). The photo sensors are located at a point along the syringe-casing where, for the un-weighted instrument, there is zero acceleration. For the standard steady-flow permeability model (Equation 1.2) to be valid for the weighted instrument, acceleration must be negligible after the timer has started.

Pressure data was monitored for each of the three weight classes using four length combinations of 20-micron plastic standards: (1) std. 1, (2) std. 2, (3) std. 1 + std. 4, and (4) std. 2 + std. 3 + std. 4. Generally, three trials were performed for each standard combination at each weight class. **Figure 3.3** shows injection pressure as a function of time for measurements on std. 1 with no weight, and for 1 lb, and 2.5 added weights. Figures for measurements made on other standard combinations are provided in Appendix 2. The arrow indicates the point at which the timer started. For each

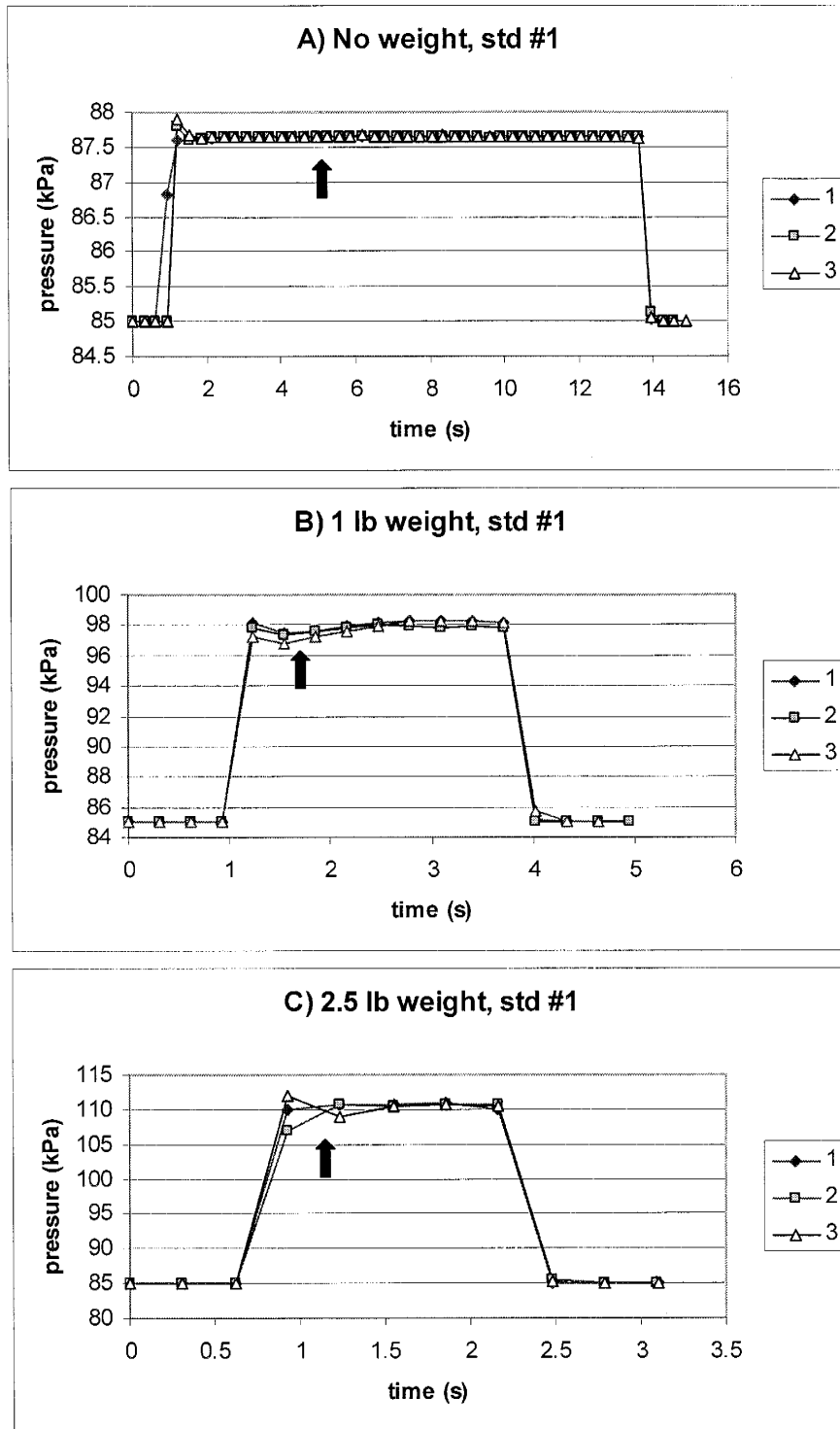


Figure 3.3. Pressure vs. time plots for measurements on std. 1 with (A) no added weight, (B) 1 lb added weight, and (C) 2.5 lb added weight. The legend indicates the trial number. Similar plots for other standard lengths are located in Appendix 2.

measurement the timer stopped at the last point, just before the valve was shut and the pressure returned to atmospheric (~ 85 kPa). Measurements made with the un-weighted instrument are the basis for performance evaluation of the weighted instrument.

A majority of weighted measurements exhibited a slight increase in pressure (piston acceleration) after the timer started. Under standard LSAMP operating conditions time, not pressure, is monitored. Injection pressure is determined using the piston fall-time through calibration. If the piston has not reached terminal velocity before timing starts, the calibration-determined pressure should still correspond to the average pressure of the measurement. The middle photo sensor, which starts the timing circuit, could be lowered to ensure weighted measurements reach terminal velocity before the timer starts. Moving the sensor would decrease the volume of gas used during the timed portion of the measurement which could decrease instrument accuracy. **Table 3.1** compares measurement duration of the three weight classes for each of the four standard combinations. The addition of the 1 lb weight reduced the measurement duration to an average of 20.3 % of the un-weighted measurement time, while the measurements made with 2.5 lb weight added were an average of 10.6% of the un-weighted duration. The percent difference in measurement duration corresponds to the difference in the pressure ratio (Equation 3.3) produced by the increase in pressure due to the added weight.

Table 3.1. Measurement duration as a function of added weight.

Standard	Average measurement duration (s)			% of non-weighted time	
	no weight	1 lb	2.5 lb	1 lb	2.5 lb
1	8.05	1.86	0.93	23.11	11.55
2	18.27	3.41	1.86	18.66	10.18
1 + 4	42.42	8.36	4.65	19.71	10.96
2 + 3 + 4	78.03	15.48	8.05	19.84	10.32

Figure 3.4 shows estimated permeability values for the 20 micron porous plastic as a function of the length of standard used for the measurement. Each data point represents the mean value of five trials. The permeability axis is stretched to exaggerate differences between measurements. Two noticeable trends can be recognized in the data: (1) estimated permeability increases slightly as a function of standard length, and (2) for a given standard length, permeability increases with increased injection pressure (amount of added weight). The first trend could be the result of imprecision in cutting and measuring the lengths of the standards. Aside from the obvious outlier (std. 1+2, 1 lb), a 4% increase in permeability is the largest difference due to length noticed within a weight class. A 4% underestimate of the standard length (0.4 - 1.6 mm depending on std.#) would explain this trend. The second trend might be due increased slippage along sleeve wall/standard interface at higher pressure.

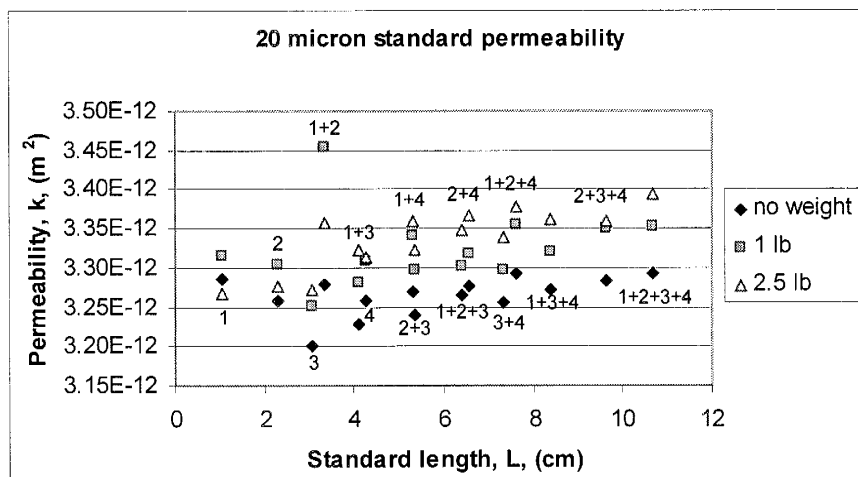


Figure 3.4. Permeability of 20-micron standard as a function of length (combination of lengths) of standard used for measurement.

Table 3.2 compares permeability estimates for 20-micron POREX® between the three permeameter weight classes. The average permeability for each weight class verifies the trend of increasing permeability with increased injection pressure. The un-weighted instrument produced less variable results (lower standard deviation and coefficient of variation). Though the weights and instrument were leveled at the onset of the experiment, the increased variability in the weighted measurements can most likely be attributed to minor chattering during the measurements. Using the permeability estimates with no added weight as a means for comparison, the weighted permeabilities are biased high with 1.81 % error in the measurements made with 1 lb added and 2.21 % error in the measurements made with 2.5 lb added.

Table 3.2. Comparison of weighted permeability estimates (m^2) with those obtained using the un-weighted instrument.

Permeability (m^2)	no weight	1 lb	2.5 lb
Average	3.26E-12	3.32E-12	3.34E-12
Standard deviation	2.54E-14	4.58E-14	3.90E-14
coefficient of variation	7.77E-03	1.38E-02	1.17E-02
% error	-	1.81	2.21

The permeability values for each weight class in **Table 3.2** are an average of the values calculated for each standard length (standard combination). **Figure 3.5** shows the ratio of length to permeability as a function of length for each weight class. In reality, from **Equation 1.1**, the length to permeability ratio is given by

$$\frac{L}{k} = \frac{A[p_1^2 - p_0^2]}{2Q\mu p_1}. \quad (3.8)$$

Permeability data were normalized by length to remove uncertainty in the measured standard lengths. This effectively removes the trend of permeability increasing with increased standard length and accentuates the differences in permeability as a function of weight. The data were fit using a linear least-squares regression (not shown), and permeability values were calculated for each weight class by inverting the slope of the regression line. The regression yielded R^2 values of: 0.9999 (no weight), 0.9996 (1 lb), and 0.9998 (2.5 lb). Such high R^2 values suggest a linear relationship between the ratio of length to permeability and length. This implies there is no real trend of permeability increasing as a function of length, and that the trend in **Figure 3.4** is likely the result of error in the cutting and length measurement of the standards.

The slopes of the regression lines from **Figure 3.5** yielded the following permeabilities: $3.27\text{E-}12 \text{ m}^2$ (no weight), $3.33\text{E-}12 \text{ m}^2$ (1 lb), and $3.36\text{E-}12 \text{ m}^2$ (2.5 lb). The percent error in the weighted measurements was 1.73 % and 2.61 % for the 1 lb and 2.5 lb measurements respectively. The permeability values and the error associated with the weighted measurements calculated from **Figure 3.5** agree well with the data presented in **Table 3.2**. The agreement of the two approaches suggests the trend of permeability increasing with increasing weight is real. A possible explanation of the trend is that as weight increases more gas bypasses the standard, at the interface of the porous plastic and flexible tubing, which results in an apparent permeability increase.

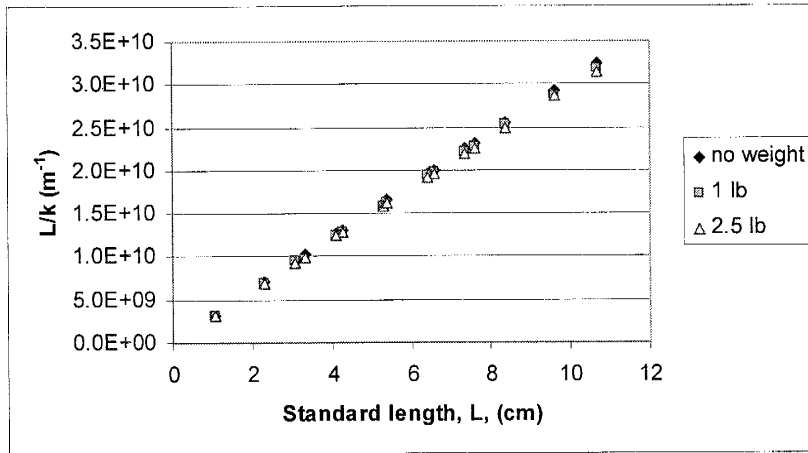


Figure 3.5. Ratio of standard length to permeability as a function of standard length.

3.4 Conclusions

The main focus of this research was to devise a method for increasing the measurement range (or decrease the measurement duration) of the LSAMP to allow for more rapid estimation of permeability on relatively low permeability materials. Two approaches were taken: (1) increasing the sample volume by varying the tip seal geometry, and (2) increasing the gas injection pressure by adding weight to the top of the syringe piston.

Three tip seal geometries were used ($r_o/r_i = 2$, $r_i = 3$ mm, $r_o/r_i = 4$, $r_i = 3$ mm, $r_o/r_i = 4$, $r_i = 1.5$ mm) to test the effect of the tip seal ratio and tip seal inner radius on the duration of a measurement. Increasing the tip seal ratio (geometric factor) for a given tip seal inner radius did not prove to have a significant effect on measurement duration, as one would expect from **Figure 1.2**. The use of tip seals with different inner radii and the same tip seal ratio produced a much better result. An increase in the tip seal inner radius significantly decreases the measurement duration and could be an effective way of

decreasing measurement time. However, if one were to change tip seal sizes or geometric factors when measuring permeability in different materials, in order to optimize piston fall time, then the different sample volumes might make comparing measurements more problematic, because of permeability scaling issues.

The effect of gas injection pressure on measurement duration was investigated by adding weight to the syringe piston. Three different amounts of weight were used for all measurements in these experiments: (1) no weight, (2) 1 lb, and (3) 2.5 lb. Weight was added externally to the piston using a fabricated weight holder and a series of steel weights. Addition of weight to the top of the piston can cause chattering in the falling piston if the weight is not leveled properly. The addition of weight proved to significantly decrease measurement duration: 20.3 % of the un-weighted duration for 1 lb, and 10.6 % of the un-weighted duration for 2.5 lb. The gas injection pressure was monitored across a range of resistances for all weight classes. A small increase in injection pressure occurred just after the timing of the measurement began (transient effects) for a majority of the weighted measurements. The error in estimated permeability (when compared to the un-weighted measurement) due to the transient effect was small: 1.77 % for 1 lb and 2.41 % for 2.5 lb. The middle photo sensor (which starts the timer) could be lowered to assure the piston reaches terminal velocity, but the reduced distance between sensors could affect the instrument's accuracy. The error in the weighted measurements resulted in a biased high permeability value, where the amount of bias increased with the amount of weight added.

The time it takes to make a measurement with the LSAMP II (or other syringe-based permeameters) can be effectively decreased by: (1) increasing the inner tip seal

radius or (2) increasing the injection pressure by adding weight to the syringe piston. Though increasing the tip seal inner radius proved to be effective, it could only be used to decrease measurement time by a factor of four. This limit is due to practical constraints on the size of a tip seal. Increasing the injection pressure by adding weight has proven to decrease the measurement duration by a factor of ten (for the addition of 2.5 lbs) with less than 3 % error.

CHAPTER 4

DESIGN AND TESTING OF A PORTABLE PRESSURE DECAY GAS PERMEAMETER

4.1 Background

Gas permeameters are a commonly employed method of estimating permeability of rock and sediment outcrops. The most common application of gas permeametry involves injecting gas at a known pressure into the rock, and measuring gas flow rate to calculate permeability. This steady-flow method, which was pioneered in the petroleum industry, traditionally involved the use of a compressed gas tank as the gas source and mass flow meters to measure flow rate. Hydrogeologists encountered a problem when applying this method to poorly consolidated sediments, in that the compressed gas tank and flow meter setup was not accurate enough on these high permeability sediments and often caused movement of the grains during measurement. A Lightweight Syringe-based Air Mini-permeameter (LSMAP) was designed [Davis et al., 1994] and modified [Suboor and Wilson, personal communication] to address the problem of measuring permeability of poorly consolidated sand deposits. The pressure used by the LSAMP is low enough such that no significant grain rearrangement occurs when used on poorly consolidated sands. A shortcoming of the design is that without modification the permeameter has

only one supply pressure (the weight of the syringe piston). This makes the practical range of the instrument (due to time limitations) approximately two orders of magnitude, while permeability commonly varies over five orders of magnitude on outcrops of hydrologic interest. Outcrop studies involving low permeability zones hosted in a poorly consolidated sand matrix brought to the forefront the need for a new permeability measurement method. Such outcrop studies require that non-destructive permeability measurements be made rapidly (1-20 seconds) across at least three orders of magnitude permeability.

The problem of measuring permeability over a wider range lends itself to two solutions: (1) use different permeameters for different permeability ranges, or (2) develop a new instrument that is capable of measuring over the desired range. Multiple devices for different permeability materials are often utilized in the laboratory. When using water to measure permeability, constant head (steady-flow) permeameters are usually used for higher permeability materials, and falling head (transient) permeameters are used for lower permeability materials. Multiple instruments do not pose any significant disadvantage in the laboratory, but would be impractical for field operation.

A laboratory-scale gas minipermeameter based on transient gas flow was designed by Jones [1992], which addressed the issue of decreasing the measurement duration (increasing the practical measurement range) of gas permeameters. Jones noted permeability measurements that required 20 minutes to achieve steady-flow conditions when measuring cores with permeabilities less than $1 \times 10^{-15} \text{ m}^2$. Jones' permeameter (PDPK-200) measures permeability over eight orders of magnitude, with a given measurement lasting no longer than 35 seconds. The PDPK-200 is a transient-based

device in which a gas at a known pressure and of a known volume is injected through a probe tip into a rock sample. The rate of pressure decay in the source tank is then monitored, and used to calculate permeability. Jones' permeameter exhibits many of the qualities that are desirable in a new permeameter design suggesting that transient methods may be most advantageous for increasing an instrument's measurement range.

4.2 Questions and Issues

Considering the work of Jones [1992] and the wide use of falling head liquid permeameters on low permeability material, it became desirable to design, construct, and test a field portable transient pressure decay gas permeameter. The PDPK-200 is a laboratory-scale device designed for measuring the permeability of consolidated materials commonly encountered in petroleum exploration. The permeameter utilizes multiple volume reservoirs to achieve a permeability measurement range of eight orders of magnitude. Our goal is to design a field portable device consisting of one reservoir volume for measuring the permeability of unconsolidated materials of hydrologic significance spanning approximately five orders of magnitude permeability. The following questions must be addressed in the early stages of model development and instrument design:

- (1) What parameters control the duration of a measurement, and which of these parameters can we change to achieve the desired measurement range?
- (2) Will pressure decay measurements be subject to nonlinearities due to thermodynamic and/or non-Darcian flow effects? If nonlinearities are present, will they be significant enough to affect permeability estimates?

The mathematical model used by Jones [1992] suggests three parameters that can be varied by the investigator which influence measurement duration: (1) the volume of the gas reservoir, (2) the initial pressure of the reservoir, and (3) the dimensions of the tip seal. The minor effect of tip seal geometry on measurement duration for steady-flow conditions is discussed in Chapter 3. Presumably tip seal geometry would have a similar second order effect on measurement duration for transient air permeability measurements. Sensitivity (with respect to measurement duration) to the reservoir volume and initial pressure will be addressed later in the Results section of this chapter.

Smith et al. [1997] found a source of systematic error when making pressure decay measurements due to non-isothermal conditions in the reservoir. A decrease in temperature occurred in the source tank due to a rapid decrease in pressure at the beginning of a measurement. In a later publication, Smith et al. [1998] outlined a means for alleviating this problem by putting fiberglass inside the source tank to act as a uniform heat source/sink, dampening temperature change. Smith et al. [1997] noted temperature deviations on the order of 0.5 degrees for measurements starting at an initial tank gauge pressure of 1.5 kPa (with reference to atmospheric).

Non-Darcian flow occurs at both low and high flow rates. Darcy's Law is described by a linear relationship between the flow rate and potential gradient. The upper limit of Darcy's Law is breached when the regular pattern of streamline flow becomes unstable and turbulent eddies begin to form [Carmen, 1956]. Turbulent flow dissipates kinetic energy as heat, which results in a nonlinear relationship between head gradient and flow rate due to head (potential) loss. Relatively high pressures induce high flow rates in a pressure decay device, causing air permeability measurements in the nonlinear

flow range. The flow rate at which the transition to turbulent flow takes place is a function of pore size and pore structure, and is related to permeability, k . The transition to non-linear flow can be characterized by a Reynolds number. The Reynolds number length scale is sometimes written as \sqrt{k} [Dullien, 1992]. For the same flow rate, higher permeability materials become non-linear. High initial pressures in a pressure decay device could induce non-linear flow effects in high permeability materials, until the pressure and flow rate decay into the linear range.

4.3 Scope

It is our goal to develop, design, and test a field portable pressure decay permeameter that can measure a wide range of permeabilities and still be sensitive enough for use on poorly consolidated sediments. This task includes:

- (1) Development of a mathematical model to describe transient gas flow through porous media for the operating conditions of interest¹.
- (2) Design of a permeameter incorporating realistic pressures and tank volumes that is optimized for field measurement on geologic materials spanning five orders of magnitude.
- (3) Testing of a prototype device and verification of the mathematical model. This involves providing evidence that the proposed pressure decay permeameter has potential to significantly improve permeability data collection in the field.

¹ Mathematical models have been developed for similar transient permeameters [Jones, 1992], but these models involve terms for gas slippage effects that are only important for extremely low permeability materials not considered in our development.

4.4 Mathematical Model

The following development is for isothermal flow of a gas from a reservoir through a porous material. While thermodynamic effects on temperature can be important for a pressure decay device, the instrument was designed to minimize these effects. Assuming the gas acts as an ideal gas, the equation of state is

$$pV = mRT \quad \text{or} \quad p = \rho RT, \quad \text{where} \quad \left(\rho = \frac{m}{V} \right). \quad (4.1)$$

Here p is pressure, V is volume, m is mass of the gas, R is the specific gas constant, T is temperature, and ρ is density. This thermodynamic expression applies both in the reservoir (left hand expression), where $V=V_T$ is the reservoir or tank volume, and porous media (right hand expression).

Assuming a constant reservoir volume (V_T) and isothermal conditions in the reservoir (T constant) provides

$$V_T \frac{dp_T}{dt} = \frac{dm_T}{dt} RT_T. \quad (4.2)$$

This expression states that the rate of pressure change in the reservoir is directly proportional to the rate of mass flux out of the tank. Isothermal conditions can be ensured by adding a heat capacitor to the reservoir. In the absence of a heat capacitor a decrease in pressure results in a decrease in temperature. With a heat capacitor, a decrease in pressure has no appreciable effect on temperature.

In the porous media, the grains become the heat capacitor. The following development is for one-dimensional flow through a porous media column of length , L ,

and cross-sectional area, A . Assuming gas slippage effects are negligible and Darcy's Law applies, volumetric and mass flux rates for a porous media are described by

$$q = -\frac{k}{\mu} \frac{dp}{dx} \quad \text{and} \quad q\rho = -\frac{k\rho}{\mu} \frac{dp}{dx}, \quad (4.3)$$

where q is Darcy velocity, k is intrinsic permeability, μ is the gas dynamic viscosity, and x is the horizontal length scale of the porous media column. Conservation of mass in the column is given by

$$\frac{\partial(\rho n)}{\partial t} + \frac{d(q\rho)}{dx} = 0, \quad (4.4)$$

Neglecting the matrix compressibility (assuming constant porosity, n), (4.4) yields:

$$\frac{\partial(\rho n)}{\partial t} = 0, \quad \text{and hence} \quad \frac{d(q\rho)}{dx} = 0 \Rightarrow q\rho = \text{constant} \Rightarrow q\rho A = \text{constant} = N_m, \quad (4.5)$$

where N_m is the rate of mass flux through the column of cross-sectional area, A .

Substituting the conservation of mass flux (4.5) into Darcy's Law (4.3) gives

$$N_m = q\rho A = -\frac{k\rho A}{\mu} \frac{dp}{dx}. \quad (4.6)$$

Assuming an ideal gas (4.1), (4.6) becomes

$$N_m = -\frac{kA}{\mu} \frac{p}{RT} \frac{dp}{dx}. \quad (4.7)$$

Rearranging and integrating (4.6),

$$\int -\frac{N_m \mu RT}{kA} dx = \int p dp. \quad (4.8)$$

Since $\frac{N_m \mu RT}{kA}$ does not depend on x or p (constant for isothermal conditions) it can be pulled outside the integral, or

$$-\frac{N_m \mu RT}{kA} \int dx = \int p dp \Rightarrow -\frac{N_m \mu RT}{kA} x = \frac{1}{2} p^2 + C' \Rightarrow -\frac{2N_m \mu RT}{kA} x = p^2 + C. \quad (4.9)$$

The constant of integration, C , is solved for by inserting the boundary condition $p = p_0$ at $x = L$, or

$$-\frac{2N_m \mu RT}{kA} L = p_0^2 + C \Rightarrow C = -\left(p_0^2 + \frac{2N_m \mu RT}{kA} L \right). \quad (4.10)$$

and (4.9) becomes

$$\frac{2N_m \mu RT}{kA} (L - x) = p^2 - p_0^2. \quad (4.11)$$

By substituting in the boundary condition at the upstream end of the column, $p = p_T$ at $x = 0$, and

$$\frac{2N_m \mu RT}{kA} L = p_T^2 - p_0^2. \quad (4.12)$$

The models for porous media (4.12) and the reservoir (4.2) are combined, assuming that all mass leaving the reservoir enters the column,

$$N_m = -\frac{dm_T}{dt}, \quad (4.13)$$

and that ideal and isothermal conditions exist in the tank (4.2), or

$$\frac{dm_T}{dt} = \frac{V_T}{RT_T} \frac{dp_T}{dt}. \quad (4.14)$$

Combining the conservation of mass for the reservoir (14) and the conservation of mass and momentum for the column (12),

$$-\frac{V_T}{RT} \frac{dp_T}{dt} \frac{2\mu RT}{kA} L = p_T^2 - p_0^2 \Rightarrow -\frac{2\mu V_T L}{kA} \frac{dp_T}{dt} = p_T^2 - p_0^2. \quad (4.15)$$

Rearranging and integrating (4.15) provides

$$-\int \frac{1}{p_T^2 - p_0^2} dp_T = \frac{kA}{2\mu V_T L} \int dt \Rightarrow -\frac{1}{2p_0} \ln \left(\frac{p_T - p_0}{p_T + p_0} \right) = \frac{kAt}{2\mu V_T L} + C. \quad (4.16)$$

Inserting the initial condition $p_T = p_i$ at $t = 0$, and solving for the constant of integration,

$$-\frac{1}{2p_0} \ln \left(\frac{p_i - p_0}{p_i + p_0} \right) = C. \quad (4.17)$$

Substituting (4.17) into (4.16), assigning $p_T = p$ at some later time, $t = \Delta t$, and solving for permeability, k ,

$$k = \frac{V_T L}{A} \frac{\mu}{p_0} \frac{1}{\Delta t} \ln \left(\frac{p_i - p_0}{p_i + p_0} \frac{p + p_0}{p - p_0} \right). \quad (4.18)$$

Equation (4.18) describes transient gas flow from a reservoir with volume, V_T , through a cylindrical porous medium of length, L , and cross-sectional area, A , with no flow boundaries on the sides.

The field permeameter involves flowing gas through a tip seal with inner radius, r_i , and outer radius, r_o , into a porous material (see Chapter 1). Tip seal application of a gas produces a hemispherical flow field which is much different than flow through a column. Accounting for the difference in flow geometry can be achieved using the

geometric factor, G_o , developed by Goggin et al. [1988], which is a function of the tip seal geometry. The term describing the geometry of flow in (4.18) is

$$\frac{L}{A}. \quad (4.19)$$

Hemispherical flow from a tip seal produces a geometry described by

$$\frac{1}{r_i G_o \left(\frac{r_o}{r_i}\right)}. \quad (4.20)$$

Both (4.19) and (4.20) ignore gas compressibility in the porous media. Substituting (4.20) for (4.19) in (4.18) yields

$$k = \frac{V_T}{r_i G_o \left(\frac{r_o}{r_i}\right)} \frac{\mu}{p_0} \frac{1}{\Delta t} \ln \left(\frac{p_i - p_0}{p_i + p_0} \frac{p + p_0}{p - p_0} \right), \quad (4.21)$$

which describes transient flow from a reservoir through a tip seal, into and through a porous medium.

4.5 Methods

Multiple reservoir volumes were constructed and equipped with a pressure transducer to monitor pressure decay as a function of time. Ultra high purity compressed nitrogen was used to pressurize the tank before each measurement. Measurements were started over a range of initial tank pressures to investigate the effect of initial pressure on measurement duration. A thermocouple was placed inside the reservoir to monitor temperature in the event that non-isothermal conditions existed in the tank. Considering the work of Smith et al. [1998], other measurements were made with a uniform heat capacitor (woven fiberglass) inserted into the reservoir to dampen possible temperature

effects. Four different porous materials of varying permeability were used to evaluate the measurement range of the permeameter. Permeability estimates obtained using the pressure decay permeameter were compared to permeability values acquired using two steady-flow methods: (1) syringe-based permeameter and (2) a continuous flow permeameter.

4.5.1 Permeameter Fabrication

A schematic diagram of the pressure decay permeameter is shown in **Figure 4.1**. Multiple tank sizes were used in the testing stage, but all were constructed using a threaded PVC nipple and two PVC caps. PVC was chosen as the tank material for the prototype because it is cheap and easily tapped, and would not deflect mechanically under the gas pressures used. Two quick-disconnect couplings were fit to the back end of the reservoir; one with a shut off for pressuring up the tank, and one to attach a pressure transducer. Three different pressure transducers were used during the testing process: (1) SenSym SDX005D4, 0-5 psi differential, (2) Motorola MPX5050DP, 0-7.25 psi differential, and (3) Omega PX800-010GV, 0-10 psig. Transducers were selected to accommodate a range of initial tank pressures. A third port was placed on the side of the reservoir for emplacement of the thermocouple. A type-K (nickel-chromium(+), nickel-aluminum(-)) exposed junction thermocouple was used to record all temperature data. The pressure transducer and thermocouple were connected to a Campbell Scientific 21-X or a National Instruments NI 4351 data logger. A ¼ inch i.d. lab cock ball valve was fit to the front of the tank and connected to the tip seal.

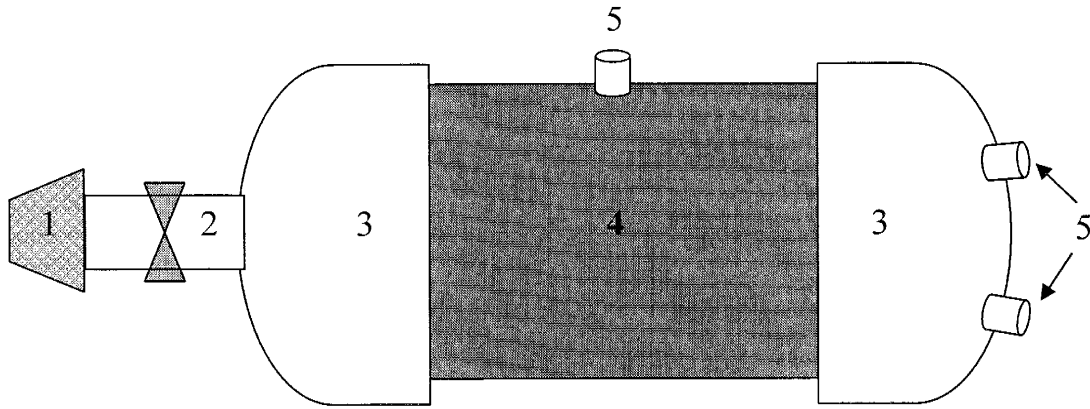


Figure 4.1. Schematic diagram of prototype pressure decay permeameter. (1) tip seal; (2) ¼ inch lab cock ball valve; (3) PVC end caps; (4) PVC threaded nipple; (5) quick disconnect couplings.

All tests were run with one of two different volume tanks. Both tanks were geometrically similar and constructed following the above procedure. The tanks are referred to as large or small based on their internal volume. The small tank was built from a 1.5 inch diameter by 4 inch PVC nipple while the large tank was made from a 2 inch diameter by 6 inch long nipple. Both tanks had 3/8 inch thick walls. Unless otherwise stated all results are for the large tank.

The tank volumes were calibrated using water. The first step taken in the process was recording the empty tank mass, m_E . After logging the empty weight, the tank and all tank fittings up to the tip seal orifice were filled with deionized water. Though the volume between the tip seal and valve is not pressurized before the valve opens, it must be included in the tank volume for permeability estimation. Room temperature was recorded to look up the density of water, ρ_W . Taking the difference of the empty and filled, m_F , tank to calculate the mass of water, m_W , in the tank, and knowing the density of water, the tank volume can be calculated using

$$V_T = \frac{m_W}{\rho_W} = \frac{m_F - m_E}{\rho_W} . \quad (4.22)$$

The above method for calculating the tank volume was repeated three times for each tank size. The average tank volumes were then used in all calculations. The average volume for each tank was: 123 cm³ for the small tank, and 388cm³ for the large tank.

Adding fiberglass to the source tank changes the tank volume. Measuring the volume of a piece of fiberglass is difficult and time consuming. Fiberglass was frequently inserted and removed from the tank, so it was impractical to re-measure the volume each time it was inserted. The density of the fiberglass used throughout permeameter testing was measured allowing for fiberglass volume to be calculated if the mass of fiberglass to be inserted was known. The fiberglass density was calculated by dividing a known mass of fiberglass by the volume of the known mass. The volume of the fiberglass used in the density calculation was measured with a pycnometer. The density of fiberglass was calculated to be 2451 kg/m³. On average, the volume of fiberglass inserted into the reservoir was only 0.2% of the total reservoir volume, and was mathematically negligible.

4.5.2 Testing Materials

Four different porous materials were used in the testing procedure: (1) Berea Sandstone, (2) Massillon Sandstone, (3) a low permeability unidentified sandstone, and (4) a laboratory fabricated permeability standard (Standard 3) previously used by Davis et al. [1994]. The materials were chosen to represent the wide range of permeability which one would expect to encounter in the field. Descriptions of the Berea and Massillon Sandstones are given in Chapter 2. The low permeability Sandstone is of unknown

origin, but was used only to test the low end of the measurement range. The laboratory fabricated standard consists of a 100 cc soil ring packed with epoxied sand grains. The fabricated standard was chosen to represent the high end of the measurement range. A description of the manufacturing process for the standard is provided by Davis et al. [1994].

4.5.3 Pressure Decay Measurement Procedure

Measurements were made by pressurizing the reservoir to an initial pressure, placing the tip seal on the sample material, opening the valve (by hand, while compressing the tip seal on the sample), and simultaneously recording pressure and time data until the tank equilibrated with atmospheric pressure. The tank was pressurized to its initial pressure by connecting the compressed gas source to the reservoir via the quick disconnect fitting with a shut off, opening the valve to the compressed gas until the desired initial pressure was achieved, and disconnecting the reservoir from the compressed gas. The reservoir was then allowed to equilibrate to room temperature, negating thermodynamic effects due to decompression from the source tank. At this point the data logger was switched on and the initial tank pressure was recorded for a small time interval to verify a constant starting pressure. To begin the measurement, the tip seal was placed on the material surface, and the ball valve was opened. Care was taken to open the valve as quickly as possible, preventing unwanted pressure losses associated with the changing cross-sectional area of flow. The tip seal remained compressed on the rock surface until the logged pressure reached that of the surroundings. Temperature was monitored by inserting a thermocouple via a quick disconnect coupling. Temperature was monitored in some experiments, but not all.

4.5.4 Steady-Flow Methods

The LSAMP II and a continuous flow permeameter permeability values were compared to permeability values obtained with the pressure decay permeameter. The measurements made with the pressure decay permeameter for comparison were started at four different initial tank pressures (gauge): (1) 30 kPa, 20 kPa, 15 kPa, and 10 kPa. Three different sample materials were used for all measurements: (1) Berea Sandstone, (2) Massillon Sandstone, and (3) the laboratory fabricated permeability standard. To assure that the same volume of rock was interrogated (same tip seal placement) for each measurement, the tip seal was clamped to the sample using two C-clamps. Once the tip seal was clamped to the sample, measurements were made with the LSAMP II, the continuous flow permeameter and the pressure decay permeameter (at four initial pressures).

Chapter 2 provides an explanation of the measurement procedure for the LSAMP II. The continuous flow permeameter consists of a compressed gas source (UHP nitrogen), a pressure transducer at the tip seal (to monitor injection pressure), and a series of three inline flow meters to measure gas flow rate. Measurements were made at multiple pressures (and flow rates) to investigate the dependence of permeability on pressure/flow rate. A complete discussion of the continuous flow permeameter is given by Davis et al. [1994], which they describe as the continuous flow air-minipermeameter (CFAMP).

4.6 Results and Discussion

Experiments were performed where pressure and (sometimes) temperature were recorded as a function of time. **Figure 4.2** is a typical plot showing the rate of pressure decay in the source tank for the Berea Sandstone (initial gauge pressure was 30 kPa). Referring to the governing equation for the calculation of permeability (4.21), all parameters are known except for the pressure time data. Atmospheric pressure, p_0 , was taken to be the ambient room pressure. Depending on how the pressure is recorded (absolute, differential, or gauge), there could be severe implications if the incorrect atmospheric pressure is chosen (see Appendix3). The choice of initial pressure, p_i , is up

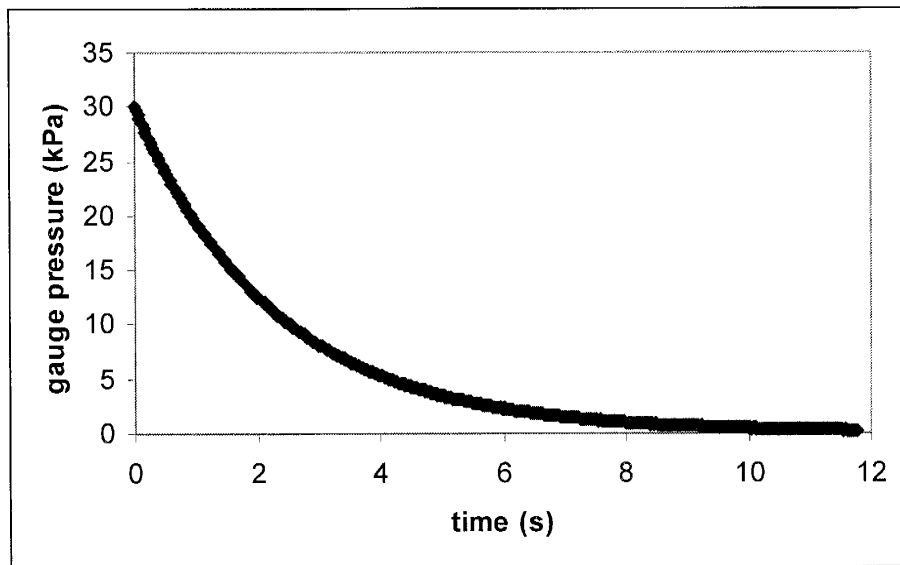


Figure 4.2. Typical plot showing the rate of pressure decay in the source tank. Measurement made on the Berea Sandstone with the small tank with an initial (gauge) pressure of 30 kPa.

to the data analyst, and need not be the highest recorded pressure. When the valve is thrown there is a pressure anomaly, as the system reacts. The initial pressure can be taken after that anomaly, or selected as any later pressure, as long as the transducer noise does not interfere. The time, Δt , is then measured from this point, and p is the pressure at some given Δt from the initial pressure, p_i . Permeability can be calculated using as few as three pressure values, an initial pressure, pressure at some later time, Δt , and atmospheric pressure. Only two pressures can be used if Δt refers to the time required for pressure to decay from its initial value to atmospheric pressure, though the accuracy and precision of the pressure transducer near atmospheric pressure is questionable.

To test the robustness of using only two or three pressure values to calculate permeability, the data were first plotted in such a way that all recorded pressures would be used to calculate permeability. Equation (4.21) can be rearranged to

$$\ln\left(\frac{p_i - p_0}{p_i + p_0} \frac{p + p_0}{p - p_0}\right) = \frac{k r_i G_o \left(\frac{r_o}{r_i}\right) p_0 \Delta t}{V_T \mu}, \quad (4.23)$$

such that permeability, k , can be calculated from the slope of the plot of $\frac{p_0 \Delta t}{\mu}$ (dimensionless time) vs. $\ln\left(\frac{p_i - p_0}{p_i + p_0} \frac{p + p_0}{p - p_0}\right)$ (transformed pressure). Using the slope of this diagnostic plot incorporates all pressure data into the calculation of permeability. If Equation (4.21) is indeed the correct mathematical model, the dimensionless time vs. transformed pressure plot should be linear. Provided the plot is linear, any two pressures (with a given Δt) from the pressure time data can be used in (4.21) to yield a single permeability value.

Figure 4.3A shows the dimensionless time vs. transformed pressure plot (diagnostic plot) for the ideal case (linear). Any deviation from linearity in the diagnostic plot suggests that the rate of pressure decay with time in the source tank does not follow the mathematical model. Throughout the testing stage for the pressure decay permeameter, two anomalous curvatures were noted in the diagnostic plot: one in which the slope was greater in the early time data (**Figure 4.3B**), and one in which the slope was less in the early time (**Figure 4.3C**). Both anomalous plots appear to achieve linear behavior in later time data. Deviation from the mathematical model suggests that either one or more of the model assumptions is violated, or that pressure is changing differently in the tank than at the tip seal as an artifact of the instrument design, as discussed in the following section.

Model assumptions include: (1) isothermal conditions exist inside the source tank, connecting valve and tip seal, and porous media, (2) Darcy's Law applies throughout the porous media over the duration of the measurement, and (3) the gas (once inside the porous media) and the porous media itself are incompressible. The design of the instrument could potentially cause differences in pressure at the tip seal and in the source tank, where the transducer is located. The pressure at the tip seal is the pressure we are interested in for the calculation of permeability, but due to design issues pressure is monitored in the reservoir.

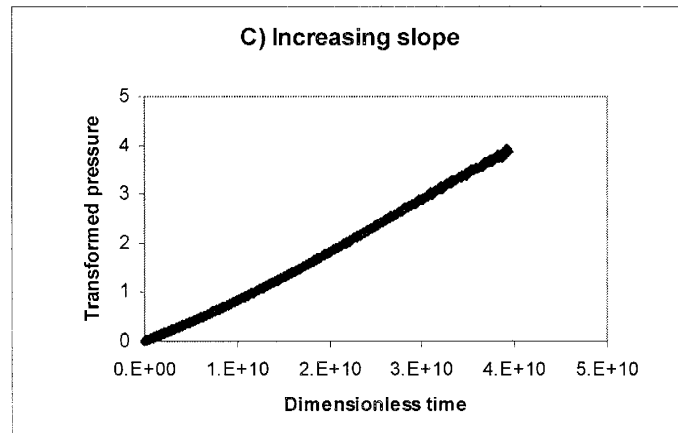
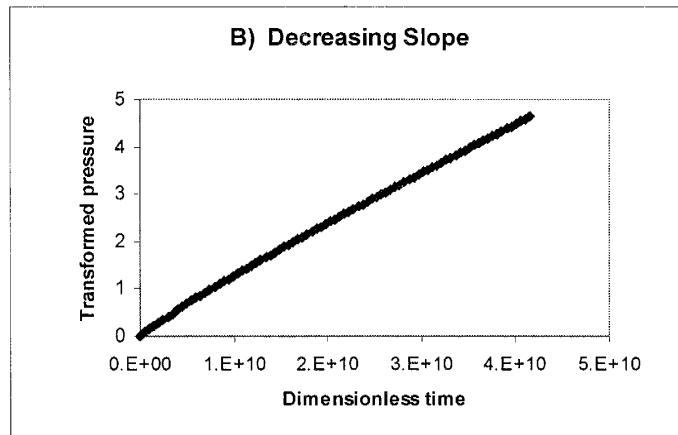
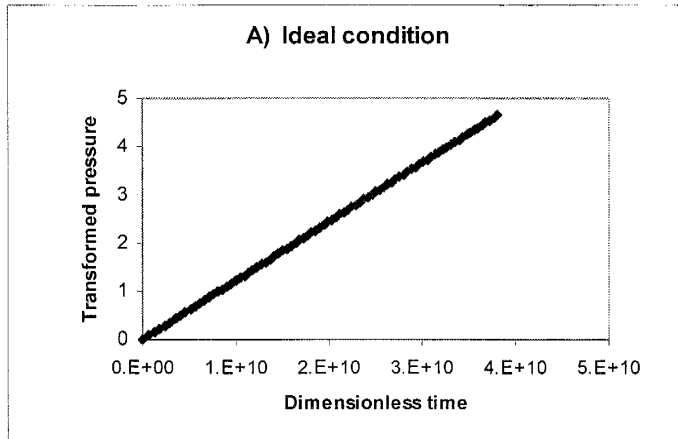


Figure 4.3. Diagnostic dimensionless time vs. transformed pressure plot. (A) The model-predicted linear plot (Berea, small tank, $p_i = 30$ kPa gauge). (B) An actual plot from recorded pressure-time data showing a steeper slope in the early time data (Berea, small tank, $p_i = 30$ kPa gauge). (C) An actual plot from recorded pressure-time data showing an increasing slope after the early time data (Massillon, small tank, $p_i = 20$ kPa gauge).

4.6.1 Pressure Anomalies

Some of the collected data show the slope of the diagnostic plot decreasing after the early time of the measurement (**Figure 4.3 B**). The slope then stabilizes and appears to follow a linear relationship. Assuming the later, linear portion of the data represent consistent model conditions, while a larger slope in the early time data equates to pressure in the source tank initially dropping more rapidly than the model predicts. The early time pressure anomaly could be attributed to thermodynamic effects (non-isothermal conditions in the reservoir), compressibility of the gas in the porous media, or as a function of the prototype design.

All measurements for which the slope decreased as the measurement progressed were made with no heat capacitor (fiberglass) in the source tank, and therefore thermodynamic effects are the most likely cause. If conditions within the reservoir are non-isothermal, one would expect a temperature drop when the valve is opened as the gas expands. Investigation of temperature effects on pressure decay measurements was achieved by inserting a thermocouple into the reservoir to simultaneously record pressure and temperature data. **Figure 4.4** shows a plot of dimensionless time vs. transformed pressure, together with a plot of the corresponding gas temperature inside the tank. Though the temperature data is noisy, it appears that in this experiment isothermal conditions do not exist in the reservoir, with temperature dropping approximately 0.5 °C when the valve is opened. The maximum deflection from linearity on the diagnostic plot can be equated to a pressure which is 3.8 kPa less than what would be expected for ideal, isothermal conditions.

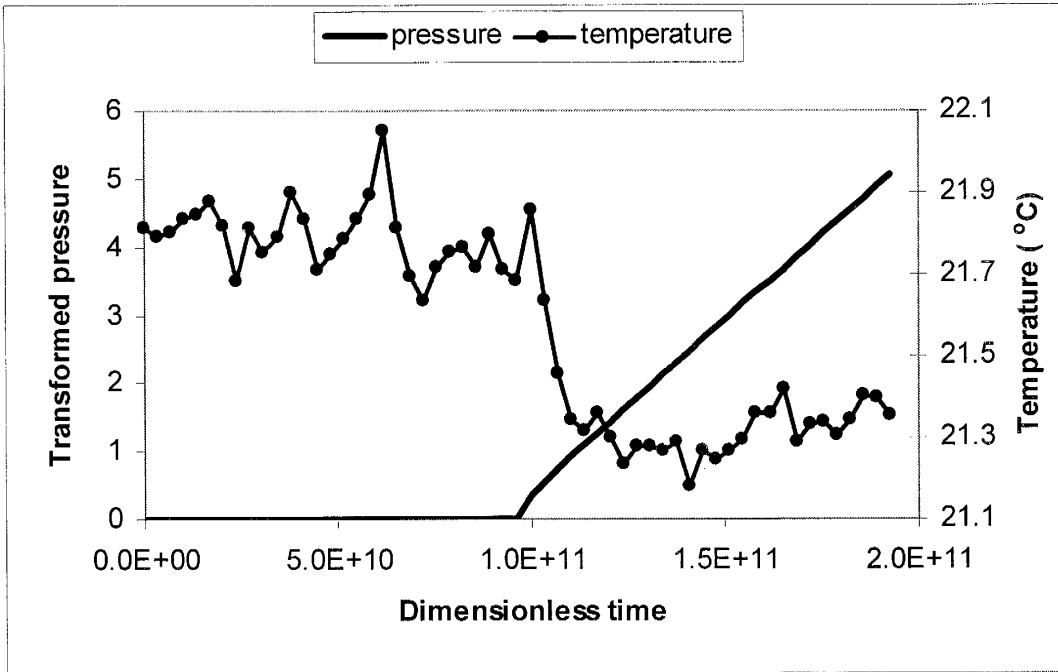


Figure 4.4. Diagnostic plot with corresponding tank temperature (Berea, small tank, $p_i = 25.5$ kPa gauge). The time at which the 0.5 °C drop in temperature occurs corresponds to the valve opening.

Other possible contributors to the pressure anomaly involve the opening of the valve at the start of a measurement and gas compressibility in the rock. The small volume (~ 3.5 cm³) between the valve and the material surface is not pressurized before the valve is opened. Thus at the onset of a measurement a rapid pressure drop occurs in the tank due to pressurization of this volume downstream of the valve. The magnitude of the initial pressure drop is a function of this volume and the reservoir volume. The larger the difference between the reservoir volume and the downstream valve volume, the smaller the initial pressure drop. Without a method of monitoring gas pressure inside the rock, it is difficult to directly measure gas compressibility effects in the porous media. If the gas were compressing in the rock, pressure would decay faster than predicted by the

model. Preliminary modeling [John Wilson, personal communication, 2002] suggested the time constant for gas compressibility was very fast, which led to the conclusion that compressibility could be left out of the model derivation. More sophisticated modeling has not been done. Along with thermodynamic effects, this pressure drop at the start of a measurement, and gas compressibility in the porous media, could contribute.

Even with a heat capacitor in the reservoir, pressure anomalies caused curvature in the diagnostic plot. Much of the data collected with the fiberglass heat capacitor in the tank exhibited an increasing slope through the early time data when plotted on the diagnostic plot (**Figure 4.3C**). Inserting fiberglass in the reservoir negates the thermodynamic effects which, apparently, are the main cause of the decrease in slope of the diagnostic plot after the early time data.

Measurements were made with and without fiberglass in the reservoir to investigate the thermodynamic effects resulting from pressurization of the small volume between the tip seal and the valve. This was achieved by pressurizing the reservoir to an initial pressure, pressing the tip seal against an impermeable object, and opening the valve to the tank. **Figure 4.5** shows the influence of the heat capacitor on tank pressure as the tip seal area is pressurized. The pressure data was normalized due to slight differences in initial pressure. The normalized pressure is the ratio of actual pressure to the pressure of stabilization (pressure at $t = 5$ s). Therefore a normalized pressure of one equates to a constant pressure (i.e. isothermal conditions). There is a 0.25 second offset in the two data sets for visual purposes.

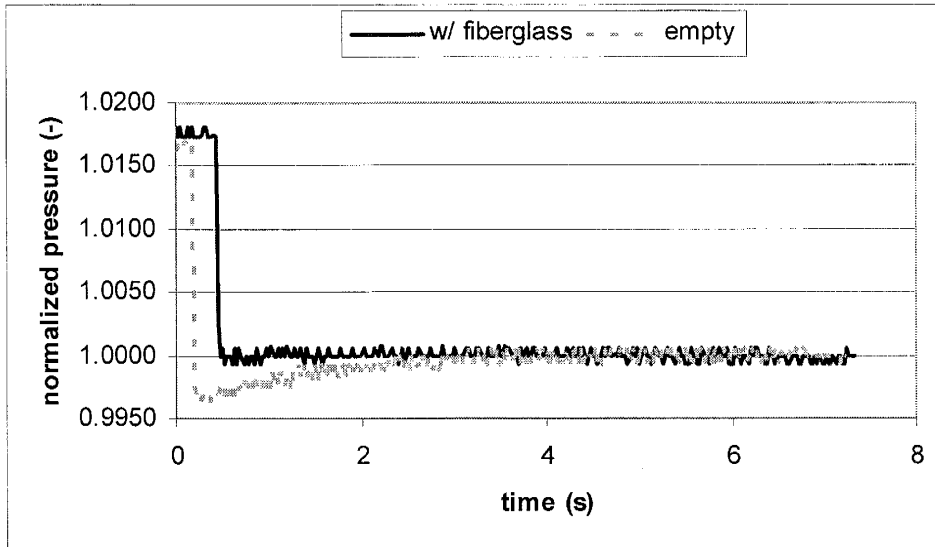


Figure 4.5. Pressure drop due to pressurization of the valve/tip seal volume at the onset of a measurement for the small reservoir with and without a heat capacitor. The 0.25 second offset in the data is for visual purposes.

The data collected with fiberglass in the tank shows that the reservoir pressure drops and immediately stabilizes. Data collected with the empty tank shows pressure dropping below the stabilization pressure and increasing to the stabilization pressure after about 3 seconds. The pressure recovery relates to the equilibration of the gas in the tank to its initial temperature (before the pressure drop). **Figure 4.5** suggests that inserting a fiberglass heat capacitor into the source tank removes the thermodynamically induced pressure anomaly.

Not all measurements made with fiberglass in the reservoir show an increase in the slope of the diagnostic plot as the measurement progresses. The anomalous change in slope is much more pronounced in high permeability materials. **Figure 4.6A-C** shows diagnostic plots for three different materials: (A) Berea Sandstone ($k \approx 8 \times 10^{-13} \text{ m}^2$), (B)

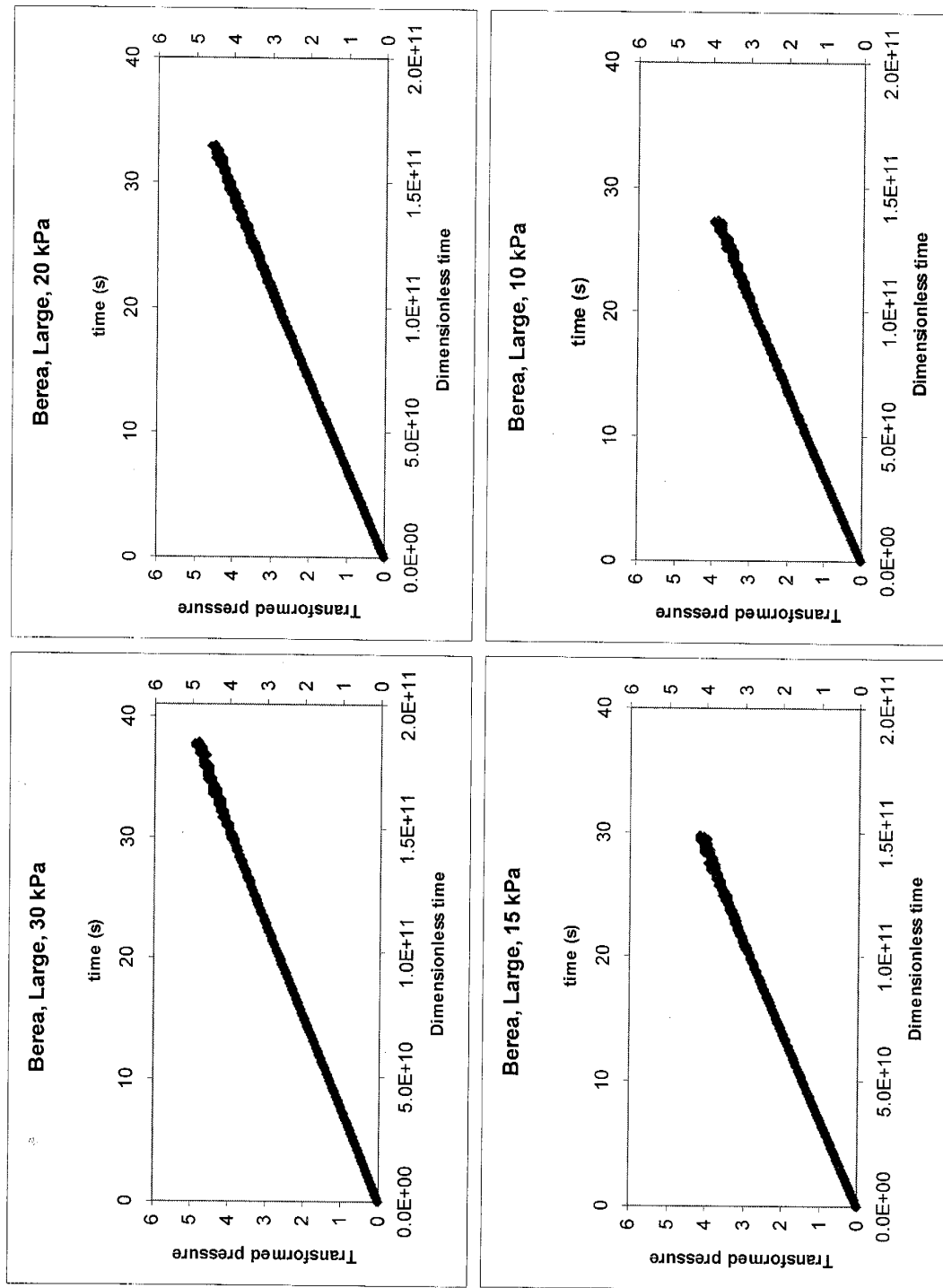


Figure 4.6A. Diagnostic plots for Berea Sandstone. Title refers to material, tank size, and initial tank gauge pressure.

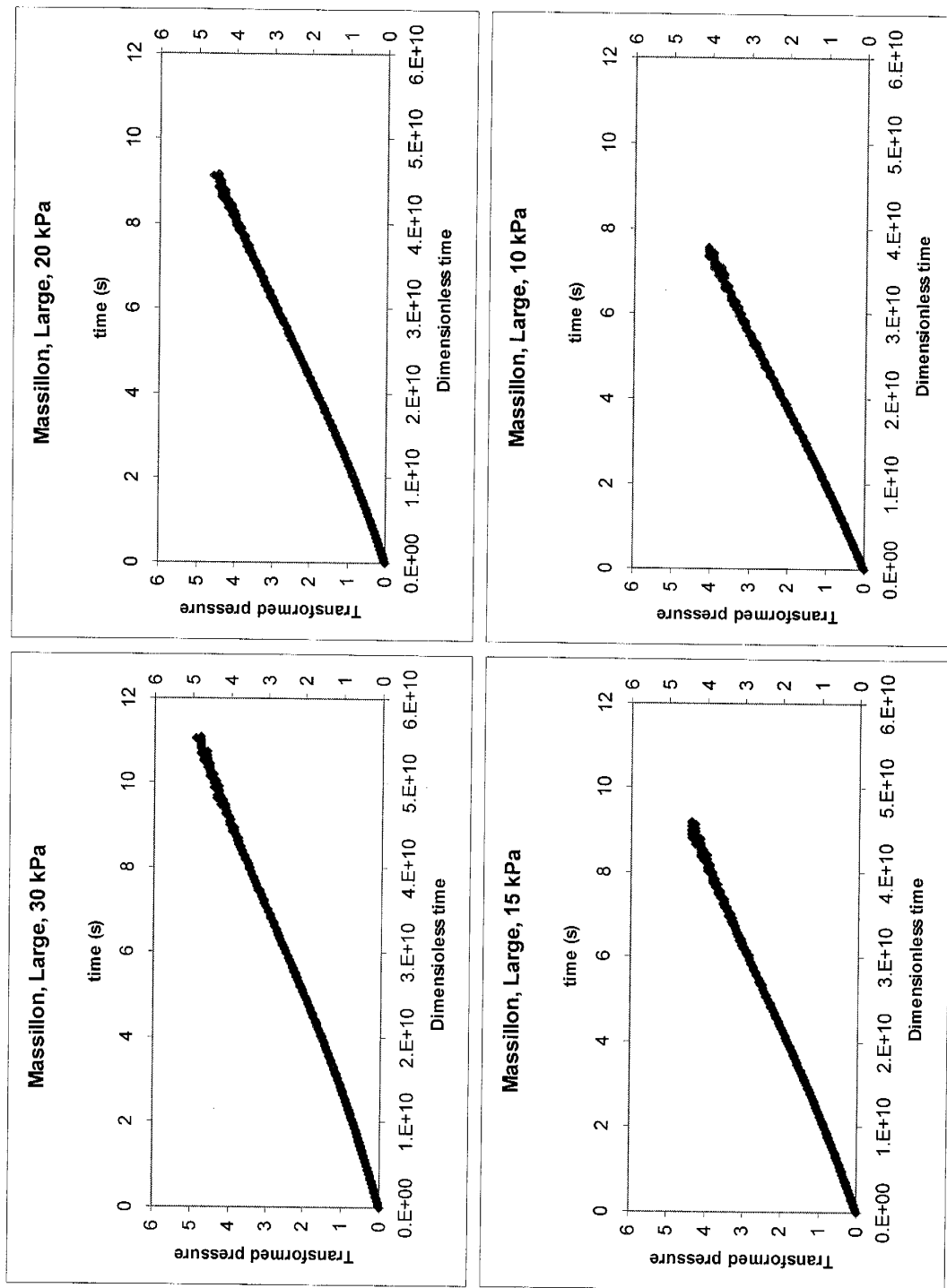


Figure 4.6B. Diagnostic plots for Massillon Sandstone. Title refers to material, tank size, and initial tank gauge pressure.

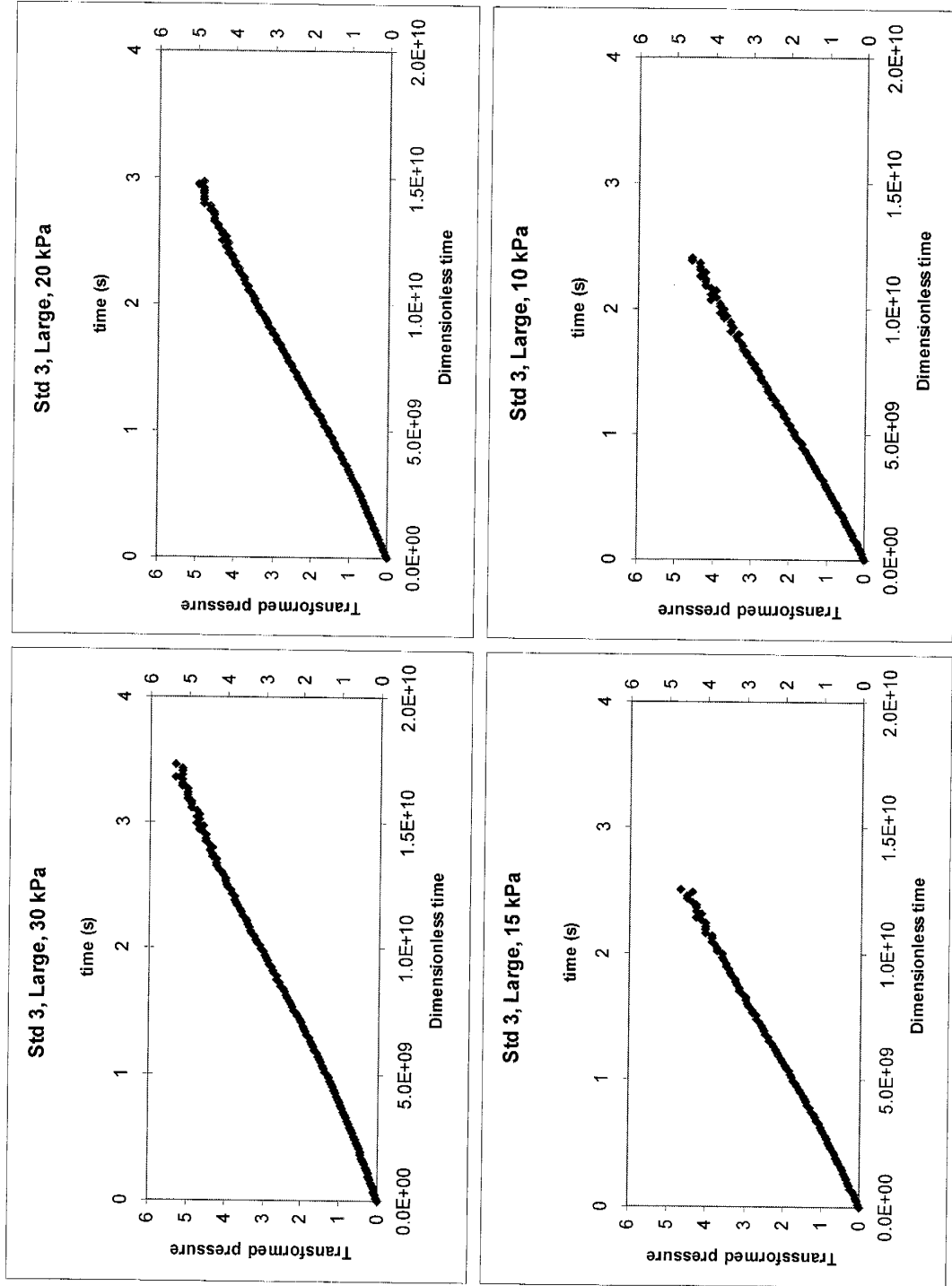


Figure 4.6C. Diagnostic plots for Standard 3. Title refers to material, tank size, and initial tank gauge pressure.

Massillon Sandstone ($k \approx 3 \times 10^{-12} \text{ m}^2$), and (C) permeability Standard 3 [Davis et al., 1994] ($k \approx 1 \times 10^{-11} \text{ m}^2$). Pressure decay measurements were made, using the large reservoir, on each of the three materials at four different initial tank pressures (gauge): 30, 20, 15, and 10 kPa. A similar set of diagnostic plots for measurements made with the small reservoir are located in Appendix 4. The increase in slope was only noticeable for the Massillon Sandstone and Standard 3, which are the two higher permeability materials.

Focusing on the diagnostic plots for either the Massillon Sandstone or Standard 3, the change in slope is most pronounced in measurements made at high initial pressures and becomes less noticeable for measurements made at lower initial pressures. There is also a noticeable difference in the duration of the measurement as a function of initial pressure; the higher the initial pressure, the longer the duration of the measurement.

4.6.2 Derivative Plots

If the diagnostic plot (**Figures 4.3 and 4.6**) has linear segments, its slope or derivative should be constant. Satisfactorily laying a straight edge to the segment, or matching it with a linear regression, indicates that the behavior fits our model (4.23). Using these measures we find that the later time behavior in all of the plots in **Figures 4.3 and 4.6** appear to be straight lines. A more exacting probe for inspecting this behavior is the local value of the slope, which can be determined from a local time derivative and also plotted versus time, or vs. another variable. It is particularly instructive to plot the local time derivative vs. pressure. The numerical derivative with respect to time of the transformed pressure, $\ln\left(\frac{P_i - P_0}{P_i + P_0} \frac{P + P_0}{P - P_0}\right)$, was calculated using a beta version of the nSights well test analysis software. The derivative algorithm used was that of Clark and

van Golf-Racht [1985]. For comparison across materials, derivatives were normalized by taking the ratio of the derivative to permeability values estimated using the LSAMP II. Permeability was used for normalization because, ideally, it is the only model parameter (for a given initial pressure, see Equation 4.21) that differs across materials. The normalized derivatives were then plotted against (1) time and (2) the corresponding reservoir pressure to investigate possible dependence of the change in slope on these two parameters. If the diagnostic plots (**Figures 4.3** and **4.6**) truly have constant slopes over a segment then their local time derivatives should also be constant. Similarly the derivative should be constant over the corresponding range of pressures.

The transformed pressure derivatives vs. time (**Figure 4.7A-C**) and reservoir pressure (**Figure 4.8A-C**) for the three sample materials are shown for comparison. Derivative plots for measurements made with the small reservoir are located in Appendix 4. Scatter in the derivative at late time and low pressure is due to transducer noise and can be safely ignored. If the stabilization of the slope on the diagnostic plot is pressure or time related, the derivatives (for all initial pressures) should converge to a constant value at the pressure or time in which the slope stabilizes.

The Berea Sandstone fits the model the best, with an apparently linear diagnostic curve (**Figure 4.6A**). The local time derivative, whether plotted vs. time (**Figure 4.7A**) or pressure (**Figure 4.8A**), is essentially constant once a startup transient passes (with an initial rapid decrease in the derivative). The derivatives for the Massillon Sandstone and Standard 3 do not have constant derivative segments. When plotted vs. time (**Figure 4.7B&C**), the derivatives for the Massillon Sandstone and Standard 3 show an initial rapid drop in the derivative due to the startup transient, then the derivatives steadily

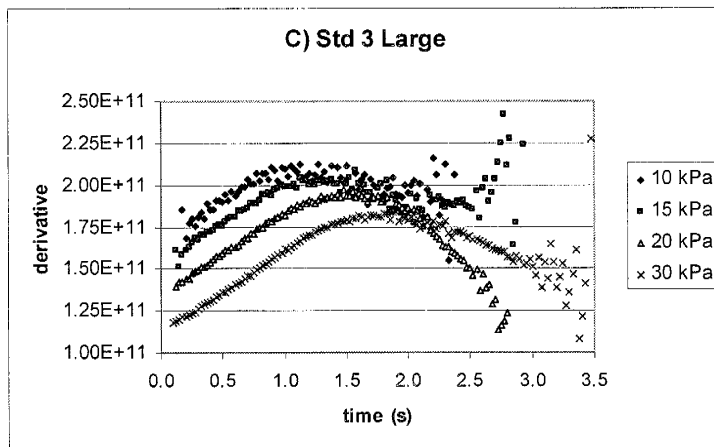
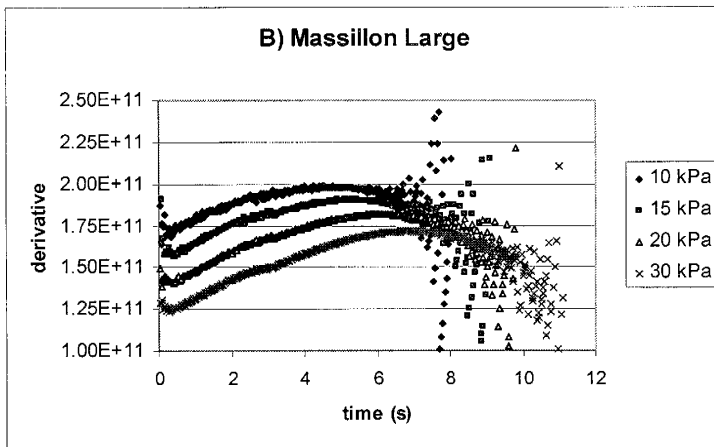
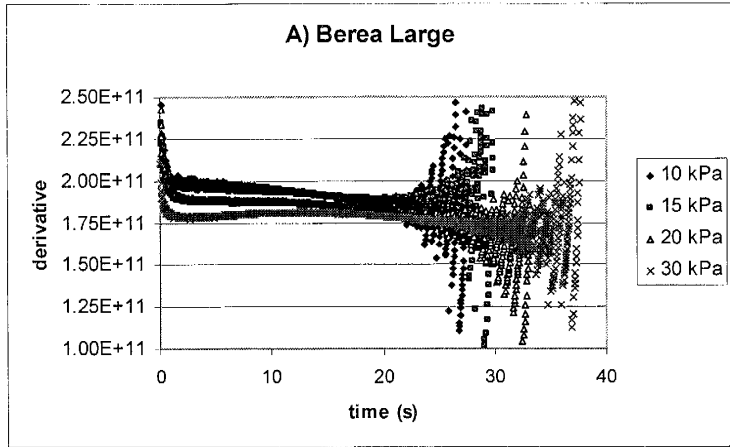


Figure 4.7. Transformed pressure derivative vs. time plots for (A) Berea Sandstone, (B) Massillon Sandstone, and (C) Standard 3. The derivative axis is stretched to accentuate differences between data collected at different initial pressures. Large in title refers to the tank used.

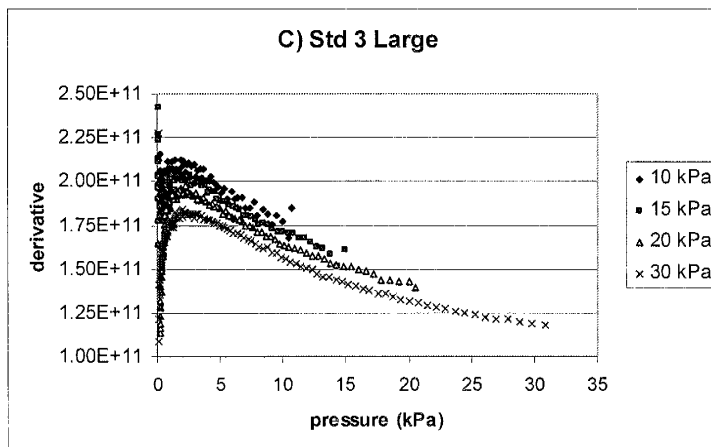
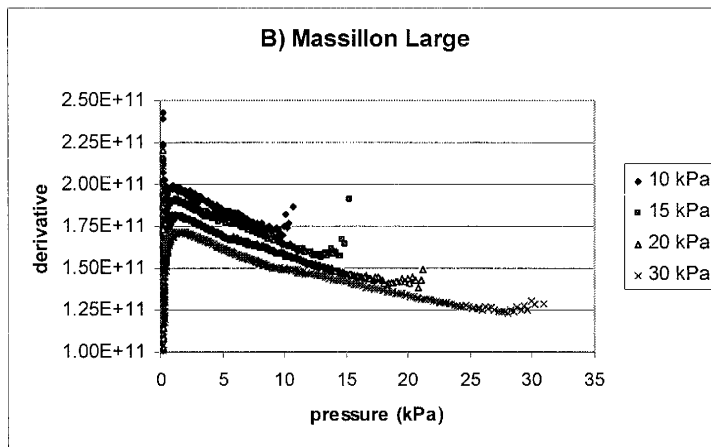
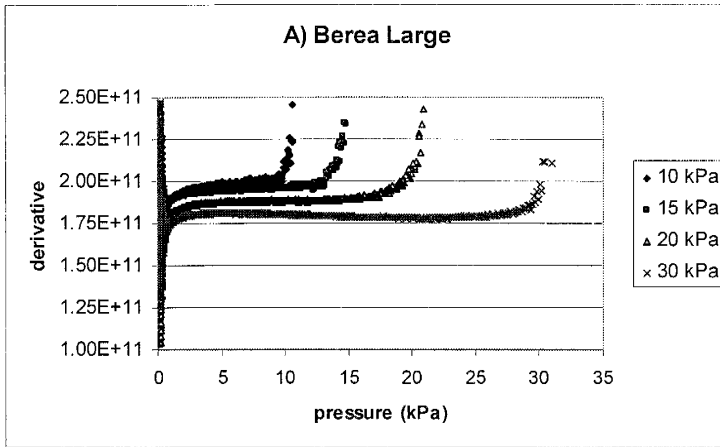


Figure 4.8. Transformed pressure derivative vs. pressure plots for (A) Berea Sandstone, (B) Massillon Sandstone, and (C) Standard 3. The derivative axis is stretched to accentuate differences between data collected at different initial pressures. Large in title refers to the tank used.

increase, reach some peak value, and then slightly drop off to noisy data. The peak in the derivatives occurs at different times for different initial pressures, equating to the change in slope occurring faster for lower initial pressures. For the same two materials, the derivatives plotted vs. pressure (**Figure 4.8B&C**) quickly decrease during the initial transient, then slowly increase as pressure decreases, achieve a maximum value, and rapidly decline to noisy data.

There is much more agreement in the location of the maximum derivative as a function of pressure, across data recorded at different initial pressures, than as a function of time. This correlation suggests that the change in slope is a pressure dependent phenomenon. The derivative peaks at a pressure of: ~ 1.5 kPa for Massillon Sandstone and ~ 2.25 kPa for Standard 3. For samples with a changing derivative, the pressure at which the derivatives peak is diagnostic of a characteristic behavior.

The normalized derivative vs. pressure for measurements started at 30 kPa on all samples is shown in **Figure 4.9**. The normalized value of the derivatives for Massillon Sandstone and Standard 3 appear to approach the normalized value of Berea Sandstone as pressure drops. Since the derivative for Berea Sandstone is fairly constant after the initial decrease, it is hypothesized that the normalized derivative value of the Berea represents linear behavior. It follows that the coincidence of the peaks in the other two derivatives with the derivative value of the Berea represents the onset of linear behavior (i.e. a constant slope) for the Massillon Sandstone and Standard 3. The following section discusses potential factors responsible for the curvature in the diagnostic plot.

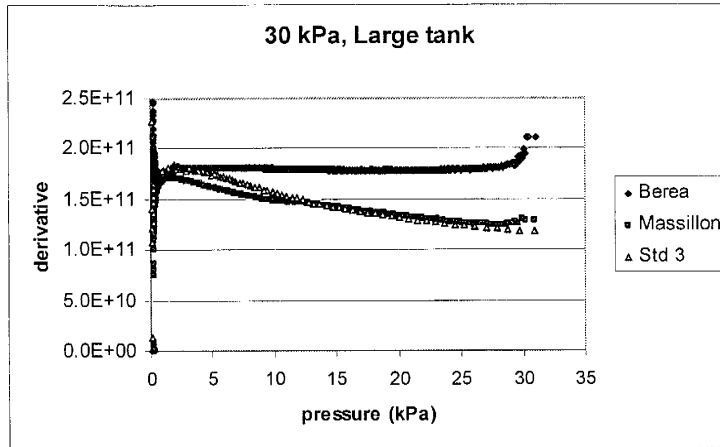


Figure 4.9. Transformed pressure derivative vs. pressure for all samples. The initial tank pressure (gauge) was 30 kPa for all samples.

4.6.3 Nonlinear Flow

The presence of pressure dependent curvature in the diagnostic plot for the Massillon Sandstone and Standard 3 implies that the model is violated at high pressure for these materials. An increasing slope on the diagnostic plot suggests pressure is decaying slower in the reservoir than the model predicts or in other words the model would underestimate permeability. The flow rates produced during the measurement are a function of injection pressure and tip seal geometry (along with the gas properties). High injection pressures correspond to high flow rates. The flow rate just below the tip seal increases as the ratio of outer to inner tip seal radii decreases (for a given inner radius) due to higher pressure gradients. Nonlinear behavior at high pressure could be explained by the transition to turbulence and violation of Darcy's Law. To test for presence of high velocity non-Darcian behavior, steady-flow measurements were made across a range of pressures for each of the materials using the continuous flow permeameter.

Steady-flow measurements were made for which tip seal injection pressure was monitored using a pressure transducer and flow rate was measured using a series of rotameters. A 2:1 tip seal (outer to inner radii) with an inner radius of 3 mm was used for all measurements. Though a 4:1 tip seal would decrease the propensity for non-Darcian flow, the 2:1 tip seal has a smaller sample volume and was used to minimize effects of sample boundaries. Darcy's Law is valid when there is a linear relationship between the flow rate and gradient (pressure). The flow rate and corresponding pressure data are plotted for each material in **Figure 4.10A-C**. A line showing a linear relationship between the flow rate and pressure was also plotted for reference to Darcian behavior. The line was derived using the steady-flow model (see Equation 1.2). Equation 1.2 was solved for flow rate, Q , given the measured pressure and an independent permeability estimate made with the LSAMP II. The experimental data for the Berea Sandstone (**Figure 4.10A**) agrees well with Darcy's Law, with slight deviation at pressures above 25 kPa. The Massillon Sandstone and Standard 3 both deviate from linear behavior. At higher pressure measured flow rates were less than would be expected for Darcian behavior. It is proposed that the lower flow rate and non-linear deviation from Darcy's Law are due to inertial effects resulting from the transition to turbulent gas flow.

Deviation from Darcy's Law occurs at a pressure (gauge) of ~ 3.5 kPa for the Massillon Sandstone, and at ~ 1.5 kPa for Standard 3. Though there is some discrepancy, these values agree fairly well with the pressure at which the derivative plots peaked (~ 1.5 kPa for Massillon Sandstone and ~ 2.25 kPa for Standard 3). Variability in the pressure for which nonlinear effects occur (for a given material) is likely due to differences in the dynamics of the two measurement techniques.

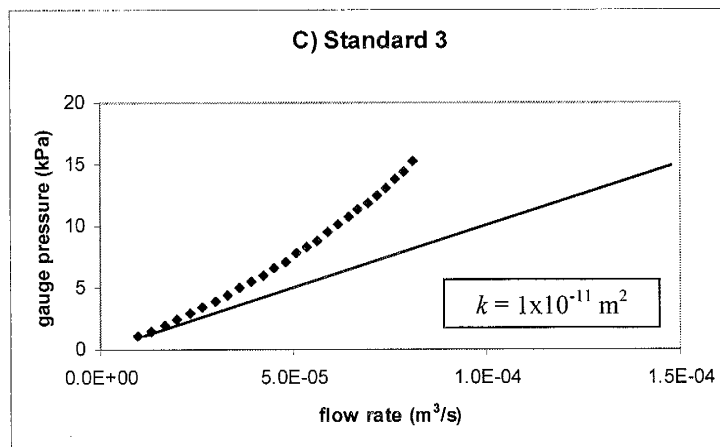
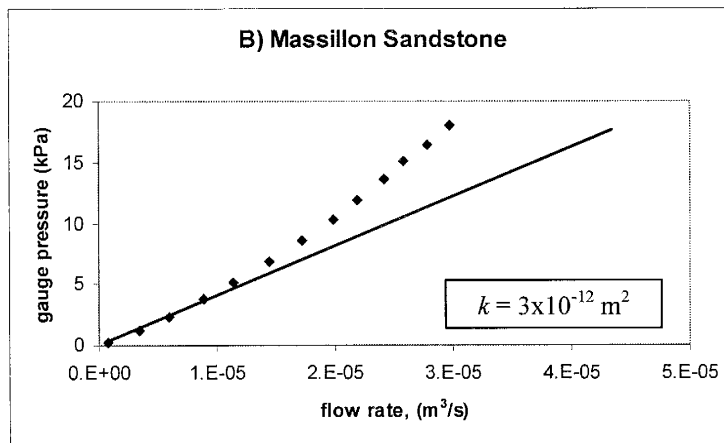
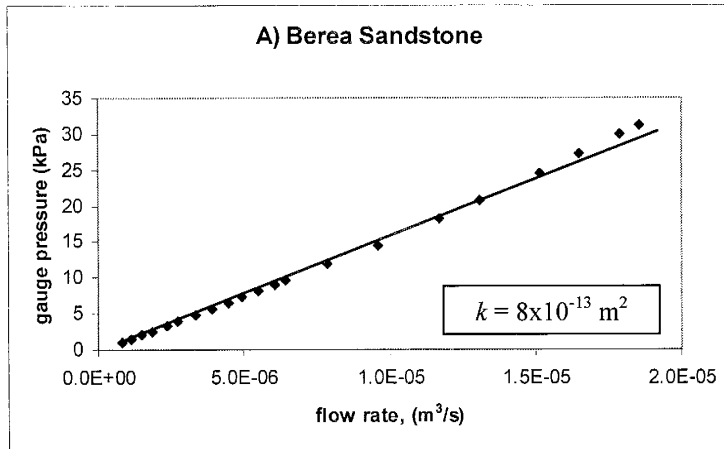


Figure 4.10. Evaluation of possible non-Darcian behavior for: (A) Berea Sandstone, (B) Massillon Sandstone, and (C) Standard 3.

Two Reynolds numbers were calculated to determine the value for which deviation from Darcy's Law occurred: (1) a Reynolds number for flow in the tip seal (before entering the rock) and (2) a Reynolds number for flow in the porous medium. The Reynolds number, Re , is given by

$$Re = \frac{\rho v d}{\mu}, \quad (4.24)$$

where ρ is the fluid density, v is the mean Darcy velocity, d is a characteristic length, and μ is the fluid viscosity. The mean velocity was calculated by dividing the measured volumetric flow rate by the cross-sectional area of the tip seal. The velocity varies both in the pipe and the porous medium. In the tip seal, the velocity reaches a maximum at the tip's center (with a minimum at its radius), while once in the rock, the maximum velocity is at the tip seal radius (with a minimum at the center).

The Reynolds number upstream of the porous medium (in the tip seal) was calculated for flow through a pipe, using the tip seal inner diameter as the characteristic length. For flow through a smooth, straight pipe, the transition to turbulence occurs at a Reynolds number of ~ 2000 . Even at the highest flow rate observed ($8.1 \times 10^{-5} \text{ m}^3/\text{s}$, Standard 3) the calculated Reynolds number was 1150, suggesting flow was laminar in the tip seal for all experiments.

The Reynolds number in rock was calculated using \sqrt{k} as the characteristic length. It is often cited that the transition to turbulent flow in porous media occurs at Reynolds numbers between 1 and 10, however the characteristic length for this Reynolds number is based on the average grain diameter. Dullien [1992] refers to departures from

laminar flow occurring at Reynolds numbers (where \sqrt{k} was the characteristic length) as low as 0.04 for compressible gas flow through porous media. The deviations from Darcy's Law (see **Figure 4.10 B&C**) occurred at Reynolds numbers of 0.05 for Massillon Sandstone and 0.10 for Standard 3. Figure 4.10 and Reynolds number calculations both suggest deviation from laminar flow at relatively low pressure in high permeability materials.

4.6.4 Comparison of Pressure Decay and Steady-Flow Methods

In order to estimate permeability using the slope of the diagnostic plot a decision had to be made as to which portion of the data (what range of pressures) should be used. Derivatives and continuous flow permeability measurements suggest that almost all of the pressure data for the Berea Sandstone can be used in the permeability calculation. Nonlinear effects occur at higher pressures in the Massillon Sandstone and Standard 3. Using all of the pressure data (the whole diagnostic plot) for these materials would result in a biased low permeability estimate.

Figure 4.11 shows the pressure dependence of all three materials on estimated permeability for measurements made with the continuous flow permeameter. As suggested by other analyses, nonlinear effects are negligible (5% difference between highest and lowest pressure) for the Berea Sandstone. Nonlinear effects in the Massillon Sandstone and Standard 3 result in much greater permeability dependence on pressure. Permeability pressure dependence ceases at the pressure for which nonlinear effects become significant (~3.5 kPa for the Massillon Sandstone, and at ~ 1.5 kPa for Standard 3). There is a significant difference in high and low (no nonlinear effects) permeability estimates: 28% difference in Massillon Sandstone and 36% difference in Standard 3.

When estimating permeability using the slope of the diagnostic plot some data has to be excluded for each of the materials. For all three materials the late time data (pressure less than 0.2 kPa) is excluded to filter the effect of transducer noise. The remaining data is used to calculate permeability for the Berea Sandstone. All data for which non-linear effects are noticeable should be omitted from Darcy flow model permeability calculation (Equation 4.21) for the Massillon Sandstone and Standard 3. The pressure at which this occurs was determined using two methods: the pressure derivative and using the continuous flow permeameter. The average pressure above which nonlinear flow occurs in each material was: 2.5 kPa for the Massillon Sandstone and 1.875 kPa for Standard 3. All pressure decay data above these pressures is excluded when calculating permeability using the slope of the diagnostic plot.

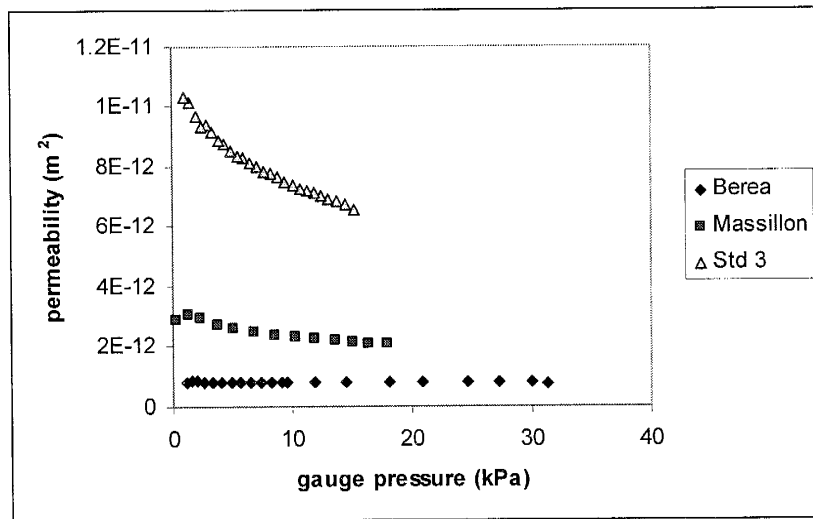


Figure 4.11. Estimated permeability dependence on injection pressure at the tip seal of a steady-flow permeameter, where permeability is estimated using Darcy's Law, ignoring non-linear effects.

With this filter on the data, continuous flow permeameter and LSAMP II measurements were made on each of the three materials for comparison with pressure decay measurements made with the large and small tanks at four initial pressures: 10, 15, 20, and 30 kPa. The tip seal ($r_i = 3\text{mm}$, $r_o/r_i = 2$) was clamped to the material for all measurements to assure the same volume of rock was interrogated.

Table 4.1 shows permeability estimated (m^2) using large (L) and small (S) tank pressure decay measurements, the continuous flow permeameter, and the LSAMP II. The range of pressures used to calculate pressure decay permeabilities varied with material: Berea ($1-p_i$ kPa), Massillon (0.2-2.5 kPa), and Standard 3 (0.1-2 kPa). Continuous flow permeability values are the average value for measurements made at different pressures. The range of pressures used is dependent on the material: Berea (1-30 kPa), Massillon (0.3-3.75 kPa), and Standard 3 (1-2 kPa). The number of measurements that were made at these ranges also depends on the material due to accuracy and precision limitations of the equipment; Berea ($n = 20$), Massillon ($n = 4$), Standard 3 ($n = 3$). The LSAMP II value is the average of three measurements, all at relatively the same pressure: Berea (1.36 kPa), Massillon (1.34 kPa), and Standard 3 (1.32 kPa).

Overall there is fairly good agreement between transient pressure decay and steady-flow (continuous flow and LSAMP II) permeability estimates. The steady-flow methods produce similar results. A few noticeable trends exist in the permeability estimates:

- (1) Pressure decay permeability estimates are consistently lower than steady-flow permeability values, even for the Berea Sandstone.

- (2) For a given initial pressure, measurements made with the small tank produce lower permeability values than corresponding value for the large tank.
- (3) Pressure decay measurements started at a higher initial pressure yield lower permeability estimates.

Table 4.1. Comparison of pressure decay permeability estimates (m^2) with two steady-flow methods: syringe-based (LSAMP) and continuous flow (CFP) permeameters.

sample	P_0 (kPa)				LSAMP	CFP
	10	15	20	30		
Std 3 L	9.83E-12	9.58E-12	9.24E-12	8.88E-12		
Std 3 S	9.65E-12	9.44E-12	9.14E-12	8.75E-12	1.12E-11	1.00E-11
Mass L	2.85E-12	2.66E-12	2.68E-12	2.45E-12		
Mass S	2.69E-12	2.60E-12	2.56E-12	2.50E-12	3.01E-12	2.92E-12
Berea L	7.35E-13	7.24E-13	7.08E-13	6.88E-13		
Berea S	7.22E-13	7.11E-13	7.00E-13	6.77E-13	7.87E-13	8.08E-13

The consistent difference between pressure decay and steady-flow permeability estimates could be the result of experimental error. A small error in the calibration of the tank volume could cause a low bias in the permeability estimate. For pressure decay measurements with fiberglass in the tank, the volume is the difference of the empty tank and fiberglass volumes. Any systematic error in the determination of either of these volumes would bias the permeability estimate. If the actual tank volume were larger than the calibrated volume, the permeability estimates for the pressure decay permeameter would fall closer to the steady-flow permeabilities. The volume used to estimate permeability should also include the tip seal volume and the volume of tubing connecting the pressure transducer. The calibration of the empty tank volume (including the tip seal

and tubing volumes) was performed by filling the tank with water, taking the difference in the full and empty tank weights, and calculating a volume (Equation 4.22). It is possible that the tank and/or tubing were not completely filled with water during volume calibration. If a small amount of air were to get trapped in the tank, the calibrated volume would be less than the actual volume. Calculations suggest a 3% (~10 cm³) underestimate of the tank volume would explain this bias.

The difference in permeability estimates for measurements made with the small and large tanks can also be explained by possible experimental error. It is quite possible that air was trapped in the tank when both tank volumes were calibrated. It is also likely that if air were to get trapped during calibration, the volume of air trapped would be relatively constant regardless of tank size. A given volume of air trapped in the tank would take a larger percentage of the total volume in the smaller tank, in increase the amount of bias in the permeability estimate.

The consistent decrease in estimated permeability with increasing initial tank pressure is more difficult to explain (see also the different peaks in the derivative plots in **Figures 4.7** and **4.8**). For steady-flow measurements, as pressure increases and Darcy's Law breaks down estimated permeability decreases (**Figure 4.11**). For all materials showing nonlinear behavior, the pressure decay permeability value is estimated using pressures for which Darcy's Law should be applicable, and thus the nonlinearity should not be a factor. The trend of decreasing permeability with increasing initial pressure is even noticeable in the Berea Sandstone estimates for which no nonlinear behavior was observed (see also **Figure 4.8A**). The behavior causing this consistent trend has a fairly large time constant. Gas compressibility in the porous media would result in an inverse

trend (higher permeability estimates for higher pressures). One possible explanation is lingering thermodynamic effects in the porous media. For higher initial pressures the gas flow rate into the rock is initially higher. This could cause heating of the gas in the rock resulting in higher gas viscosity, more resistance to flow, and a lower permeability estimate.

4.6.5 Instrument Range

The pressure decay permeameter's capability for measuring over a wide range of permeability was investigated using two materials: Standard 3 and a low permeability sandstone. A major goal of the permeameter design was to have the capability of measuring permeability over five orders of magnitude with the duration of the measurement taking less than 20 seconds. Equation (4.24) shows the governing equation (4.21) solved for the duration of the measurement.

$$\Delta t = \frac{V_T}{r_i G_o \left(\frac{r_o}{r_i}\right)} \frac{\mu}{P_0} \frac{1}{k} \ln \left(\frac{P_i - P_0}{P_i + P_0} \frac{P + P_0}{P - P_0} \right). \quad (4.25)$$

Three model parameters (other than permeability) control the duration of a measurement: (1) tip seal geometry, (2) tank volume, and (3) initial tank pressure. The control of tip seal geometry on measurement duration was discussed in Chapter 3. It was concluded that even though increasing the inner radius of the tip seal decreases measurement duration, a practical limit exists for the size of the inner radius that can be used on the materials of interest. Measurement duration for high permeability materials is small even for low initial pressures and large tank sizes, so low permeability materials are the focus of decreasing the measurement duration. A similar size limit exists for the tank volume. A very small volume would make measurements fast, but would have

significant effect on the accuracy and precision of the device. Initial pressure is the only parameter considered to provide control of measurement duration for low permeability materials.

Measurement duration could also be reduced by employing a high precision transducer. None of the transducers used for these experiments were accurate within approximately 0.1 kPa. Since the transducer does not accurately sense small changes in pressure, data recorded at higher rates of pressure decay are more reliable. If the transducer could precisely and accurately measure small changes in pressure, data measured across much smaller pressure drops could be used to estimate permeability.

If running a measurement to atmospheric pressure was a requirement, using a high initial pressure would not decrease the measurement duration, but in fact increase it. If the diagnostic plot does not exhibit an anomalous curvature, any portion of the data can be used to estimate permeability. Nonlinear effects occur at high pressures in high permeability materials. For Darcy's Law to be satisfied, permeability should be estimated using the low pressure data for these materials. Using high initial pressures on low permeability materials increases the rate of pressure decay at the beginning of a measurement. A relatively high rate of pressure decay reduces the effect of transducer noise on the data. Starting measurements at high pressures and using only a small portion of the early time data could significantly increase the low end of the measurement range.

The high end of the measurement range was determined to be the permeability of Standard 3, approximately $1 \times 10^{-11} \text{ m}^2$. Even with the large volume tank, measurement duration (for Standard 3) from an initial pressure of 5 kPa to atmospheric pressure was 2 seconds. Nonlinear flow effects would be a factor at low pressures for permeabilities

higher than this, and the accuracy of the instrument would be jeopardized. The instrument could be modified to extend the range upward. Decreasing the tip seal size would help, but it would also lower the porous media support of the measurement, which is inappropriate for higher permeability sediments which have larger pores. Increasing the tank volume presents physical size constraints for a field portable device.

To test the low end of the measurement range, pressure decay measurements were made on a low permeability sandstone. Pressure decay permeability estimates were then compared to estimates made with the continuous flow permeameter. The pressure decay measurement was made with the small tank at an initial pressure of 30 kPa. After the valve was opened, the time required for the tank pressure to decay to 1.9 kPa (the measurement was stopped here) was 30 minutes. Using all of the data collected over the 30 minute duration, permeability was estimated to be $3.12 \times 10^{-15} \text{ m}^2$. 30 minutes is much too long for a measurement in the field, so it was decided to use the data collected from the initial pressure (30 kPa) to a pressure of 28 kPa. A high initial pressure was used to maximize the rate of pressure decay in the tank (reduce transducer noise) for a small pressure drop. Measurements on low permeability materials could be made at lower initial pressures with a smaller pressure drop if a more accurate and precise transducer was used. The 2 kPa pressure drop required 27 seconds. Permeability estimated from this data was $3.02 \times 10^{-15} \text{ m}^2$. The estimate using 30 minutes of data and 27 seconds were only different by 3%. The continuous flow permeameter permeability estimate was $3.23 \times 10^{-15} \text{ m}^2$, which is 3.5% greater than the value using 30 minutes of data, and 7.5% greater than the value for 27 seconds of data. The differences between transient pressure

decay and steady-flow permeability estimates are consistent with the differences noted in the above comparison (steady-flow $k >$ transient k).

4.7 Conclusions

The objective of this research was to design, fabricate, and test a transient pressure decay permeameter for use in the field. It was motivated by the need of a new method for rapidly acquiring permeability estimates in the field across many orders of magnitude. The work included development of a mathematical model and designing a prototype permeameter for model validation. Testing of the pressure decay permeameter included investigating the effect of reservoir volume and initial tank pressure on the duration (practical range) of a measurement for four different porous materials. Steady-flow permeability estimates were made on three materials for comparison with the pressure decay values.

4.7.1 Model Validation

Pressure decay data is presented using the diagnostic plot (see Equation 4.23). If the model assumptions are not violated the diagnostic should be linear, and permeability can be estimated from the slope. If the plot is linear, only a small percentage of the pressure decay data needs to be collected to estimate permeability. Deviations from linearity on the diagnostic plot are used to identify anomalous behavior.

Two anomalous curvatures were noted in the diagnostic plot; one in which the slope decreased, and one that increased, after the early time data. The decreasing slope is attributed mainly to thermodynamic effects in the tank and pressurization of the downstream portion of the valve at the start of a measurement. Inserting a heat capacitor

in the tank dampens thermodynamic effects. The increasing slope is only noticeable for the two highest permeability materials (Massillon Sandstone and Standard 3). An increasing slope on the diagnostic plot equates to pressure decaying slower in the early time than predicted by the model. Two methods are used to investigate the possibility of nonlinear behavior: (1) calculation of numerical derivatives for transformed pressure, and (2) recording steady-flow measurements across a range of pressures, monitoring flow rate to check the validity of Darcy's Law. Both methods show deviations from linear behavior occurring at a specific pressure: 2.5 kPa for the Massillon Sandstone and 1.875 kPa for Standard 3.

Pressure decay permeability estimates were made using a large (388 cm³) and small (123 cm³) tank at four initial tank pressure for comparison with two steady-flow methods (continuous flow permeameter and LSAMP II). Permeability values were calculated using only the pressure data for which Darcy's Law applies. Pressure decay measurements made with the large tank consistently yield higher permeability estimates than the small tank. The difference in permeability values acquired by the two tanks could be explained by possible error in the calibration of the tank volumes. The steady-flow estimates agree well with one another, but pressure decay permeability values are systematically less than steady-flow values. This too could be explained by error in calibration of the tank volume. Pressure decay measurements made at higher initial pressure consistently yield lower permeability values. There is lack of hard evidence to provide an explanation for this anomaly. We speculate that the behavior is not the result of nonlinear and/or compressibility effects due to their relatively fast time constants. A possible explanation is the presence of thermodynamic effects in the porous media.

When the valve is opened, the gas pressure in the porous media jumps in response, heating the gas. As the gas heats up, its viscosity increases, increasing resistance to flow and reducing the rate of pressure decay. The heat capacity of the solid attenuates this effect, but if the initial pressure jump is large enough, it will be noticeable. The gas will also be heated by friction. Higher initial pressures result in higher flow rates at the beginning of the measurement. Increased frictional heating for higher velocity flow could cause a lingering temperature effect, which together with the thermodynamic effect would result in relatively slower pressure decay for higher initial pressure measurements.

The pressure decay permeameter is clearly capable of measuring over approximately (1×10^{-11} – 3×10^{-15} m²) four orders of magnitude permeability with all measurements requiring less than 30 seconds. The time required to make a measurement on high permeability materials is very short, and must be started at lower pressure to assure nonlinear effects are not a factor. While the low end of the range (1×10^{-15} m²) is the lowest we tested, the instrument should be capable of lower measurements by using a smaller pressure drop, or larger time between pressure observations. Inspection of the diagnostic plot verifies permeability can be calculated using only early time data, which significantly decreases the required measurement duration. For pressure decay measurements starting at an initial pressure of 30 kPa on a low permeability sandstone, the difference between using 30 minutes and 27 seconds of data is 3%. The 30 minutes of data records pressure dropping to 1.9 kPa, while the 27 seconds of data only goes to 28 kPa. This suggests that for low permeability materials starting measurements at high initial pressures (for faster rate of pressure decay) and recording only the early pressure data does not introduce significant error.

4.7.2 Recommendations for Future Work

More work is required before a field portable pressure decay permeameter can be constructed. Specifically, four questions must be addressed:

- (1) How will the tank be pressurized during field use?
- (2) What type of valve should be used on the tank, and where will it be located?
- (3) How will pressure and time data be acquired in the field?
- (4) What pressure ranges will be necessary to measure across five orders of magnitude permeability?

For all measurements made thus far, the tank has been pressurized using compressed nitrogen. Using a compressed gas tank in the field greatly inhibits the portability of the pressure decay instrument, and robs it of the advantages it holds over a conventional steady-flow device, which also uses a compressed gas tank. Potential methods for pressurizing the tank in the field are: (1) using a hand pump or (2) a battery operated miniature air pump. Using a hand pump would decrease the amount of power required to run the permeameter, but would most likely increase the overall bulk of the materials needed in the field. A miniature air pump (golf ball size) is used in the LSAMP II to fill the syringe with air at the beginning of a measurement. A similar pump could be used, but it would have to work at much higher pressures and likely require an air filter to prevent dust from entering the tank.

The type of valve and its placement are issues with the prototype device. A manually opening lab cock ball valve is used in the prototype design. Though the valve can be opened easily and rapidly, it would be more advantageous to use an (electronic)

solenoid valve to provide consistency in opening speed. The more serious issue with valve selection is the volume of gas between the valve and the material surface which remains un-pressurized until the valve opens. Care should be taken in selecting a valve that minimizes this volume and the initial pressure drop at the onset of a measurement.

Two options are available for recording pressure and time data in the field. A data logger could be used and pressure/time data could be recorded as it was during the instrument testing. Using a data logger should be avoided if possible, it would significantly increase the size and production cost of the instrument. An alternative method would be to program a circuit to measure the time it takes for the tank pressure to decay across a known pressure drop. Multiple pressure ranges could be made available to retain the instrument range and avoid nonlinear flow effects.

Using multiple pressure ranges to accommodate a wide permeability range requires some additional testing. A major task would be determining in the field when nonlinear flow is likely to occur as a function of initial tank pressure. Permeability estimates made with data exhibiting nonlinear effects are no less than 50 % of the true permeability (62% for Massillon, large tank, $p_i = 30$ kPa). The Reynolds numbers calculated for the steady flow measurements (Section 4.6.3) could be used to determine a threshold permeability for which nonlinear effects should be negligible, given a prescribed pressure drop. Permeability estimates in the field could be checked against this threshold permeability, for the given pressure drop, to determine the likelihood of nonlinear effects. If a nonlinear effect is suspected for a particular pressure range, the operator could then set the instrument to use the next lowest pressure drop and repeat the process until the correct pressure is used.

CHAPTER 5

CONCLUSIONS

The main goal of this research was to assess and improve the operational characteristics of gas permeameters, with particular focus on rapid field-collection of permeability data across a wide range. This task included three more focused studies, to which Chapters 2-4 are dedicated. Chapter 2 is a comparison of the original LSAMP and design improvements made with the LSAMP II as they apply to measurement repeatability when measurement averaging, and also includes an analysis of instrument error on measurement variability. Chapter 3 presents the testing of modifications to the LSAMP II and investigating their effects of measurement duration. Chapter 4 discusses the development, fabrication, and testing of a new transient pressure decay permeameter, with particular focus on measurement duration and range. Thorough discussion of results and conclusions are provided in the respective chapters.

5.1 Gas Permeameter Operation

The main focus of the work presented in Chapter 2 was to assess the effects of modifications made the LSAMP in the design of the LSAMP II. Many of the results from the comparison of the LSAMP and LSAMP II apply to operation of all gas

permeameters that use a tip seal. Making repeated measurements at a point (measurement averaging) is commonly practiced by operators of permeameters requiring tip seal injection. There are two separate motivations for taking the mean value of 3-5 measurements at a point: (1) reduction of instrument noise and (2) averaging small-scale permeability heterogeneities.

Results of the LSAMP comparison study suggest that when averaging measurements, removing the tip seal between measurements causes a significant increase in measurement variability. This increase in variability is due to small changes in the volume of rock interrogated by the permeameter each time the tip seal is removed and replaced between measurements. Gas permeameters are extremely sensitive to the area just below the tip seal, so even slight changes in tip seal position can result noticeably different permeability estimates. If measurements are made with a noisy instrument, the variability noticed when the tip seal is moved will be a combination of instrument noise and permeability heterogeneity. For measurements made (with tip seal movement) with a more precise instrument, variability between measurements will be almost entirely the result of permeability heterogeneity.

Instrument error for the LSAMP II was found to be a minor contribution to measurement variability for most permeability materials. This suggests making repeated measurements at a point to decrease instrument noise is unnecessary and possibly a waste of time. As the extreme high end of the LSAMP II's measurement range is approached, instrument error could play a larger role in measurement variability and averaging point estimates should be considered when making measurements in this range.

5.2 LSAMP II Modification

The unmodified LSAMP II can only measure two orders of magnitude permeability due to practical time constraints. The goal of this study was to modify the LSAMP II to decrease its measurement duration. Two methods were tested to decrease the time required to make measurements with the LSAMP II: (1) using different tip seal geometries to change the permeameter sample volume and (2) adding weight to the syringe piston to increase gas injection pressure. The results of this study apply specifically to syringe-based permeameters. Using different size tip seals, in particular ones having different inner radii, proved to be effective in decreasing measurement duration. Though the results for changing tip seal geometry were promising, application of this method is limited due to practical constraints on tip seal size. Adding weight proved to be a more useful means for reducing measurement duration.

Measurements were made on various length combinations of POREX® porous plastics (see Appendix 1) with no added weight, addition of the 696.67 g (1lb + weight holder), and 1377.02 g weight (2.5 lb + weight holder). Addition of weight proved to significantly decrease measurement duration: 20.3 % of un-weighted duration for 1 lb, and 10.6 % of the un-weighted duration for 2.5 lb. The error in estimated permeability (when compared to the un-weighted measurement) due to a pressure transient during the measurement interval was small: 1.77 % for 1 lb and 2.41 % for 2.5 lb. If the 3-way valve, which opens the pressurized syringe and tubing to the tip seal, were moved to the tip seal, addition of more weight may be possible, further decreasing measurement duration (increasing measurement range).

5.3 Pressure Decay Permeameter

The main motivation for developing the transient pressure decay permeameter was to increase the range of permeability that can be measured in the field. A mathematical model was developed and a prototype device was fabricated to test the permeability measurement range that the pressure decay permeameter could offer. Measurements were made on four sample materials with a wide range of permeability, at four different initial tank pressures, using two different volume tanks. Smith [1998] noted non-isothermal conditions in the gas reservoir for a similar type device, so a fiberglass heat capacitor was placed in the tank for many measurements. Data was analyzed using a diagnostic dimensionless plot. If the model is satisfied, the diagnostic plot should be linear.

Results showed two types of anomalous behavior. One anomaly was attributed to thermodynamic effects in the tank due to rapidly decaying pressure at the onset of a measurement. This was conclusion was based on the fact that measurements made with the heat capacitor in the tank did not exhibit the anomaly. The other anomalous behavior equated to tank pressure decaying slower than the model predicted, and was noticed only in high permeability materials. Derivatives of transformed pressure and steady-flow measurements, across a range of injection pressures, suggest the pressure anomaly is due to inertial effects at higher pressures.

The tested range of the pressure decay permeameter was greater than four orders of magnitude ($1 \times 10^{-11} - 3 \times 10^{-15} \text{ m}^2$). This range is made possible by using only early time pressure decay data rather than the decay from initial tank pressure to atmospheric

pressure. The instrument's range could be extended by using a more precise and accurate pressure transducer.

More work is required before a field portable device can be constructed. Instrumentation and design issues include: how the tank will be pressurized in the field, what type of valve should be used between the tank and the tip seal, what type of pressure transducer is required, and what range of pressures must be used to retain the measurement range without worrying about nonlinear effects.

REFERENCES

1. Aronson, E.C., 1999. *Modeling investigations on gas permeameters: spatial weighting functions and layered systems*, M.S. Special Report, New Mexico Institute of Mining and Technology, Socorro, New Mexico.
2. Carmen, P.C., 1956, *Flow of gases through porous media*, Butherworths Scientific Publications, London, 182 p.
3. Chandler, M.A., Kocurek, G., Goggin, D.J., and Lake, L.W., 1989. Effects of stratigraphic heterogeneity on permeability in eolian sandstone sequence, Page Sandstone, Northern Arizona, *AAPG Bulletin*, v. 73 (5), 658-668.
4. Clark, D.G. and van Golf-Racht, T.D., 1985. Pressure derivative approach to transient test analysis: A high permeability North Sea reservoir example, *Journal of Petroleum Technology*, v. 37 (12), 2023-2039.
5. Davis, J.M., Lohmann, R.C., Phillips, F.M., Wilson, J.L., and Love, D.W., 1993. Architecture of the Sierra Ladrone Formation, central New Mexico: Depositional controls on permeability correlation structure, *GSA Bulletin*, v. 105, 998-1007.
6. Davis, J.M., 1994. *A conceptual sedimentological-geostatistical model of aquifer heterogeneity based on outcrop studies*, PhD. Thesis, New Mexico Institute of Mining and Technology, Socorro, New Mexico.
7. Davis, J.M., Wilson, J.L., and Phillips, F.M., 1994. A portable air-minipermeameter for rapid in-situ field measurements, *Ground Water*, v. 32 (2), 258-266.
8. Dullien, F.A.L., 1992. *Porous media: Fluid transport and pore structure*, Academic Press, San Diego.
9. Dykstra, H. and Parsons, R.L., 1950. The prediction of oil recovery by water flood, Secondary recovery in the U.S.A., 2nd ed., *American Petroleum Inst.*, 160-174.

10. Eijpe, R. and Weber, K.J., 1971. Mini-permeameters for consolidated rock and unconsolidated sand, *AAPG Bulletin*, v. 55 (2), 307-309.
11. Ferris, S.M., 1995. *Characterization of physical properties and statistical description of permeability distribution of an upper portion of the Great Miami Aquifer near Fernald, Ohio*, M.S. Thesis, University of Cincinnati, Cincinnati, Ohio.
12. Goggin, D.J., Thrasher, R.L., and Lake, L.W., 1988. A theoretical and experimental analysis of minipermeameter response including gas slippage and high velocity flow effects, *In Situ*, v. 12 (1-2), 79-116.
13. Herrin, J.M., 2001. *Characteristics of deformation bands in poorly lithified sand: Rio Grande Rift, New Mexico*, M.S. Thesis, New Mexico Institute of Mining and Technology, Socorro, New Mexico.
14. Hong, S, 1999. *Anisotropic hydraulic conductivity of faulted poorly consolidated eolian sands: Bosque, New Mexico*, M.S. Thesis, New Mexico Institute of Mining and Technology, Socorro, New Mexico.
15. Jones, S.C., 1992. The profile permeameter: A new, fast, accurate minipermeameter, paper *SPE 24757* presented at the 67th Annual Technical Conference, Soc. of Pet. Eng., Washington D.C., Oct 4-7, 1992.
16. Kirkham, D., 1946. Field method for determination of air permeability of soil in its undisturbed state, *Soil Sci. Soc. Am. Proc.*, v. 11, 93-99.
17. Molz, F.J., Dinwiddie, C.L., and Wilson, J.L., 2002. A physical basis for calculating instrument spatial weighting functions in homogeneous systems, *Water Resources Research*, in press.
18. Rawling, G.C., Goodwin, L.B., and Wilson, J.L., 2001. Internal architecture, permeability structure, and hydrologic significance of contrasting fault-zone types, *Geology*, v. 29 (1), 43-46.
19. Sigda, J., 1997. *Effects of small-displacement faults on the permeability distribution of poorly consolidated Santa Fe Group sands, Rio Grande rift New Mexico*, M.S. Thesis, New Mexico Institute of Mining and Technology, Socorro, New Mexico.

20. Sigda, J.M., Goodwin, L.B., Mozley, P.S., and Wilson, J.L., 1999. Permeability alteration in small-displacement faults in poorly lithified sediments; Rio Grande Rift, central New Mexico, Faults and subsurface fluid flow in the shallow crust, *AGU Monograph* 113, 51-68.
21. Sigda, J.M. and Wilson, J.L., 2002. Are faults preferential flow paths through semi-arid and arid vadose zones?, submitted to *Water Resources Research*.
22. Smith, J.E., Robin, J.L., and Elrick, D.E., 1997. A source of systematic error in transient-flow air permeameter measurements, *Soil Sci. Soc. Am. J.*, v. 61, 1563-1568.
23. Smith, J.E., Robin, J.L., and Elrick, D.E., 1998. Improved transient-flow air permeameter design: Dampening the temperature effects, *Soil Sci. Soc. Am. J.*, v. 62, 1220-1227.
24. Suboor, M.A., 1994. *The operating characteristics of minipermeameter and its ability to investigate small scale permeability heterogeneity*, M.S. Thesis, New Mexico Institute of Mining and Technology, Socorro, New Mexico.
25. Tartakovsky, D.M., Moulton, and J.D., Zlotnik, 2000. Kinematic structure of minipermeameter flow, *Water Resources Research*, v. 36 (9), 2433-2442.
26. Taylor, R.G., 1997. *Effect of water saturation on air permeability in unconsolidated sands of Oyster, Virginia*, M.S. Thesis, New Mexico Institute of Mining and Technology, Socorro, New Mexico.
27. Titzel, C.S., 1997. *Quantification of the permeability distribution within sand and gravel lithofacies in a southern portion of the Miami Valley Aquifer*, M.S. Thesis, Wright State University, Dayton, Ohio.
28. Tidwell, V.C. and Wilson, J.L., 1997. Laboratory method for investigating permeability upscaling, *Water Resources Research*, v. 33 (7), 1607-1616.

APPENDIX 1: POREX[®] Porous Plastic Standards

When using an instrument such as a gas permeameter, it is good practice to periodically check the instrument for drift that could bias permeability estimates. The presence of a leak in the measurement system can easily be identified, but ensuring that permeability estimates are repeatable is more difficult. A permeability standard must be used to check for instrument drift and verify precision. The gas permeameter could be calibrated with one or more small blocks of porous rock, but unless the rock is completely homogeneous accounting for differences in permeability due to tip seal placement on the rock face is difficult. Desirable qualities in a standard are: (1) the material is relatively homogeneous, (2) no use of the tip seal is required, and (3) the material has a low thermal capacity. Porous plastic manufactured by the Porex Corporation (500 Bohannon Rd., Fairburn, GA 30213-2828) satisfied the above qualifications.

Porex porous plastic products are available in many different polymers, shapes, and pore sizes. Common applications include: filters for gases and liquids, diffusers, vents, and mufflers. For more information on Porex Porous Plastic Components see www.porex.com.

Porex standard rod products were chosen for construction of the permeability standards. The porous plastic rods are made from a polyethylene polymer, have a ½ inch diameter, and come in 1 ft lengths. The assembly of a permeability standard requires three materials: (1) the porous plastic rod, (2) flexible tubing with a slightly smaller inner diameter than the diameter of the rod (ID = 7/16 in), and (3) a male and female quick disconnect fitting at the ends. First, a length of Porex plastic is cut from the rod and its

length is measured (for use in the calculation of permeability). The piece of plastic is then inserted in a section of tubing and the fittings installed on each end of the tubing, on either side of the Porex plastic. The tubing provides a seal on the outer wall of the rod so that a pressure gradient can be imposed across the sample.

Porex plastics with three different pore sizes were chosen for use as permeability standards: 20 μm , 35 μm , and 120 μm . Of the three pore sizes, the 20 μm plastic was used most extensively. Permeability estimates for the different materials were made with the LSAMP II. **Table A1.1** gives the mean permeability for each of the samples. Permeability increases with pore size, though the permeability range is very small. The standard deviation in estimated permeability is very low hence the Porex porous plastic provides a good material to use as a permeability standard.

Table A1.1. Mean and standard deviation permeability by Porex plastic pore size.

permeability (m^2)	20 μm	35 μm	120 μm
average	1.24E-11	2.05E-11	3.65E-11
standard deviation	2.05E-14	7.51E-14	1.38E-13

The permeability standards used in the testing of the weighted LSAMP II (Chapter 3) were all 20 μm porous plastic. The measured lengths of each standard, its mean, and standard deviation permeability are given in **Table A1.2**. The permeability varies only slightly across samples (standard deviation = 3.6107E-14 m^2) and there appears to be no systematic bias due to sample length. The relatively high standard deviation for the 2 cm standard can be attributed to one outlier.

Table A1.2. Measured length of permeability standards used to test weighted LSAMP.
Statistics for each length are based on five LSAMP II measurements.

standard #	length (cm)	mean permeability (m²)	standard deviation permeability (m²)
1	1.047	3.29E-12	4.29263E-15
2	2.298	3.26E-12	1.31128E-14
3	3.068	3.20E-12	6.21388E-15
4	4.260	3.26E-12	3.61817E-15

APPENDIX 2: LSAMP II Modification, Pressure vs. Time Plots

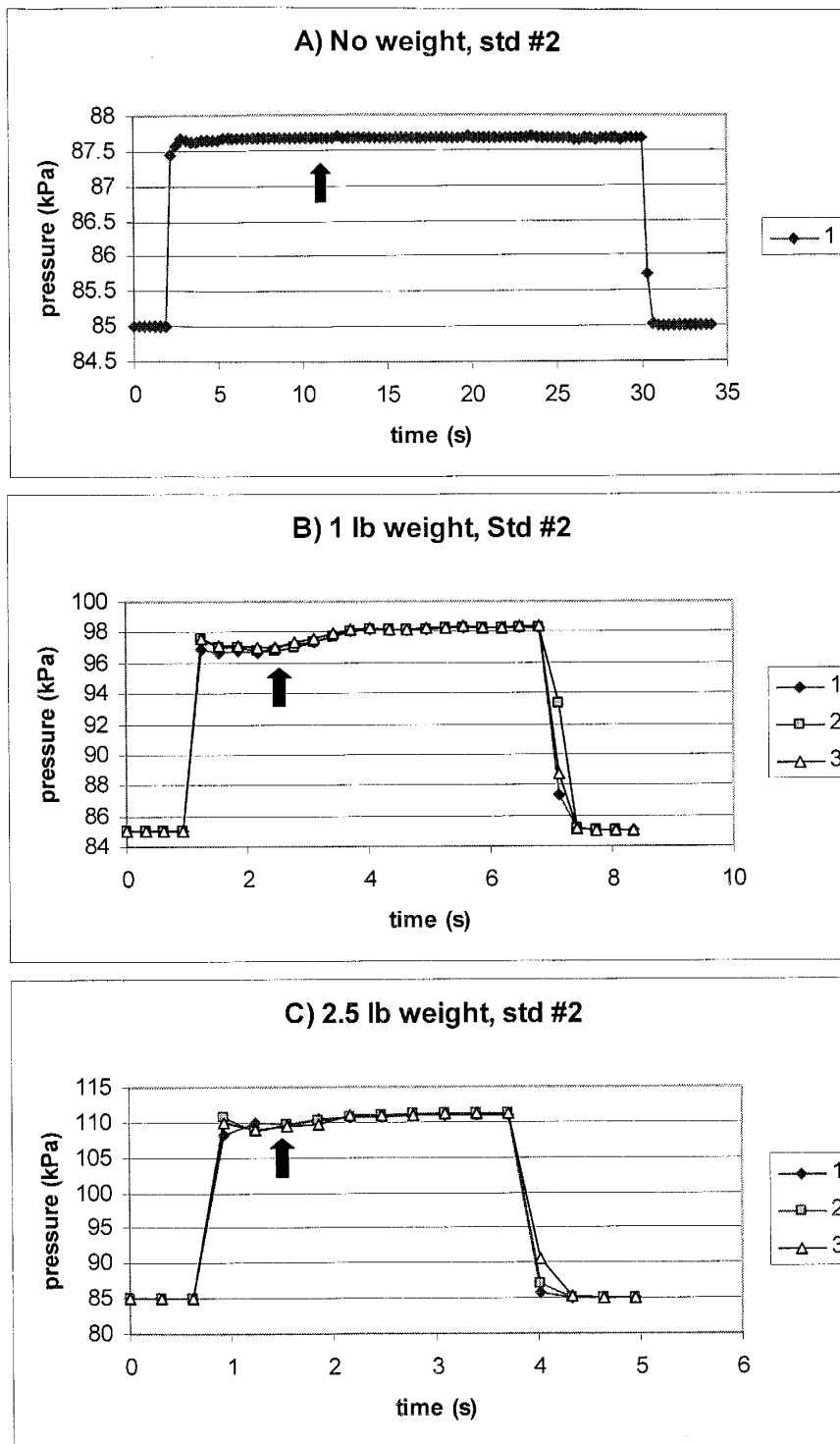


Figure A2.1. Pressure vs. time plots for all three weight classes on (A-C) Std. 2, (D-F) Std. 1 + 4, and (G-I) Std. 2 + 3 + 4.

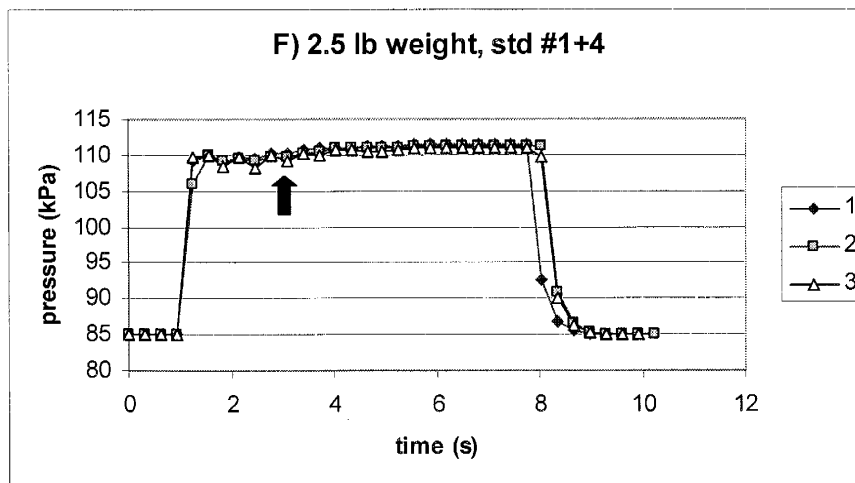
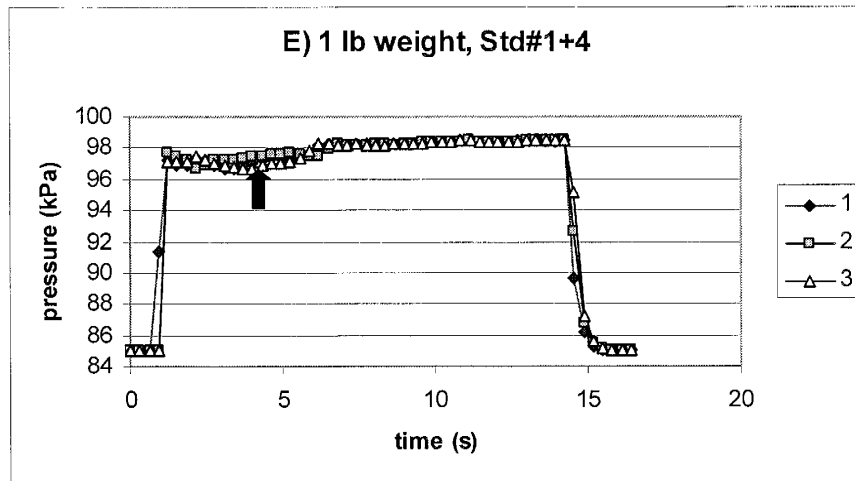
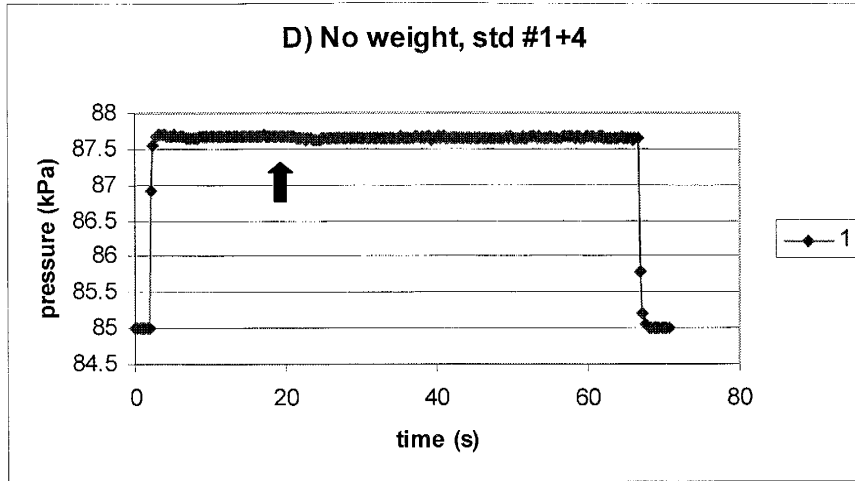


Figure A2.1. Pressure vs. time plots for all three weight classes on (A-C) Std. 2, (D-F) Std. 1 + 4, and (G-I) Std. 2 + 3 + 4.

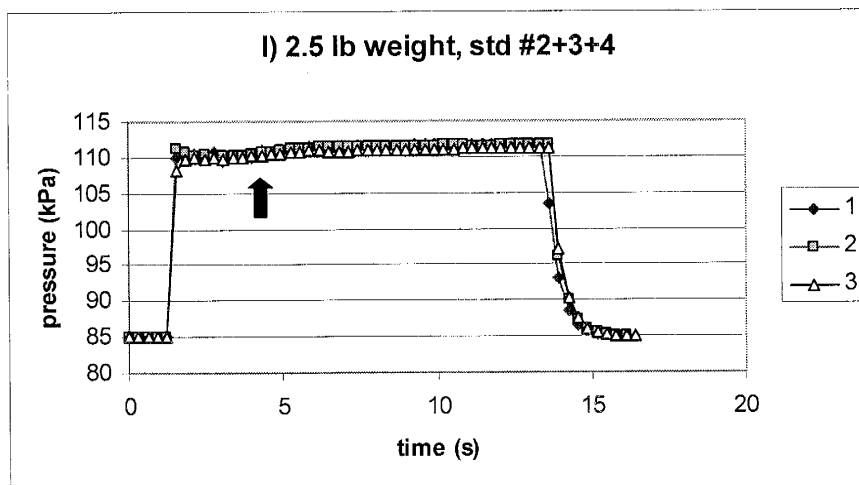
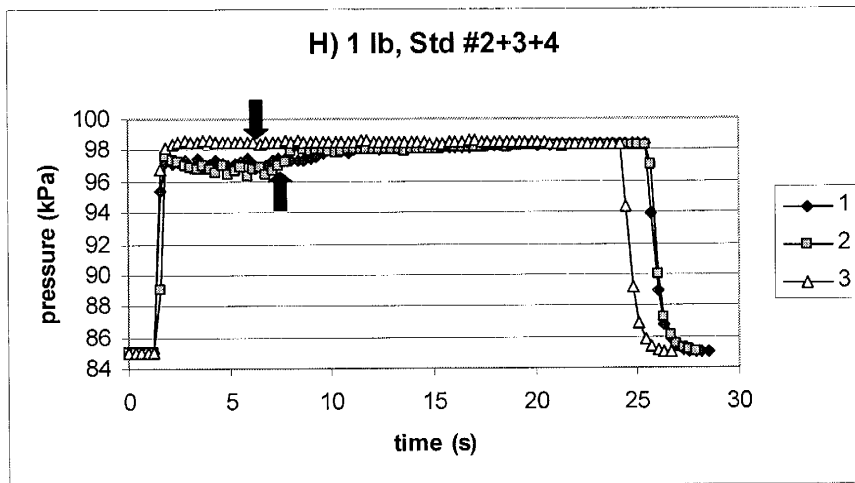
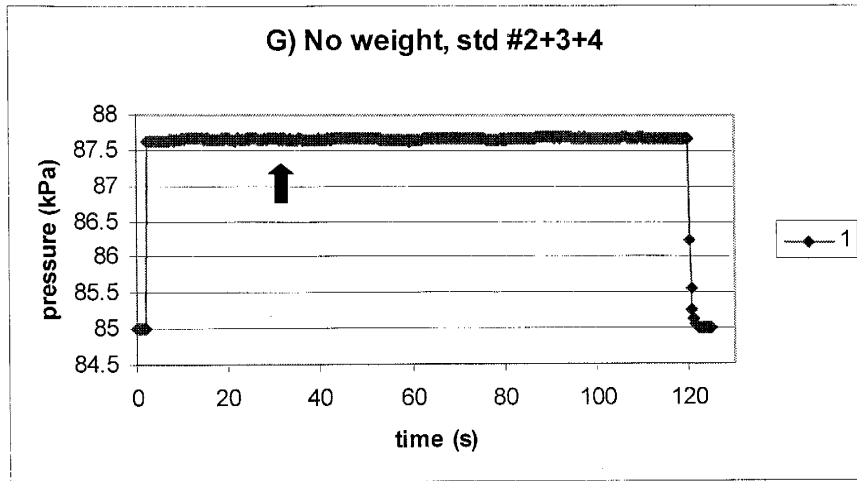


Figure A2.1. Pressure vs. time plots for all three weight classes on (A-C) Std. 2, (D-F) Std. 1 + 4, and (G-I) Std. 2 + 3 + 4.

APPENDIX 3: Pressure Decay Permeameter Model Sensitivity to Atmospheric Pressure

Calculation of permeability (using Equation 4.21) from pressure decay permeability data requires knowledge of atmospheric pressure at the time of the measurement. Atmospheric pressure, p_0 , can be retrieved from a local barometer (preferably at the site of the measurements), but should not be taken from online or published weather data. The values posted by the National Weather Service are typically corrected to mean sea level (1 atm), which is not the value that should be used for permeability calculation. The error associated with using the incorrect value for atmospheric pressure depends on the type of transducer used.

Pressure data recorded using a transducer comes in one of three forms of pressure: (1) absolute pressure, (2) differential pressure, or (3) gauge pressure. Absolute pressure transducers include atmospheric pressure in their value, while differential (with one port open to the atmosphere) and gauge pressure transducers record the pressure in excess of atmospheric. Inspecting Equation (4.21), there are three pressure forms in the equation: (1) atmospheric pressure (absolute pressure), (2) tank pressure (t) plus atmospheric pressure (absolute pressure), and (3) tank pressure (t) minus atmospheric pressure (differential pressure). Regardless of how pressure data is recorded (absolute or differential) knowledge of p_0 is required. If absolute pressure is recorded, to calculate # 3 above, p_0 must be subtracted from the recorded data. If differential or gauge pressure is recorded, the actual value for # 3 is that recorded by the transducer and # 2 can be calculated by adding $2 \times p_0$ to the recorded data.

Sensitivity to atmospheric pressure was explored for use of both absolute and differential pressure data. The true atmospheric pressure was assumed to be 85 kPa. Other model parameters set for the analysis were: permeability, k , of $1 \times 10^{-12} \text{ m}^2$, inner tip seal radius, r_i , of 3 mm, geometric factor, G_o , of 4.432 (4:1 tip seal), a tank volume, V_T , of 120 cm^3 , and a gas viscosity of $1.75 \times 10^{-5} \text{ Pa}\cdot\text{s}$. The same set of parameters was used in both analyses. Synthetic pressure data, ranging from 115-85.1 kPa (absolute) and 30-0.1 kPa (gauge), and the model were used to generate corresponding time data using the true atmospheric pressure (85 kPa). Transformed pressure data was then calculated using the above pressure ranges for five different initial pressures: 86, 85.5, 85, 84.5, and 84 kPa. It is assumed that the pressure and corresponding time data is correct, so dimensionless time data was calculated using the true time data (calculated for $p_0 = 85 \text{ kPa}$) and each of the five atmospheric pressures.

Figure A3.1 shows the behavior of the diagnostic plot as a function of the chosen atmospheric pressure for: (A) absolute pressure data and (B) differential pressure data. There is a drastic difference in the character of the two plots. The slope of the diagnostic plot (**Figure A3.1B**) when differential pressure is used is essentially independent of the atmospheric pressure. The diagnostic plot (**Figure A3.1A**) for the absolute pressure data does not show much deviation from the true behavior until to a transformed pressure of ~ 1.5 . At this point, data for which too high an atmospheric pressure was used increase in slope and data with too low an atmospheric pressure decrease in slope, with the true atmospheric pressure producing a constant slope. The larger the deviations (positive or negative) from the true atmospheric pressure produce greater deviations from the true behavior. This implies that when using an absolute pressure transducer extreme

accuracy and precision in the estimate of atmospheric pressure is required. There seem to be no severe consequences for using the incorrect atmospheric pressure for data collected with a differential or gauge transducer.

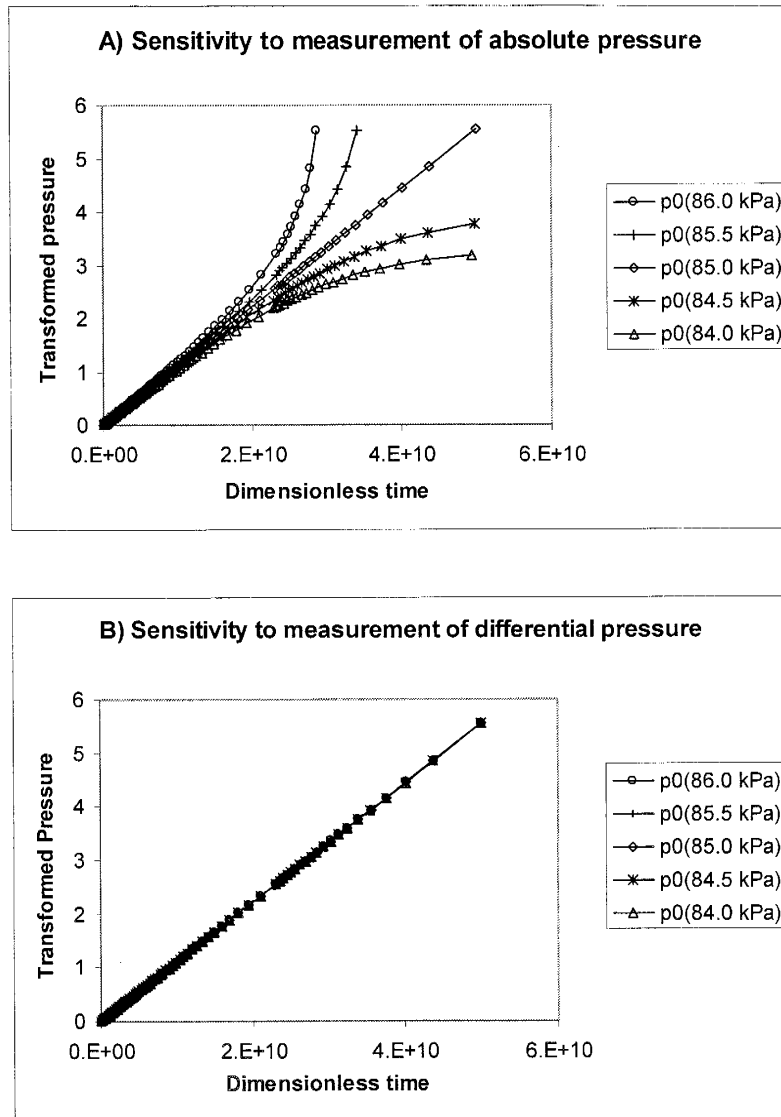


Figure A3.1. Pressure decay model sensitivity to atmospheric pressure. Sensitivity depends on whether pressure data is in (A) absolute or (B) differential pressure.

APPENDIX 4: Pressure Decay Permeameter Plots (Small Reservoir)

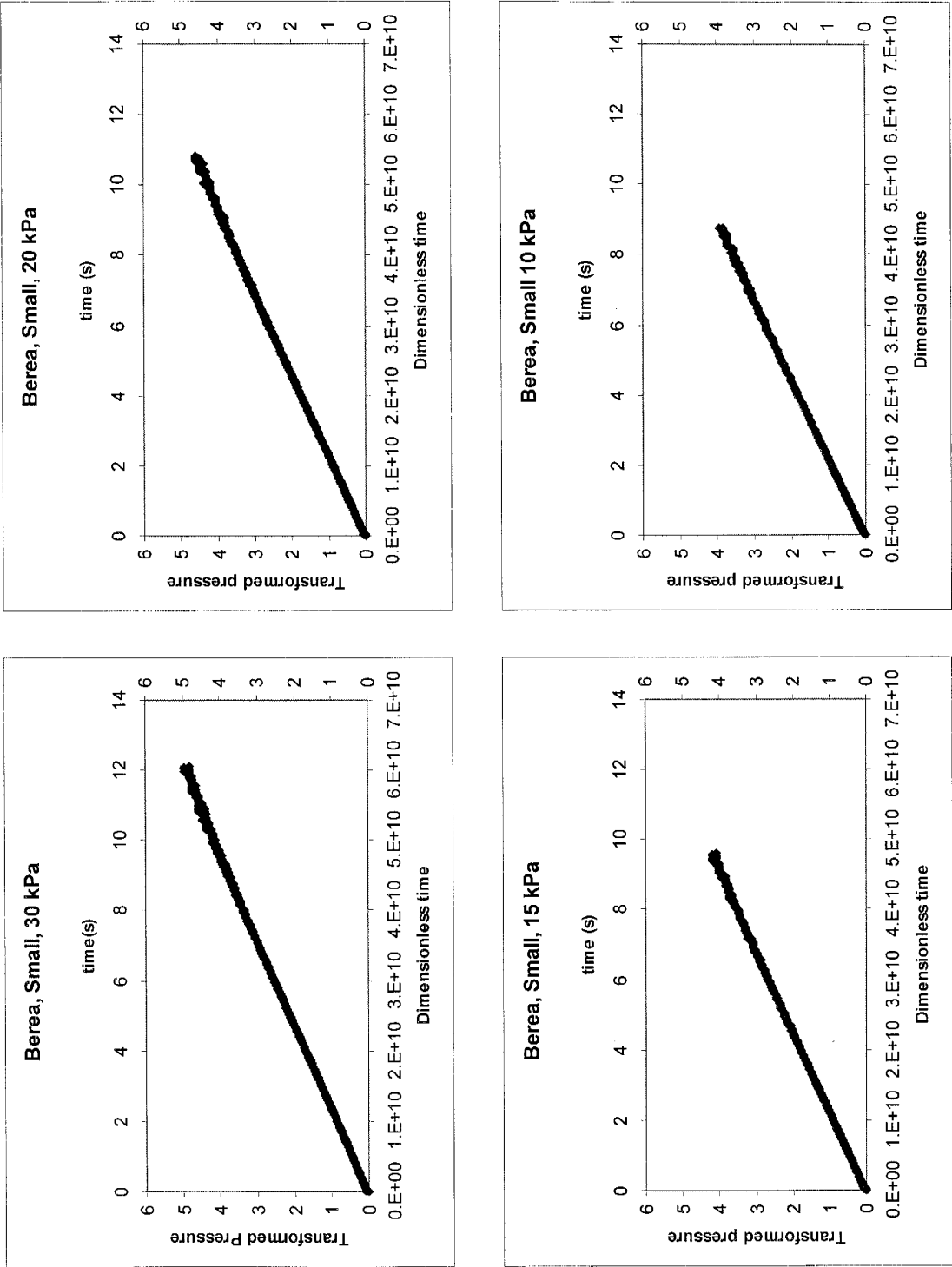


Figure A4.1. Diagnostic plots for Berea Sandstone. Title refers to material, tank size, and initial tank gauge pressure.

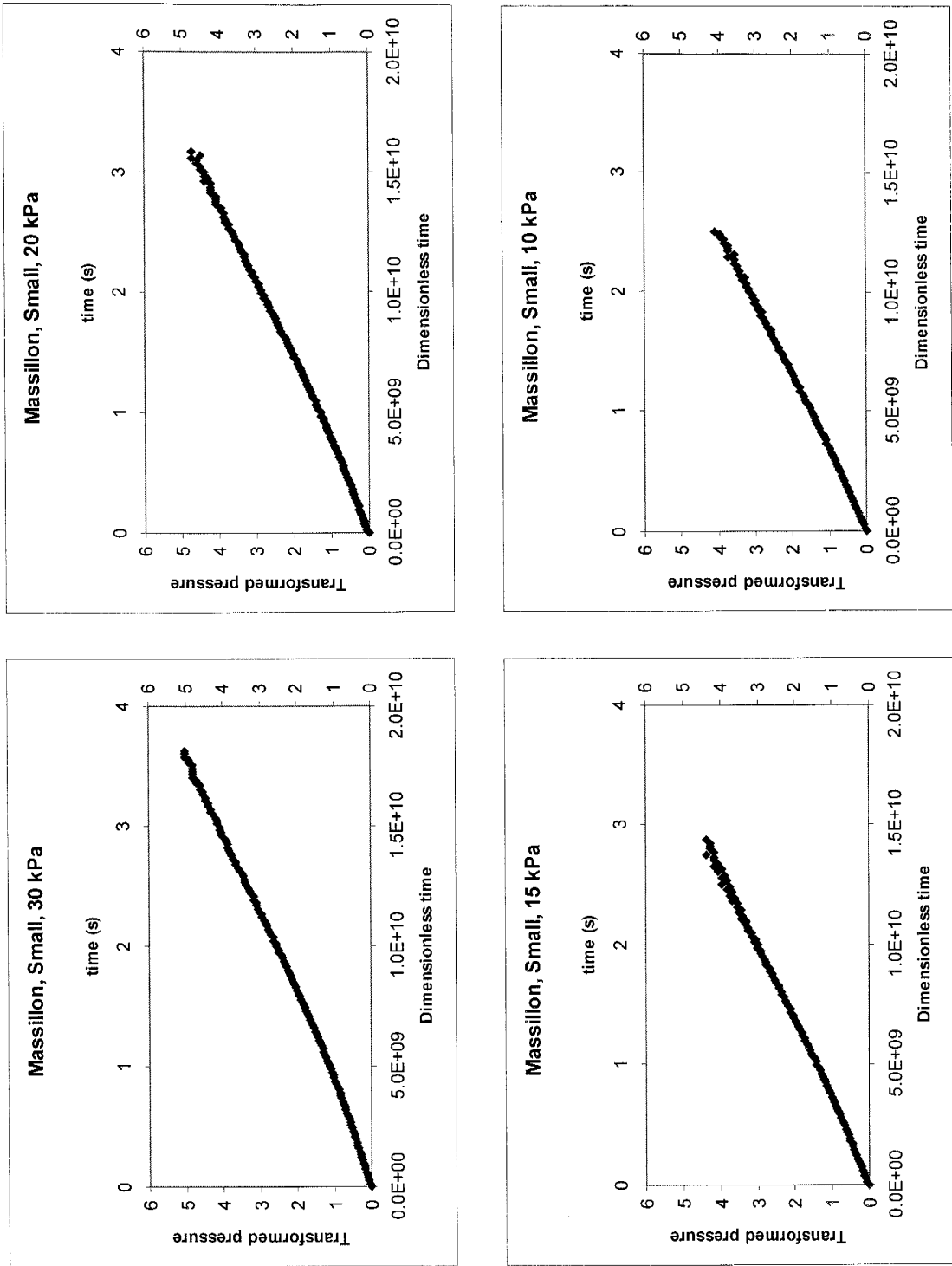


Figure A4.2. Diagnostic plots for Massillon Sandstone. Title refers to material, tank size, and initial tank gauge pressure.

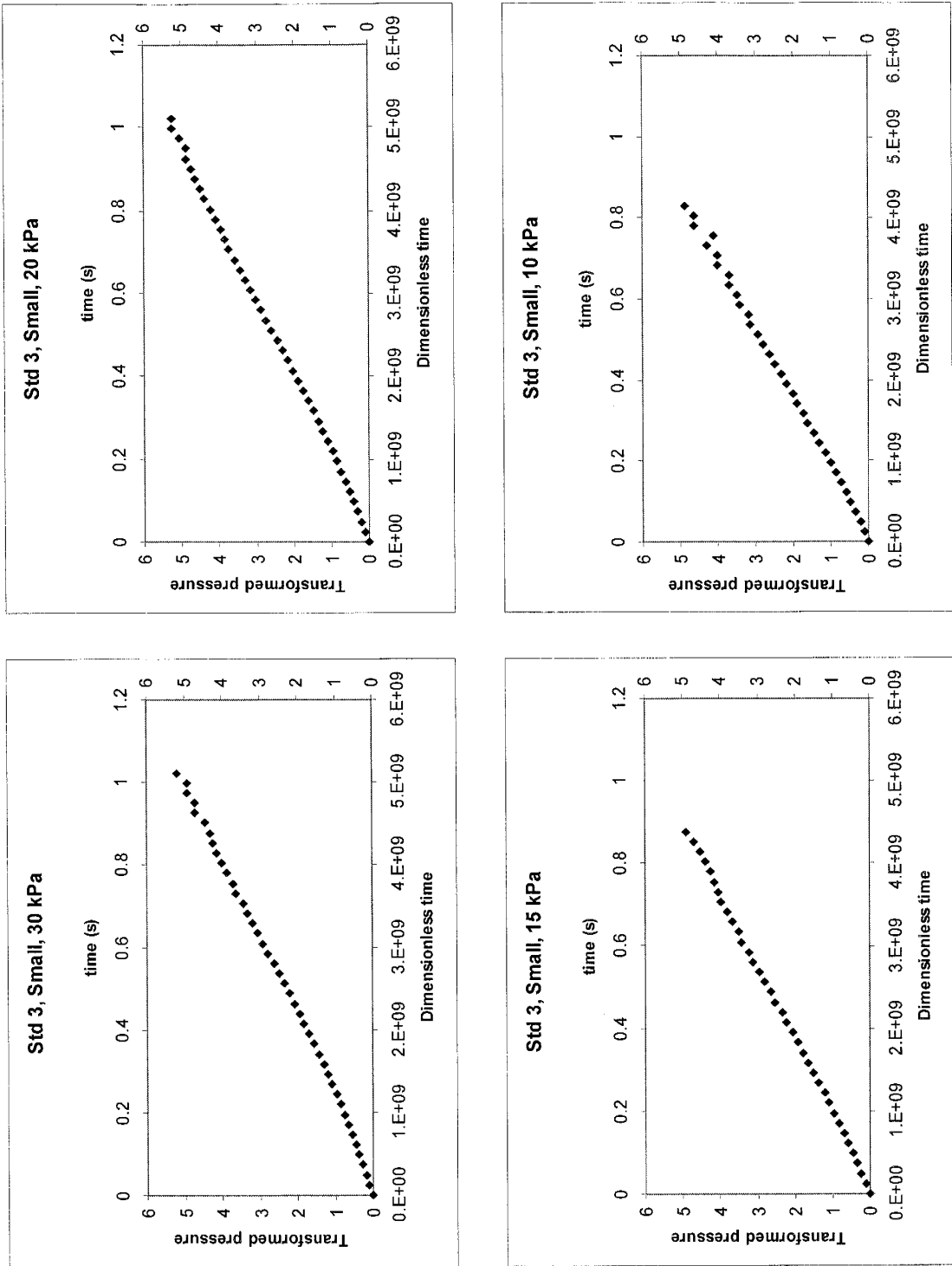


Figure A4.3. Diagnostic plots for Standard 3. Title refers to material, tank size, and initial tank gauge pressure.

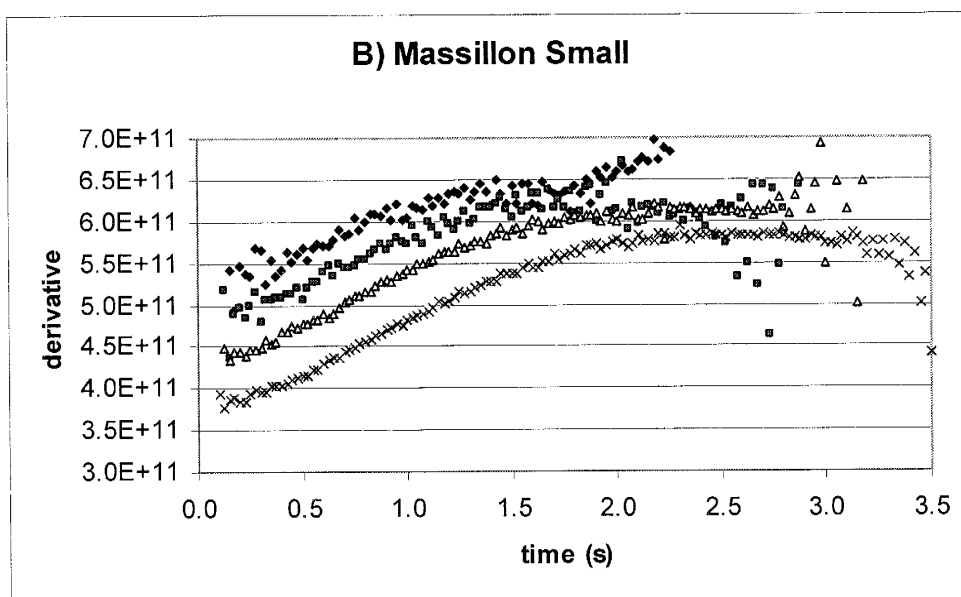
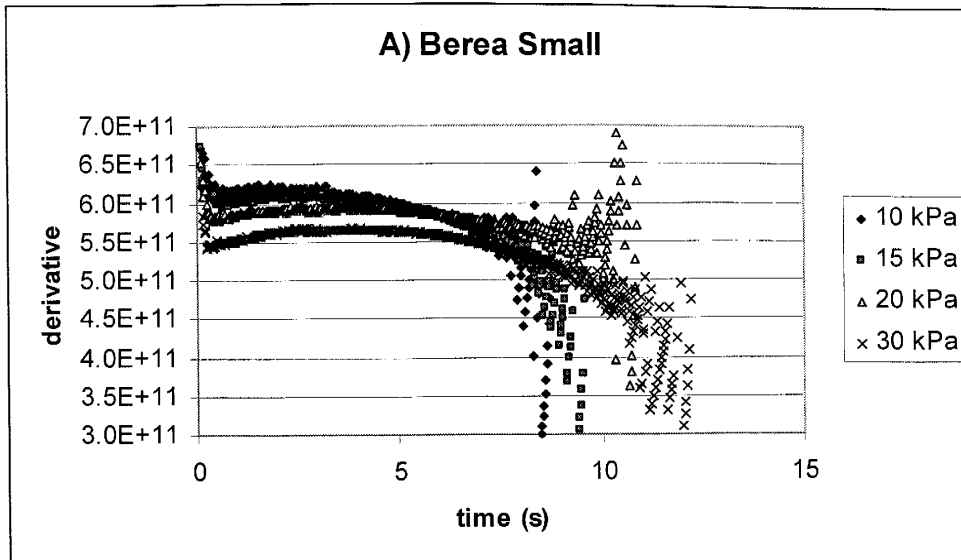


Figure A4.4. Transformed pressure derivative vs. time plots for (A) Berea Sandstone and (B) Massillon Sandstone. The derivative axis is stretched to accentuate differences between data collected at different initial pressures. Small in title refers to the tank used.

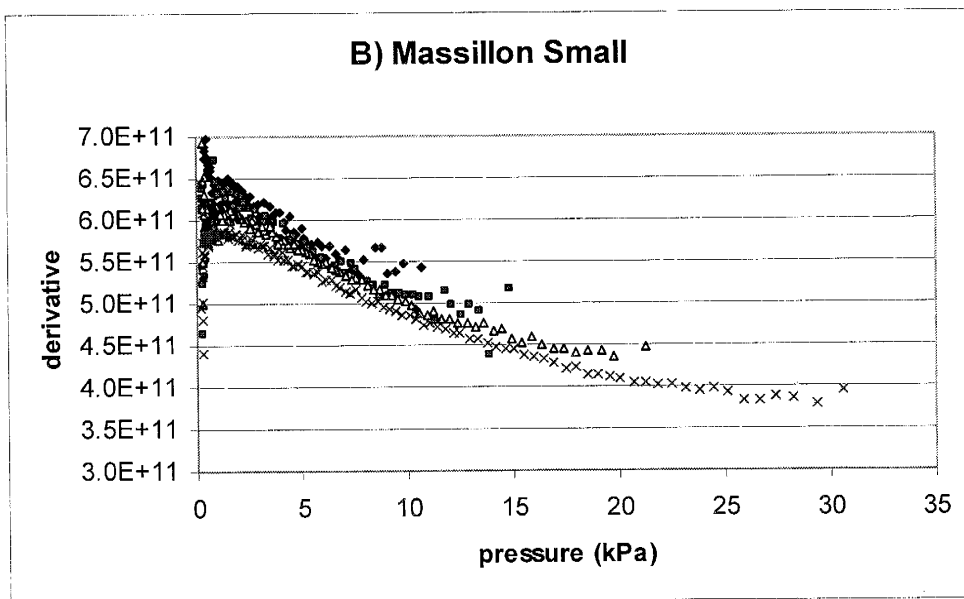
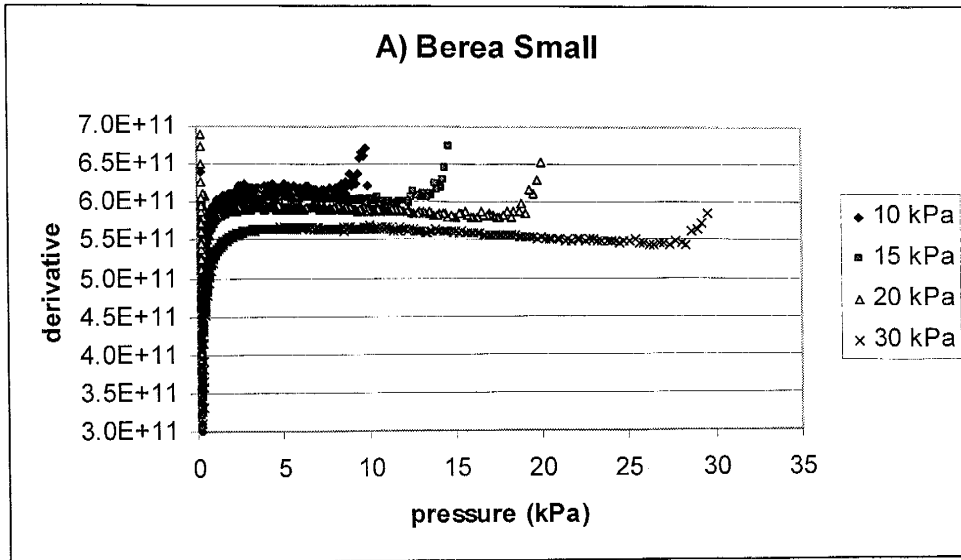
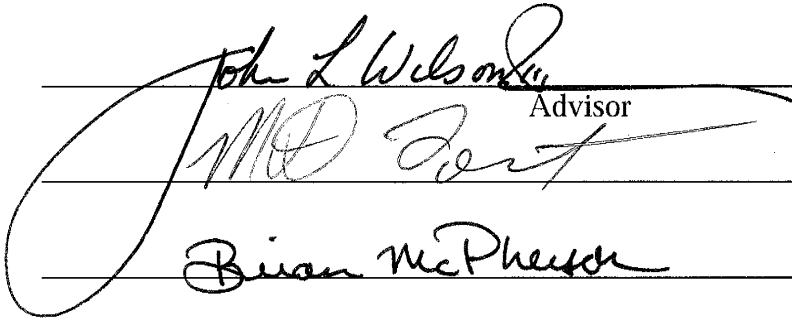




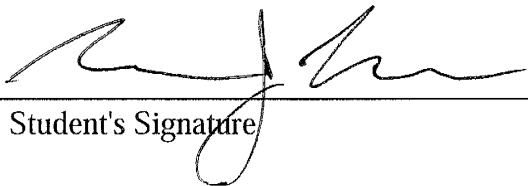
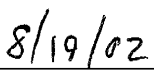
Figure A4.5. Transformed pressure derivative vs. pressure plots for (A) Berea Sandstone and (B) Massillon Sandstone. The derivative axis is stretched to accentuate differences between data collected at different initial pressures. Small in title refers to the tank used.

This thesis is accepted on behalf of the
Faculty of the Institute by the following committee:

 _____
Advisor
 _____
 _____

 _____
Date

I release this document to the New Mexico Institute of Mining and Technology.

 _____
Student's Signature
 _____
Date